

TOOL LIFE ENHANCEMENT OF COATED CARBIDE TOOLS  
USED FOR MILLING OF H13 TOOL STEEL

Tool Life Enhancement of Coated Carbide Tools used for Milling of H13 Tool Steel

By

Shahereen Chowdhury

A Thesis

Submitted to the School of Graduate Studies in Partial Fulfillment of the Requirements  
for the Degree of  
Doctor of Philosophy

McMaster University

© Copyright by Shahereen Chowdhury, January 2020

DOCTOR OF PHILOSOPHY (2020)  
(Mechanical Engineering)

McMaster University  
Hamilton, Ontario

TITLE: Tool Life Enhancement of Coated Carbide Tools used  
for Milling of H13 Tool Steel.

AUTHOR: Shahereen Chowdhury

SUPERVISOR: Dr. Stephen C. Veldhuis

SUPERVISORY COMMITTEE: Dr. Peidong Wu

Dr. Kathryn Grandfield

EXTERNAL MEMBER: Dr. Robert J. Klassen

*To my father Md. Matlubar Rahman Chowdhury, a cancer survivor, a person who taught me the art of survival while remaining happy.*

*To my mother Teslima Rahman, for accepting me the way I am and shaping me into the woman and mother I am today.*

*To my husband Dr. Kazi Arafat Rahman, for making my sky much wider and brighter.*

*To my daughter, my ultimate sunshine, Zwena Alinah, for making be a better person each day and walking with me to the finish line hand in hand.*

## ACKNOWLEDGMENTS

I would like to express my profound gratitude to my supervisor Prof. Stephen C. Veldhuis, for his guidance, advice and support while encouraging me to follow my own ideas. I thank him for his kindness and trust.

I would also like to sincerely thank Dr. Bipasha Bose for inspiring and supporting my ideas.

This work would not succeed without her precious advice.

My utmost gratitude to Dr. German Fox-Rabinovich and Dr. Abul Fazal M. Arif for their continuous guidance, help and support.

A special thanks to my friends Farhad Molaiekiya, Mostafa Yakut, Mohammad Shariful Islam Chowdhury and Ali Aliakbari Khoei for their immense support. Their encouragement and kind words were a constant source of inspiration during this period.

I acknowledge the Natural Sciences and Engineering Research Council of Canada (NSERC) and the Canadian Network for Research and Innovation in Machining Technology (CANRIMT) for their financial support.

## TABLE OF CONTENTS

LIST OF TABLES .....	x
LIST OF FIGURES .....	xi
LAY ABSTRACT .....	xiv
ABSTRACT .....	xv
Chapter 1. INTRODUCTION.....	17
1.1 Background.....	17
1.1.1 Literature Review .....	17
Tool Wear and Tool Wear Mechanisms.....	17
Milling of H13 Tool Steel .....	20
PVD Tool Coating.....	23
Coating Development: Effect of PVD Coating Composition.....	26
Process Development: Effect of PVD Coating Deposition Parameter .....	27
Optimization for Application: Effect of PVD Coating Architecture .....	28
Mechanical Surface Treatment of PVD coatings .....	32
1.1.2 Research Gaps.....	37
1.2 Motivation and Research Objective.....	39
1.2.1 Motivation.....	39
1.2.2 Research Objective .....	39
1.3 Thesis Organization .....	41
1.3.1 General technical overview .....	41

1.3.2	Chapter contents .....	42
1.4	Note to the Reader .....	43
1.5	References.....	43
Chapter 2.	IMPROVEMENT OF WEAR PERFORMANCE OF NANO-MULTILAYER PVD COATINGS UNDER DRY HARD END MILLING CONDITIONS BASED ON THEIR ARCHITECTURAL DEVELOPMENT .....	49
2.1	Introduction.....	49
2.2	Materials and Methods .....	52
2.3	Results and Discussion.....	57
2.3.1	Structural Analysis.....	57
2.3.2	Mechanical properties.....	57
Residual stress .....		57
Micro-mechanical properties.....		60
2.3.3	Tool Life and Wear Performance Studies .....	66
2.4	Conclusion .....	70
2.5	References.....	71
Chapter 3.	EFFECT OF INTERLAYER THICKNESS ON NANO-MULTILAYER COATING PERFORMANCE DURING HIGH SPEED DRY MILLING OF H13 TOOL STEEL.....	74
3.1	Introduction.....	74
3.2	Experimental Details.....	79
3.2.1	Substrate Specification .....	79

3.2.2	Coating Deposition .....	79
3.2.3	Determination of Micro-Mechanical Properties of Coatings .....	81
3.2.4	Cutting Performance of Coated Tools .....	83
3.3	Results and Discussion .....	83
3.3.1	Structural Analysis.....	83
3.3.2	Micro-Mechanical Property Analysis.....	85
3.3.3	Tool Life Analysis .....	95
3.4	Conclusions.....	98
3.5	References.....	99
 Chapter 4. IMPROVEMENT IN COATED CARBIDE TOOL LIFE FOLLOWING THE APPLICATION OF SURFACE TREATMENT TECHNIQUE-WIDE PEENING CLEANING (WPC) WHILE WET MILLING OF H13 TOOL STEEL.....		
		104
4.1	Introduction.....	104
4.2	Experimental Details.....	107
4.2.1	Coating deposition .....	107
4.2.2	Post-treatment process .....	108
4.2.3	Determination of micro-mechanical properties of coatings .....	108
4.2.4	Cutting performance .....	110
4.3	Results and Discussion .....	111
4.3.1	Effect on cutting-edge geometry and coating roughness.....	111
4.3.2	Analysis of Micro-mechanical properties.....	112
4.3.3	Coating adhesion and tool life analysis .....	121



4.4	Conclusion .....	129
4.5	References .....	130
Chapter 5. CONCLUSIONS AND FUTURE WORKS .....		136
5.1	General Conclusions .....	136
5.2	Research Contributions .....	141
5.3	Directions for Future Work.....	142
PUBLICATIONS.....		143

## LIST OF TABLES

Table 1.1 Nominal chemical composition of H13 tool steel (wt%) [15].	21
Table 1.2 Mechanical and thermal properties of H13 tool steel ( 45-58 HRC) [16].	21
Table 1.3 Wear patterns observed in literature for milling of H13 tool steel	22
Table 1.4 Summary of research on the coating interlayer.	31
Table 1.5 Literature on currently available techniques for the post-treatment of coated tools.	33
Table 2.1 Different architectures of TiAlCrSiYN-based coatings.	53
Table 2.2 Cutting parameters used for the tool life evaluation.	54
Table 2.3 Residual stress values in the studied coatings.	60
Table 2.4 Micro-mechanical properties of the studied coatings	61
Table 2.5 Penetration depth after 30 s and 300 s during nano impact test (20–30 mN).	61
Table 2.6 Scratch crack propagation resistance of the studied coatings.	64
Table 3.1 Coatings studied for tool life and micro-mechanical property evaluation.	81
Table 3.2 Cutting parameters used for the tool-life evaluation.	83
Table 3.3 Residual stress in the studied coatings when $E$ is 500 GPa for all crystal axis.	86
Table 3.4 Variation of dimensionless parameter $H^3/E^2$ and $H/E$ with the interlayer thickness.	88
Table 4.1 WPC conditions applied on coatings studied for tool life and micro-mechanical property evaluation	108
Table 4.2 Cutting parameters used for the tool-life evaluation.	111
Table 4.3 Surface profile ( $Ra$ and $Rt$ ) at a roughness sampling length of 250 $\mu\text{m}$ due to the variation of WPC conditions	114
Table 4.4 Value of $H^3/E^2$ and $H/E$ ratio at a depth of penetration of 180 nm for WPC process time variation at a process pressure of 0.2 MPa ( $E \sim 500$ GPa)	116
Table 4.5 Comparison of ramped load scratch test and wear test data for the variation of WPC process time at a WPC pressure of 0.2 MPa	123

## LIST OF FIGURES

Figure 1.1 (a) Tool wear schematic; Failure mechanisms in (b) continuous cutting and (c) interrupted cutting adapted from [4].	18
Figure 1.2 Typical tool life curve versus cutting time/length.	19
Figure 1.3 Influence of coatings on wear mechanisms and contact conditions adapted from [28].	24
Figure 1.4 Coating-substrate system properties adapted from [30].	25
Figure 1.5 Toughening mechanisms of a multilayer coating.	29
Figure 1.6 (a) schematic of the work capability of aerosol; (b) Effect of grain quality on the maximum penetration and film roughness.	36
Figure 2.1 TEM (transmission electron microscope, JEOL FS2200, JEO USA, Inc., Peabody, MA, USA) image of FIB cross-section of TiAlCrSiYN-based coatings: (a) monolayer; (b) multilayer; (c) multilayer with interlayer. Thickness of alternating nanolayers in multilayered coatings is 20–40 nm, thickness of TiAlCrN interlayer is 100 nm.	58
Figure 2.2 X-ray diffractograms of different TiAlCrSiYN-based coating architectures with different thickness.	59
Figure 2.3 30 s impact fatigue fracture resistance data at 20 mN for the studied coatings: (a) TiAlCrSiYN monolayer, 3 $\mu\text{m}$ ; TiAlCrN/TiAlCrSiYN multilayer with TiAlCrN interlayer (b) 2 $\mu\text{m}$ , (c) 3 $\mu\text{m}$ .	62
Figure 2.4 (a) Impact fatigue fracture resistance at 25–30 mN, 300 s for the studied coatings, SEM images (b) TiAlCrSiYN monolayer, 3 $\mu\text{m}$ ; (c) TiAlCrN/TiAlCrSiYN multilayer, 2 $\mu\text{m}$ and multilayer with TiAlCrN interlayer (d) 2 $\mu\text{m}$ , (e) 3 $\mu\text{m}$ .	63
Figure 2.5 SEM images of a micro-scratch test on the 3 $\mu\text{m}$ multilayer with interlayer, with higher magnification images of the deformation at the (a) $L_{c1}$ and (c) $L_{c2}$ failures.	65
Figure 2.6 FIB cross-section of multilayer TiAlCrSiYN/TiAlCrN coating on the cutting edge.	66
Figure 2.7 Tool-life data of the studied coatings vs. length of cut (m): (a) flank wear; (b) rake wear; (c) chipping intensity; (d) average cutting forces.	68
Figure 2.8 XPS (X-ray photoelectron spectroscopy, Physical Electronics (PHI) Quantera II spectrometer, Physical Electronics, Inc, Chanhassen, MN, USA) data for tribo-films formed on the worn surface of TiAlCrSiYN/TiAlCrN multilayer with interlayer coatings of different thickness (of 2 and 3 $\mu\text{m}$ ) during running-in stage (after machining of 30 m).	69

Figure 3.1 Comparison of micro-mechanical properties of a TiAlCrSiYN/TiAlCrN multilayer coating with a TiAlCrN interlayer [23].	77
Figure 3.2 Schematic diagram of interlayer thickness effect on the coating substrate adhesion (a), and on the entire coating structure shear strength in a reference plane (b,c), with the same roughness of cemented carbide substrate [22]; $t_i$ and $t_c$ represent interlayer and coating thicknesses respectively.	78
Figure 3.3 (a) Microstructure with back-scattered electron (BSE) at 12,000x magnification; (b) surface profile ( $Rt$ and $Ra$ ) at a roughness sampling length of 250 $\mu\text{m}$ and average WC grain diameter $d_g$ of the tool substrate; (c) surface profile of the substrate.	80
Figure 3.4 SEM images of the focused ion beam (FIB) cross-section showing (a) alternating nano-layers, the interlayer in the studied multilayer coatings, and the variation of interlayer thickness (b) ( $100 \pm 30$ nm), (c) ( $300 \pm 30$ nm), and (d) ( $500 \pm 30$ nm).	84
Figure 3.5 X-ray diffraction patterns of TiAlCrSiYN-based coatings with different interlayer thickness from 100 to 500 nm. Mark C represents the cubic (B1) phase.	85
Figure 3.6 (a) Depth dependent hardness variation at a load range of 5–100 mN; (b) mechanical properties of the studied coatings obtained through nano-indentation tests (elasticity obtained by taking the Poisson's ratio of all coatings to be 0.25).	87
Figure 3.7 Comparison of (a) critical load for crack initiation in coating, $L_{c1}$ and (b) critical load for coating failure, $L_{c2}$ due to the variation of interlayer thickness within the multilayer coatings.	89
Figure 3.8 (a–c) Microscopic images of the ramped load scratch test track showing the cohesive (a) and adhesive (c) failure within the studied coating (same failure mechanism for all the studied coatings).	90
Figure 3.9 (a–d) Evolution of penetration depth at different passes during repetitive wear test at 1.5 N.	91
Figure 3.10 Microscopic images of the wear track after 15th pass at a repetitive load of 1.5 N, for coatings with interlayer thickness (a) 100 nm, (b) 300 nm, and (c) 500 nm.	92
Figure 3.11 Nano-impact testing, (a) probability distribution vs final penetration depth; (b) penetration depth at a load of 25 mN; SEM image of the impact site for the coating with (c) 100 nm, (d) 300 nm, and (e) 500 nm interlayer.	94
Figure 3.12 Tool-life data of the studied coatings vs. machining length (m): (a) flank wear; (b) rake wear; (c) chipping intensity; (d) resultant cutting forces.	97
Figure 4.1 SEM image and corresponding point EDS on the cutting edges for variation of WPC pressure of (a, d) 0.2 MPa; (b, e) 0.3 MPa; (c, f) 0.4 MPa.	113
Figure 4.2 SEM image of the cutting edges for variation of WPC time of (a) 2 s; (b) 4 s; (c) 8 s.	113

Figure 4.3 Cutting edge radius for (a) WPC process pressure variation for a process time of 4 s; (b) WPC process time variation for a process pressure of 0.2 MPa.....	114
Figure 4.4 Depth dependent hardness variation at a load range of 5–100 mN (a) WPC process pressure variation for a process time of 4 s; (b) WPC process time variation for a process pressure of 0.2 MPa. ....	115
Figure 4.5 Depth dependent value of (a) $H^3/E^2$ and (b) $H/E$ ratio for WPC process pressure variation at a process time of 4 s. ( $E \sim 500$ GPa).....	116
Figure 4.6 (a) load-depth penetration curve; (b) Representative stress vs strain , for as deposited coating and treated coating at a pressure of 0.4 MPa for 4 s; Comparison of yield stress for (c) WPC process pressure variation s; (d) WPC process time variation. ....	119
Figure 4.7 Nano-impact testing, (a) final depth after 300 s of impacting ; (b) (final-initial); (b inset) first 50 s depth of penetration for WPC process pressure variation, (c) final depth after 300 s of impacting; (d) (final-initial); (d inset) first 50 s depth of penetration for WPC process time variation at a load of 15 mN. ....	121
Figure 4.8 Comparison of (a) critical load for crack initiation , $Lc_1$ and (b) critical load for coating failure, $Lc_2$ (c) wear test data for the variation of WPC pressure.....	122
Figure 4.9 SEM images of the ramped load scratch test track showing the (a) cohesive; (b) semicircular cracks and (c) adhesive failure (same failure mechanism for all the studied coatings-including the as deposited one); EDS of the delaminated part of the scratch track (d, e, f) Ti- Ka 1, (g, h, i) W La 1 for the variation of WPC process pressure. ....	125
Figure 4.10 Tool-life data of the studied coatings vs. machining length (m); (a,b) flank and rake chipping intensity with WPC pressure variation; (c,d) flank and rake chipping intensity with WPC time variation. ....	126
Figure 4.11 Wear evolution vs machining length (m); (a, c) flank and rake face for as deposited coating; (b, d) flank and rake face for treated coating at 0.2 MPa and 4 s. ....	128

## **LAY ABSTRACT**

Over the last 50 years, PVD (physical vapor deposition) coatings have played an increasingly important role in manufacturing where tool cost takes up 3% of the total expenses of the production process. Optimization of these coatings can expedite production wherever machining is conducted under extreme cutting conditions and consequent high material removal rates. These considerations assert significant importance on conducting research on PVD coating development specifically for milling of H13 tool steel, the material widely used in the mold and die industry. This research work seeks to enhance the micro-mechanical and adhesion properties of PVD coatings through architectural design and careful process development while relating desired properties to the high-performance milling of H13 tool steel.

## ABSTRACT

Dry High speed and wet milling strategies have both been used to machine hardened die and mold H13 tool steel (HRC 45-58). The TiAlCrSiYN-based family of PVD coatings prepared with various architectures (mono-, multi- and multilayer with an TiAlCrN interlayer) were studied to evaluate the coating micro-mechanical properties that affect tool life during dry high-speed milling of H13 tool steel. A systematic design of varying TiAlCrN interlayer thickness within a multilayer coating structure was developed and its influence on coating properties and cutting performance was investigated. A comprehensive characterization of the coatings was performed using a transmission electron microscope (TEM), focused ion beam (FIB), scanning electron microscope (SEM), X-ray powder diffraction (XRD), room-temperature nanoindentation, a nano-impact, ramped load scratch and a repetitive load wear test. The incorporation of an interlayer into the multilayer coating structure was found to increase the crack propagation resistance (CPRs) to 5.8 compared to 1.9 for the multilayer and 1.6 for the monolayer coatings, which resulted in a 60% tool life increase. The wear test at a load of 1.5 N showed that although the 500nm interlayer exhibited the best coating adhesion, a decline in the  $H^3/E^2$  ratio was observed to worsen the machining performance. An approximate 40% increase in the tool life was achieved with the 300 nm interlayer by obtaining a balance between mechanical and adhesion properties. To investigate the tool performance during the wet milling of hardened tool steels, the (AlCrN-TiAlN) bi-layer PVD coating was post-treated by WPC (Wide Peening Cleaning) at various pressures and times. Fatigue resistance of the coating

following the application of post treatment was observed to improve as the micro-mechanical characteristics (such as  $H^3/E^2$  ratio, yield stress) were increased. A deterioration in the coating's adhesion with increasing WPC pressure was also observed as measured by wear test applying a load of 1 N. Through experimentation a balance between fatigue resistance and adhesion was found with tool life being improved by 35% at a WPC applied pressure of 0.2 MPa.

**keywords:** milling; multilayer; interlayer; WPC treatment, PVD coating, micro-mechanical property assessment.



## **Chapter 1. INTRODUCTION**

### **1.1 Background**

Improvement of tool life and machining productivity through the application of Physical Vapor Deposition (PVD) coatings on cutting tools has been a major research interest over the past several years. Several promising developments were made in this field during the machining of H13 tool steel in its hardened state. However, excessive tool wear due to poor low cycle fatigue performance presents a major challenge during an intermittent cutting process such as milling. This is more crucial in wet H13 milling where thermal fatigue is a limiting factor of tool life. Furthermore, extreme cutting conditions during milling cause high stress and temperature in the cutting zone. The primary motivation of this study is to perform an in-depth investigation on the micro-mechanical and adhesion properties of PVD coatings to optimize their design for both wet and dry milling of H13 tool steel.

#### **1.1.1 Literature Review**

##### ***Tool Wear and Tool Wear Mechanisms***

Metal cutting is a process in which a sharp tool moves relative to a work piece and shears away thin layers of bulk material, generating a new surface (Figure 1.1a). The sheared material comes in the form of a ‘chip’ that flows or effectively slides over the surface of the tool and eventually separates. Thus, the thermal, mechanical and chemical interactions between the cutting tool, work piece and the environment lead to various forms of tool wear such as flank wear, crater wear, notch wear, tool edge chipping and build up edge (BUE)

formation. Consequently, the geometry and surface topography of the cutting tool change near the cutting-edge. The underlying wear mechanisms— such as adhesion, abrasion, oxidation, and diffusion responsible for these tool wear patterns [2] generally act in parallel, although one is usually predominant over the others. The decisive factors in determining which of these mechanisms predominate during a wear process are the type of interaction between the tool and the workpiece (continuous, intermittent), cutting tools (material, geometry), cutting parameters (cutting speed, feed and depth of cut), the workpiece material involved and the external environment (wet and dry condition) [3] as illustrated in Figure 1.1 (b, c).

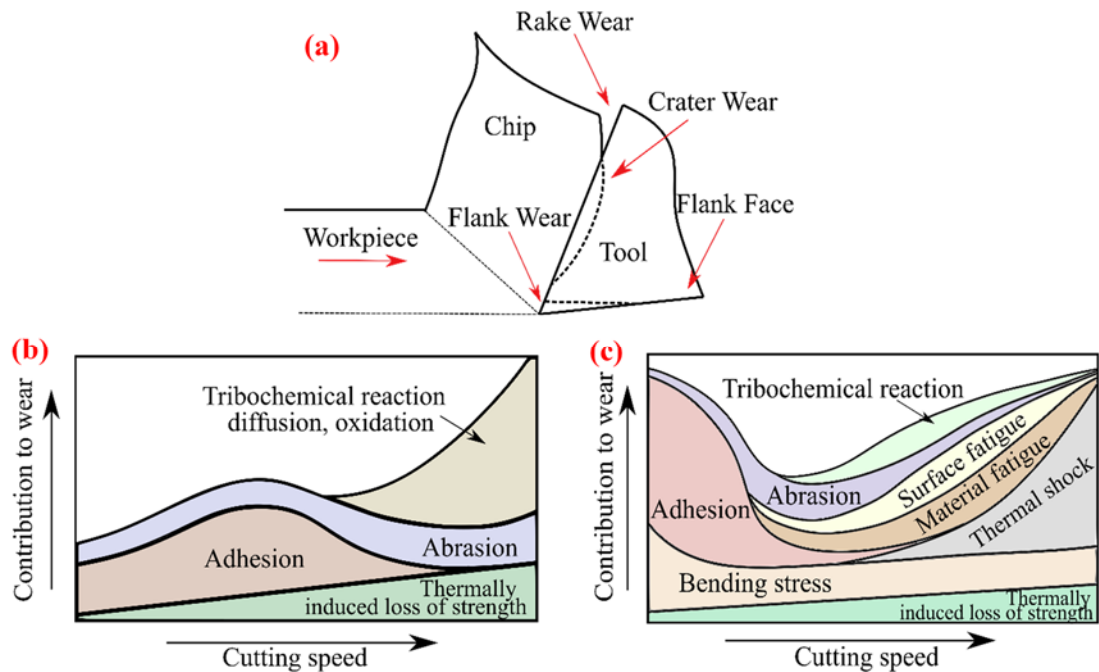


Figure 1.1 (a) Tool wear schematic; Failure mechanisms in (b) continuous cutting and (c) interrupted cutting adapted from [4].

The term ‘Tool life’ refers to the total machining length and/or time before a cutting tool needs to be replaced due to increased power consumption and/or degradation of surface quality caused by progressive tool wear. It is generally measured in terms of flank wear width. According to the ISO 8688-2 standard, a flank wear of 300  $\mu\text{m}$  is considered to be the end of the functional life of a cutting tool. However, process conditions, desired part quality and the pattern of tool wear each play an important role in determining the tool life criteria in actual practice.

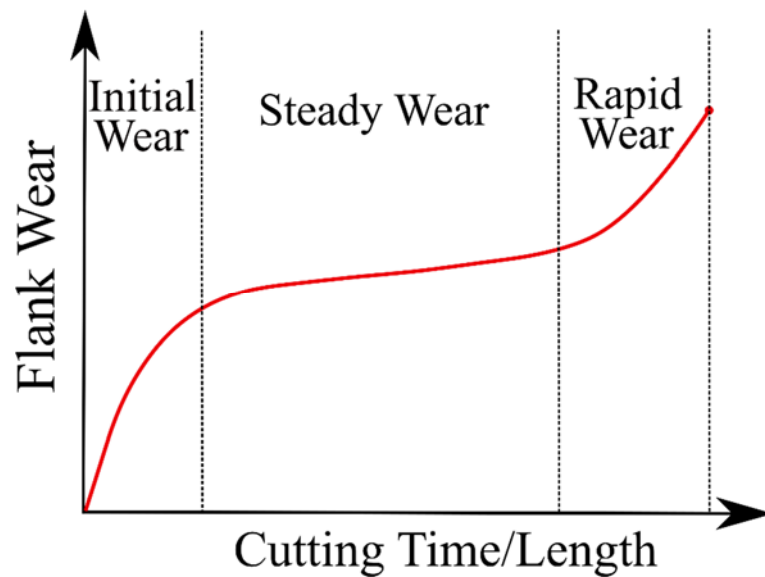


Figure 1.2 Typical tool life curve versus cutting time/length.

The characteristic tool wear versus machining length curve displayed in Figure 1.2 can be divided into three stages: the running-in stage, characterized by the high wear rate and adaptation of the tool/coating system to the cutting process followed by the stable wear stage and completed by the catastrophic wear stage, during which the tool wear rapidly intensifies until the tool reaches failure [5]. A potential tool material's ability to enhance

the machining performance under specific tool wear patterns and application is evaluated by repeated cutting trials.

### ***Milling of H13 Tool Steel***

H13, hot work tool steels (45–58 HRC) are extensively used for pressure die casting, extrusion, hot forging and extrusion mandrels due to the combined properties of high hot-hardness and toughness [6]. They also possess high-temperature strength and wear resistance [7]. The nominal chemical composition (wt%) and mechanical (HRC range 45-58) as well as thermal properties of H13 tool steel are presented in Table 1.1 and Table 1.2 respectively .

Mold and die machining traditionally performed by electrical discharge machining (EDM) and grinding processes, results in a relatively low material removal rate (EDM) as well as damaged surface layers [8] for both methods if the processes are not carefully controlled. Recent practice involves direct milling of H13 in its hardened state as a competitive finish and semi-finish process [9-11]. Recent developments in tool materials and coatings have also been applied to diminish part distortion generated during heat treatment [12]. Milling of H13 tool steel at a lower cutting speed is usually carried out under wet condition but in recent years high speed machining (HSM) [13, 14] and high feed machining have become more common. Dewes et al. [13] stated that the advantages of HSM such as high material removal rate, low cutting forces, minimum workpiece distortion, better surface finish, and reduced burr formation, have significant potential to improve productivity.

Table 1.1 Nominal chemical composition of H13 tool steel (wt%) [15].

<b>C</b>	<b>Mn</b>	<b>Si</b>	<b>Cr</b>	<b>Mo</b>	<b>V</b>	<b>Ni</b>	<b>Fe</b>
0.32-0.45	0.02-0.05	0.08-1.2	4.75-5.50	1.10-1.75	0.80-1.2	0-0.30	Bal.

Table 1.2 Mechanical and thermal properties of H13 tool steel ( 45-58 HRC) [16].

<b>Yield Strength (MPa)</b>	<b>Tensile Strength (MPa)</b>	<b>Elastic Modulus (GPa)</b>	<b>Thermal Conductivity (W/mK)</b>	<b>RT Density (Kg/m<sup>3</sup>)</b>	<b>Melting Point (° C)</b>
1280-1520	1420-1820	210	25	7800	1427

Conventionally, high speed milling is conducted in the dry cutting condition [15]. This is done to avoid the high temperature gradient present during wet milling [17] at a high speed as well as to alleviate environmental effects. However, the elevated temperature in the cutting zone [18] during the high-performance milling operation of hardened tool steel generates higher mechanical and thermal surges on the cutting tool edge, which significantly distinguish milling from single-point machining [17]. This in turn strongly deteriorates the mechanical properties of the cutting tool. Thus, high performance milling of H13 tool steel dies and moulds in their hardened state presents a challenge.

The aforementioned factors contribute to the different tool wear patterns listed in Table 1.3. According to a literature survey, flank wear, crater wear and chipping are the dominant wear modes that are highly dependent on the cutting parameters. Adhesion and BUE formation were also observed at lower cutting speeds and feeds [19]. Moreover, Gu et al.[17] previously demonstrated that mechanical impacts on the cutting tool increase

when a dry cutting condition is used as well as when cutting speed and feed rate increase. As a result, micro-cracks develop on the flank face of the cutting tool, parallel to the cutting edge. Furthermore, the cutting edge undergoes micro chipping due to the high mechanical load present at a feed rate of 0.315 mm/tooth or above. Similarly, in the presence of lubricant, the flank face of the tool develops thermal cracks due to the thermal surges which can also lead to chipping at a cutting speed range of 120-240 m/min. It is worth mentioning that the machinability of H13 tool steel is also affected by its composition and hardness [20].

Table 1.3 Wear patterns observed in literature for milling of H13 tool steel

Flank wear ● Crater wear ● Adhesion ● Chipping ● Thermal cracks ■ BUE or BUL formation ■ Fracture ■		
Author	Process Parameter	Tool Material/ Coating
Beake et al. (2015)[1]	DoC: 0.3 mm	
	Feed: 0.5 mm/tooth Speed: 160 m/min Workpiece hardness: (46-48) HRC	WC-Co/PVD AlTiN ●●● WC-Co/PVD AlCrN ●●● WC-Co/PVD AlCrN/TiAlN ●●●●
<b>Wet condition</b>		
Fox et al. (2014)[21]	DoC: 5 mm	
	Feed: 0.06 mm/tooth Speed: 500 m/min Workpiece hardness: (55-57) HRC	WC-Co/ PVD TiAlCrSiYN/TiAlCrN ●●● WC-Co/PVD TiAlCrSiYN ●●●■
<b>Dry condition</b>		
Cui et al. (2013)[15]	DoC: 0.3 mm	
	Feed: 0.1 mm/tooth Speed: 200-1200 m/min Workpiece hardness: (46-47) HRC	CBN (Cubic Boron Nitride) ●●●■
<b>Dry condition</b>		

Ning et al. (2008)[18]	DoC: 5 mm Feed: 0.06 mm/tooth Speed: 300 m/min Workpiece hardness: (55-57) HRC <b>Dry condition</b>	WC-Co /PVD nano-multilayered TiAlCrN/NbN ●●●● WC-Co/PVD TiAlCrN ●●●●
Yamamoto et al. (2003)[22]	DoC: 5 mm Feed: 0.06 mm/tooth Speed: 220 m/min Workpiece hardness: (48-56) HRC <b>Dry condition</b>	WC-Co/PVD TiCrAlN ● WC-Co/PVD TiAlN ●
Toh (2003)[23]	DoC: 10, 15 and 20 mm Feed: 0.06 mm/tooth Speed: 314 m/min Workpiece hardness: 52 HRC <b>Wet and Dry condition</b>	WC-Co/PVD AlTiN ●●
Braghini et al. (2001)[24]	DoC: 1 mm Feed: 0.02 mm/rev Speed: 60-100 m/min Workpiece hardness: (48-56) HRC <b>Dry condition</b>	PCBN (Polycrystalline Cubic Boron Nitride) ●●● WC-Co uncoated ●●
Elbestawi et al. (1997)[25]	DoC: 0.625 up to 2 mm Feed: 0.0254 to 0.1 mm/tooth Speed: 220 to 1320 m/min Workpiece hardness: up to 57 HRC <b>Wet and Dry condition</b>	PCBN (Polycrystalline Cubic Boron Nitride) ●●●●■

### ***PVD Tool Coating***

Different tool material classes are actively used in modern machining, such as high-speed steel (HSS), cemented carbide, ceramic, cermet, CBN, PCBN and diamond. Hardened steels are commonly machined with PCBN and ceramic tools. However, coated carbide tools are often used in hardened steel machining as an economical alternative to costly PCBN and ceramic tools due to the recent developments in cemented carbide grades, coating materials and coating deposition technologies [26]. Coating deposited on different

tool substrate materials by Chemical Vapor Deposition (CVD), Physical Vapor Deposition (PVD), and thermal spray techniques have been developed to enhance tool performance over the past 50 years. PVD coatings are more preferable for solid carbide milling tools for their ability to control thickness on the edges ensuring a sharper cutting edge [27].

Klocke et al. [28] mentioned two major ways (direct and indirect) by which a coating influences tool wear, as shown in Figure 1.3. Wear mechanisms such as adhesion, abrasion, tribo-oxidation and diffusion were considered as surface effects and fatigue as a typical volume effect that leads to the loss of tool material due to fracture and the formation of cracks. Whereas coating technology directly affects these wear mechanisms, variation of contact conditions through altering the generation of friction and heat is an indirect way of influencing wear.

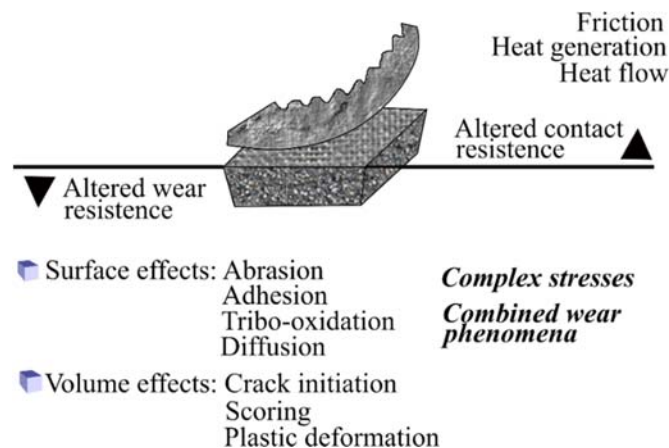


Figure 1.3 Influence of coatings on wear mechanisms and contact conditions adapted from [28].

The effects of the coating substrate system on various aspects of machining are shown in Figure 1.4. Bouzakis et al. [29] demonstrated with FEM that, the maximum



equivalent stress in 4 $\mu$ m TiAlN coating deposited on HW-K05/K20 indexable inserts reaches 5.6 GPa on the cutting-edge during dry milling (cutting speed,  $v_c=200$ m/min, axial and radial depth of cut= 3mm) of hardened steel . In comparison, the coating yield stress on the cutting edge of the flank surface is 5.9 GPa. The maximum equivalent stress (3 GPa) is less in the coated tool substrate than in that of the uncoated tool (4.9 GPa). Furthermore, the maximum temperature of the coated insert reaches 266°C at a tool-chip contact time of 4.8 ms, compared with 652°C in the uncoated tool during the same tool-chip contact time.

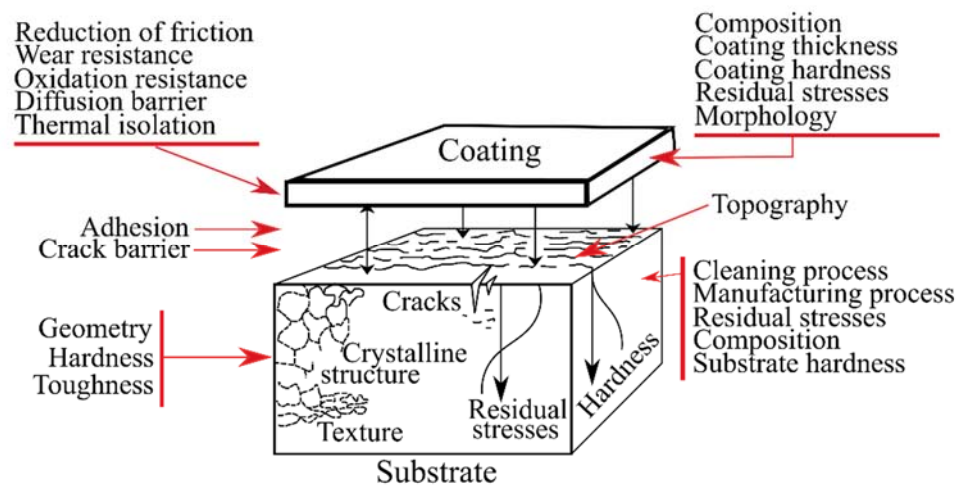


Figure 1.4 Coating-substrate system properties adapted from [30].

The ability of the coated tool surface to generate protective tribo-films under aggressive friction condition between the tool and chip, is known as ‘self-organization’ [31]. The formation of a protective film (such as  $Al_2O_3$ ) on the surface of TiAlN coatings is a well-known example [28]. According to Fox-Rabinovich and Totten [31], mechanical energy is transformed into heat during friction accumulating into friction surfaces. This ‘activation’ stage may be followed by a ‘passivation’ stage during which excessive free

energy is reduced by the formation of protective tribo-films through reactions with the environment. Such a spontaneous formation of dissipative structures only occurs in conditions far from equilibrium (i.e. friction). The transition occurs from the running-in to the stable wear stage during machining when the optimal frictional surface conditions are reached. This reduces the friction coefficient and the wear rate.

Loffler [4] presented a systematic approach for developing coating technology. He divided the design process into three stages:

- 1) Coating development (analysis of the coating's composition, microstructure and properties)
- 2) Process development (evaluating the effect of process parameters on coating properties)
- 3) Optimization for an application (characterization of the application, evaluation of the restrictions, selection of the coating and substrate).

#### *Coating Development: Effect of PVD Coating Composition*

Alloying elements that permeate into the matrix lattice create a solid solution in the coating layer during the deposition process. This in turn, produces multi component coatings such as binary, ternary and quaternary coatings. The cutting performance of the first generation of successful binary PVD coatings (TiN and CrN) was improved by the inclusion of Al to form ternary TiAlN and CrAlN coatings [32]. Previously Ding et al. [33] characterized the influence of the Al/Cr atomic ratio (between 0 and 0.6) on the mechanical properties of CrAlN coatings. Coating hardness first increases with the inclusion of Al, but reduces as more Al is added. This decrease of hardness can be attributed to the formation of a hcp-

AlN phase, which has a lower strength than the fcc-AlN phase. A similar pattern was also observed in the TiAlN coating.

Studies of coatings with quaternary or even more components were limited to TiAlN based coatings with additional elements such as V, Y, Si, Cr, W, Zr. High temperature oxidation resistance was noticeably enhanced for the TiAlYN [34] and TiAlCrN [35] coatings. Yamamoto et al. [36] investigated the structural and mechanical characteristics of a TiCrAlN-based coating following the addition of Si and Y (at a fixed Si + Y ratio of 0.05) and reported an improvement in coating properties which included increased chemical stability, reduced adhering of the workpiece material to the tool surface and increased oxidation resistance. The addition of Si provides benefits in terms of grain refinement and the addition of Y obstructs grain coarsening at the elevated temperatures associated with HSM.

Moreover, super hard nanocomposite coatings can be an alternative to traditional transitional metal nitrides used in cutting tools where nc-TiN/a-Si<sub>3</sub>N<sub>4</sub> nanocomposites exhibit high oxidation resistance up to temperatures greater than 800 °C [37]. Recent research has also been conducted on AlTiN/SiN<sub>x</sub> nanocomposites for dry machining processes involving down milling [38].

#### *Process Development: Effect of PVD Coating Deposition Parameter*

One of the most influential process parameters during PVD coating deposition is the substrate bias voltage, which determines the energy of ion bombardment during the process. A higher bombardment energy during high negative bias voltage increases nucleation,

thereby producing a finer structure. Consequently, the increase in bias voltage results in an increase of coating hardness and elastic modulus [39, 40]. Further, as the negative bias voltage is raised, compressive residual stress increases to a certain point due to the reopening of the already deposited coating by high energy ions. However, this increase is disrupted by the activation of diffusion with high ion bombardment [41, 42]. Multiple factors affect the relation between substrate bias and coating adhesion [40]. Moreover, bias voltage can also affect the preferential orientation of the coating [41].

During a reaction deposition, nitrogen can be introduced into the chamber in the form of  $N_2$  gas to create compounds such as TiN and TiAlN. It was previously observed [43, 44] that an increase in the partial pressure of the reactive gas results in a higher deposition rate up to a certain point which is defined by target poisoning which takes place at a higher value.

#### *Optimization for Application: Effect of PVD Coating Architecture*

##### **Multilayer Structure**

The development of coating architecture is obtained through the transition from monolayer to multilayer and then an interlayer introduced into the structure of a multilayer coating. High performance milling (HSM and high feed) induces high mechanical and thermal loads on the cutting edge as well as high temperature in the cutting zone. The coatings need to possess multifunctionality under these conditions, which is a role best fulfilled by multilayer coatings [45]. These coatings are prepared at an atomic scale and consist of multiple layers up to several nanometers thick. A multilayer coating is considered to be an

effective way to improve toughness of a ceramic coatings [46]. Holleck [47] stated that the main mechanisms by which the multilayer strengthens a coating include: crack deflection at the interface between the sublayers, interface delamination, ductile interlayer ligament bridging, and blunting of crack tips due to nanoplasticity as shown in Figure 1.5.

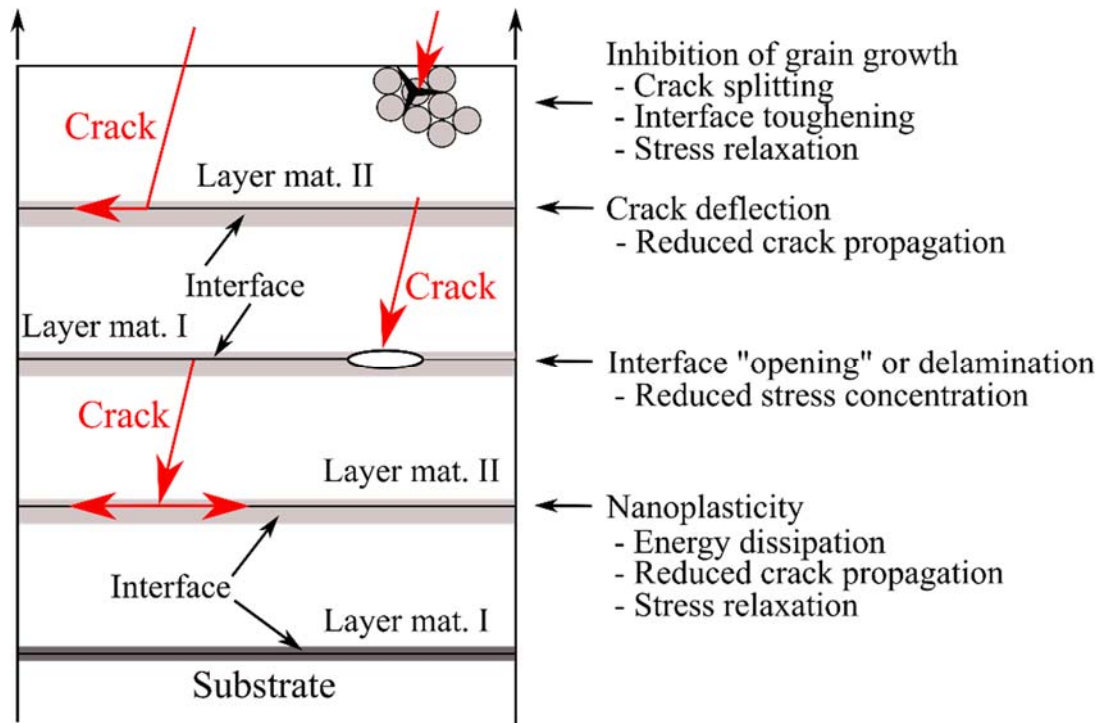


Figure 1.5 Toughening mechanisms of a multilayer coating.

Suresha et al. [48] studied the cracking patterns in monolayer TiN and multilayered TiN/AlTiN at an indentation load of 20 N. The experimental findings showed that multilayering reduces indentation-induced cracking (edge and shear cracking) compared to the monolayer TiN coating.

Furthermore, a large amount of accumulated residual stress may lead to the detachment of layers from the multilayer coating system. It was previously observed that

substrate and coating residual stresses developed during machining processes that make use of PVD coated cemented carbide tools, have a dominant effect on coated tool life [49]. Bielawski [50] evaluated the effect of coating thickness on the magnitude of residual stress using a TiN/Si coating whose thickness varied from 1 to 12  $\mu\text{m}$ . The results of this study demonstrated that, the level of stress in the coating had changed as the coating thickness was increased from  $\sim 100$  MPa (compressive) to  $\sim 75$  MPa (tensile).

In one of the most recent developments of a multilayer coating for high speed milling operations, Fox-Rabinovich et al. [51] evaluated the performance of two nanomultilayered TiAlCrSiYN/TiAlCrN coatings with respective 55% and 60% Al content while machining a Ni-based super alloy. The coating with the higher Al content had better scratch propagation resistance than both the one with the lesser Al content and the monolayered benchmark sample.

### **Coating with Interlayer**

One of the major challenges of coating deposition is adhesion of the coating to the substrate. In recent years, this issue has been addressed by developing a coating architecture with the incorporation of an interlayer as shown in Table 1.4.

Studies on this subject conclude that this improves coating adhesion to the substrate. However, the selection of an appropriate interlayer [52] and the optimization of its thickness in relation to the substrate roughness [53] is needed to ensure sufficient coating adhesion.

Table 1.4 Summary of research on the coating interlayer.

Author	Coating Material	Process Studied	Important observations
Beake et al. (2015) [1]	Coating <b>AlCrN</b> Interlayer: <b>TiAlN</b>	Wet milling of H13 Cutting speed: 160 m/min DOC: 0.3 mm	<ul style="list-style-type: none"> <li>• Improved fatigue resistance.</li> <li>• Higher load support as indicated by a higher <math>H^3/E^2</math> ratio.</li> <li>• Cutting edge chipping due to thermal fatigue and crater wear with buildup edge formation.</li> <li>• Superior coating integrity as indicated by the micro-scratch test.</li> </ul>
Bouzakis et al. (2010) [52]	Coating <b>TiAlN</b> Interlayer <b>W/WN,</b> <b>Ti/TiN, Cr/CrN</b>	Dry milling of 42CrMo4 Cutting speed: 200 m/min DOC: 3mm	<ul style="list-style-type: none"> <li>• Cr-adhesive nanolayer exhibits improved cutting performance compared to that of the W or Ti adhesive interlayers.</li> <li>• Negative effect of Ti and W interlayers on coating adhesion.</li> </ul>
Bouzakis et al. (2010) [53]	Coating <b>TiAlN</b> Interlayer <b>Cr/CrN</b>	Dry milling of 42CrMo4 QT Cutting speed: 200 m/min DOC: 3mm	<ul style="list-style-type: none"> <li>• Coating adhesion and the ensuing cutting performance can be improved if the graded Cr/CrN interlayer thickness is adapted to the substrate roughness.</li> </ul>
Hong et al. (2011) [54]	Coating: <b>CrAlSiN</b> Interlayer: <b>Cr</b>		<ul style="list-style-type: none"> <li>• Lower hardness of the coating system with the thicker Cr interlayer.</li> <li>• Improved adhesion due to the reduction in shear stress at the coating and substrate interface.</li> </ul>
Kloche et al. (2011) [55]	Coating <b>Pt-Ir</b> Interlayer <b>Ni or Cr</b>	glass molding tools	<ul style="list-style-type: none"> <li>• Cr and Ni interlayers improved the coating adhesion as well as strength of the entire structure.</li> <li>• The enhancement is more significant in Cr interlayer.</li> <li>• The effectiveness of the adhesive interlayers depends on the thickness adjusted in terms of the substrate roughness <math>R_t</math>.</li> </ul>
Shahsavari et al. (2016) [56]	Coating <b>DLC</b> Interlayer	Tribological Service	<ul style="list-style-type: none"> <li>• Good adhesion for a Cr interlayer thickness of up to 10 and 20 nm having</li> </ul>

	<b>Cr</b>		<p>a hardness value of 17 GPa and 24 GPa, respectively.</p> <ul style="list-style-type: none"> <li>• The mechanism of mechanical interlocking between Cr interlayer and DLC coating improves adhesion.</li> </ul>
Cemin et al. (2015) [57]	Coating <b>DLC</b> Interlayer <b>a-SiC<sub>x</sub>:H</b>	Tribological Service	<ul style="list-style-type: none"> <li>• Improved adhesion of a-C:H films after the incorporation of a-SiC<sub>x</sub>:H interlayers deposited under optimized experimental conditions enhances the lifespan of the coated components.</li> </ul>

### *Mechanical Surface Treatment of PVD coatings*

Lower compressive residual stress or tensile stress in the coating layer could lead to the formation of surface cracks and delamination of a coating from the substrate [58]. More importantly this has a detrimental effect on the fatigue life of the coated cutting tools during milling. However, compressive residual stress induced into the coating can be used to strengthen it, because more energy would then be needed to initiate a crack. At the present, the mechanical surface treatment of a coating is one of many ways to induce surface compressive residual stress into the coating system.

Table 1.5 outlines recent developments in mechanical surface treatments of coated tools used for machining. Most of these research works focused on the micro-blasting of coated tools for milling operations. This past research confirms that mechanical surface treatment can enhance tool life during milling where low cycle fatigue resistance of tools plays an important role. Furthermore, an elaborate analysis of various process parameters associated with micro-blasting exhibited the influence of the type and size of shot particles, the medium of shot particle delivery, process pressure and process duration upon surface



integrity, microstructure, micro-mechanical properties and overall cutting performance of coated tools.

Table 1.5 Literature on currently available techniques for the post-treatment of coated tools.

<b>Author</b>	<b>Technique (Coating)</b>	<b>Application</b>	<b>Significant observations</b>
Jacob et al. (2017) [59]	micro-blasting (AlTiN)	Dry turning martensitic stainless steel.	<p><b>Change in AlTiN coating properties</b></p> <ul style="list-style-type: none"> <li>• Coating hardness.</li> <li>• Grain refinement.</li> <li>• Roughness increase.</li> </ul> <p><b>Tool wear</b></p> <ul style="list-style-type: none"> <li>• Tool life was prolonged at a lower cutting speed of 120m/min. A further increase in cutting speed resulted in a similar tool life with no change in wear pattern (coating delamination, built-up edge and notch wear) compare to the untreated one at all speeds.</li> </ul>
Abusuilik (2015) [60]	Micro-blasting (TiAlN)	Drilling AISI 304	<p><b>Change in TiAlN coating properties</b></p> <ul style="list-style-type: none"> <li>• Decreased amount of material transfer and wear volume on the counter surface.</li> </ul> <p><b>Tool wear</b></p> <ul style="list-style-type: none"> <li>• Stabilization of the spindle torque and drilling regularity.</li> <li>• Short and uniform chips were obtained from the drill bit (Compared to long chips in untreated tools)</li> </ul>
Bouzakis et al. (2011) [61]	Dry Micro-blasting (TiAlN)	Milling of AISI 4140	<p>Micro-blasting with particle variation (sharp-edged Al<sub>2</sub>O<sub>3</sub> and smooth spherical ZrO<sub>2</sub> particles)</p> <p><b>Coating properties</b></p> <ul style="list-style-type: none"> <li>• Abrasion during micro-blasting is less intense and coating deformation is higher for spherical particles.</li> <li>• Substrate exposure occurs at a lower pressure in spherical particles.</li> </ul>

---

			<ul style="list-style-type: none"> <li>• Roughness <math>R_t</math> grows when sharp-edged grains are used.</li> <li>• Greater hardness improvement upon use of spherical particles under the same conditions.</li> <li>• As pressure grows, the cutting-edge radius is more significantly enlarged with the use of sharp-edged particles.</li> </ul> <p><b>Tool wear</b></p> <ul style="list-style-type: none"> <li>• Cutting performance deteriorates more rapidly at micro-blasting pressure over 0.4MPa when spherical particles are used.</li> </ul>
Bouzakis et al. (2011) [62]	Wet Micro-blasting (TiAlN)	Milling of AISI 4140 (42 Cr Mo 4 QT)	<p>Micro-blasting with particle size variation (10 <math>\mu\text{m}</math> and 100 <math>\mu\text{m}</math> sharp-edged <math>\text{Al}_2\text{O}_3</math>)</p> <p><b>Coating properties</b></p> <ul style="list-style-type: none"> <li>• Intensive removal of coating material via micro-chippings by fine particles over the same treatment duration.</li> <li>• Intensive deterioration of surface roughness with the use of fine particles.</li> <li>• Reduction of nano hardness with the use of fine particles under the same conditions.</li> <li>• Yield stress growth vs. pressure is greater when coarse particles are applied under the same conditions.</li> <li>• Cutting edge radius is more enlarged when coarse particles are used.</li> </ul> <p><b>Tool wear</b></p> <ul style="list-style-type: none"> <li>• Cutting performance can be reduced with the use of fine particles at a micro-blasting pressure of 0.4 MPa.</li> <li>• Risk of local substrate revelation is greater for coarse particles at micro-blasting pressures over 0.3 MPa.</li> <li>• Tool blasted by coarse particles at a low pressure of 0.2 MPa, has led to a significant tool life improvement.</li> </ul>

---

Bouzakis et al (2011) [63]	Wet and dry Micro-blasting (TiAlN)	Milling of AISI 4140 (42 Cr Mo 4 QT)	Micro-blasting under wet and dry environmental conditions. <b>Coating properties</b> <ul style="list-style-type: none"> <li>• Surface roughness increased after wet blasting process.</li> <li>• Similer nano hardness for both the wet and dry conditions.</li> <li>• Cutting edge radius becomes higher with increasing pressure in the dry condition.</li> <li>• Coating thickness is severely reduced in the dry condition with increasing particle size.</li> </ul> <b>Tool wear</b> <ul style="list-style-type: none"> <li>• A significant improvement of tool life is observed in the wet condition with increasing particle size.</li> </ul>
Bouzakis et al (2009) [64]	Dry Micro- blasting (TiAlN)	Milling of AISI 4140 (42 Cr Mo 4 QT)	Micro-blasting process pressure and duration. <b>Coating properties</b> <ul style="list-style-type: none"> <li>• Minimal coating thickness reduction on the rake face was observed at an increased pressure and time.</li> <li>• The growth in pressure and time intensifies the effect of cutting-edge geometry.</li> <li>• Coating superficial strength is enhanced by the increase of blasting pressure and duration.</li> </ul> <b>Tool wear</b> <ul style="list-style-type: none"> <li>• The micro-blasted tool at a pressure of 0.2 MPa exhibited the best cutting performance.</li> </ul>

WPC (Wide Peening Cleaning) is a shot peening process [Japan Patent No. 1594395] that provides improved control of process parameters where peening particles impact the

surface at a much higher velocity as compared to regular peening. This technique provides an alternative to other mechanical surface treatment processes for coated cutting tool.

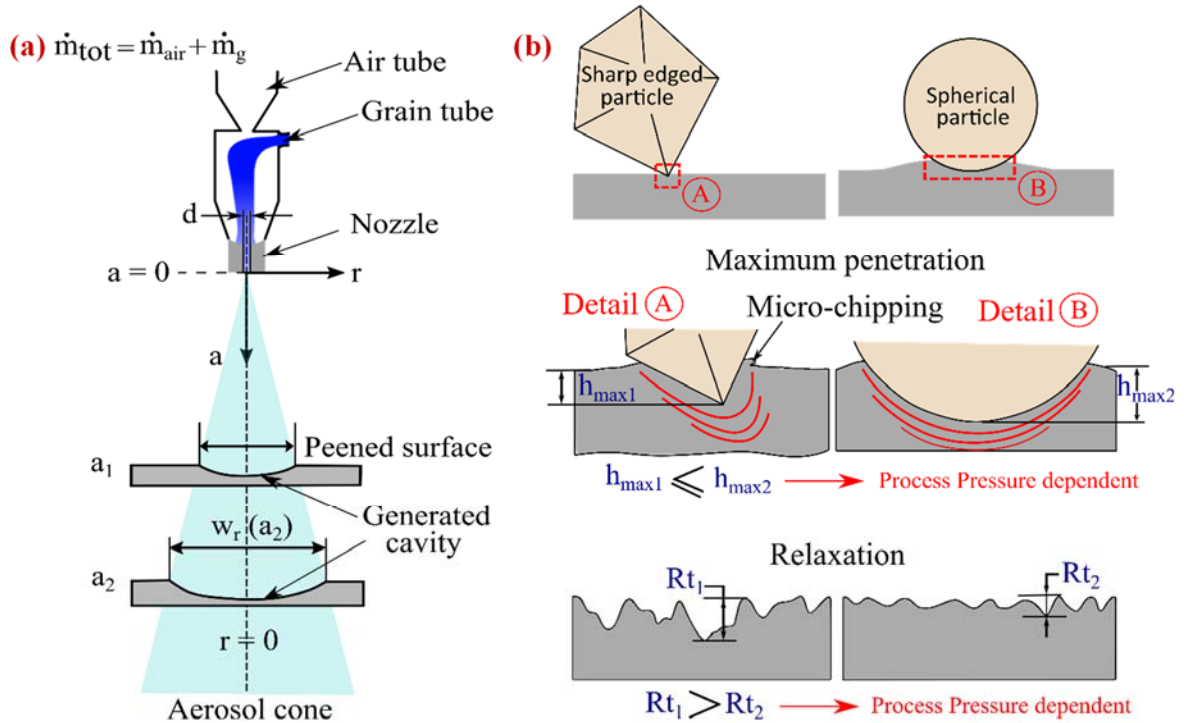


Figure 1.6 (a) schematic of the work capability of aerosol; (b) Effect of grain quality on the maximum penetration and film roughness.

Figure 1.6a depicts the relationship between different process parameters during peening. An aerosol mixture of the peened particles and the carrying fluid (in this case air) is passed through a nozzle. The work capability of the aerosol can be expressed as the degree of deformation caused by the peening particles. This work capability increases along with size, since a larger particle has a greater mass and higher kinetic energy (as long as the speed is in the same range). A higher peening pressure also increases the work capability as the peening particles accelerate along with the faster moving carrier air flow. The grain type

(density and shape) has a significant influence on the work capability as shown in Figure 1.6b. Sharp-edged particles generate more erosion than the similarly sized spherical ones when both are accelerated at the same speed. Each particle shape has a considerably different energy distribution when colliding with a peened surface. Therefore, micro-roughening caused by sharp-edged particles is always greater than that by spherical ones. Moreover, the distance (a) between the jet and the peened surface also affects surface roughness. As this distance increases, the surface roughness decreases due to the distribution of energy over a larger area. Consequently, the optimum peening distance is a function of the grain type and size. Another factor is process duration, in which smaller particles produce more impacts per pound, thereby requiring less exposure time. Conversely, a longer exposure time is required to acceptably cover the tool when soft particles are peened on a hard material than when hard ones impact a soft material. Thus, for any given set of experimental conditions such as shot type, shape, size and distance between the nozzle and the surface, the two most important variables that affect the peening process are pressure and duration of application.

### **1.1.2 Research Gaps**

The available literature provides an overview of the current state of the art developments in cutting tool PVD coatings during both wet and dry milling of H13 tool steel under extreme cutting conditions. However, the research goals of this PhD study are based on areas not covered in literature:

1. Although a large number of studies can be found concerning interlayer design in DLC coatings [56], little research has been conducted on the coatings suitable for hardened steel milling.
2. One of the most significant problems with multilayer coating architecture is that the increase in compressive residual stress deteriorates the adhesion of a coating to the substrate [51]. This can be mitigated by incorporating an interlayer within the coating structure. However, no studies were found concerning the improvement of coating adhesion through the combination of a multilayer coating with an interlayer.
3. WPC is a relatively new mechanical surface treatment technique. The few studies that deal with it are usually limited to studying the impact of peening on bulk material properties. Further investigation is required to better understand the impact of this treatment process on surfaces specifically for coating development applied to H13 milling.
4. No previous investigation was found with regards to the coating's substrate adhesive properties following a post treatment process which involved inducing compressive residual stress to strengthen the surface. Under the given circumstances, adhesion becomes a key property in predicting the performance of the post-treated coated tool.
5. The wear mechanisms and the tool wear patterns of the coating after post treatment are seldom covered in the literature. However, milling performance is strongly dependent on these two parameters.

## **1.2 Motivation and Research Objective**

### **1.2.1 Motivation**

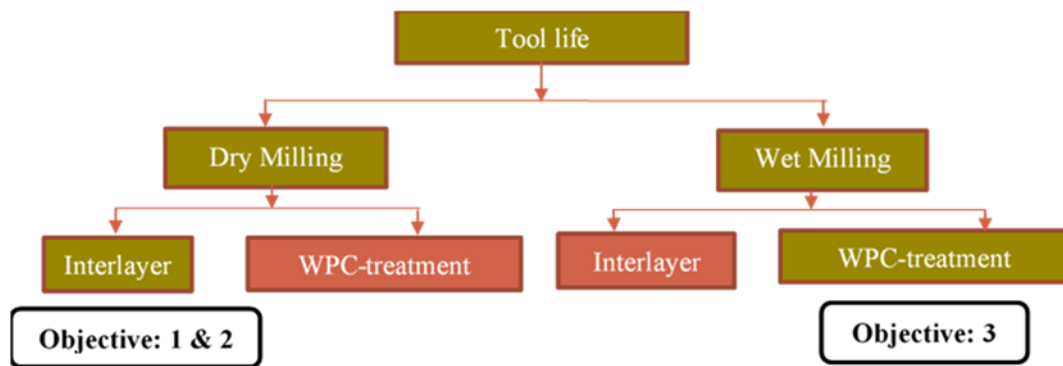
High performance (high speed and high feed) milling of hardened H13 Tool steel is used to increase material removal rate (MRR) in modern manufacturing practice. However, this milling operation is carried out under extreme cutting conditions. Moreover, the milling of hardened H13 poses its own challenges. Since the tool wear pattern rapidly progresses from flank and crater wear to chipping. Thus, it is of paramount importance to enhance the low cycle fatigue resistance of the cutting tools. This can be achieved either by multilayer coating architecture design or by compressive surface strengthening of the coating. However, this induces high compressive residual stress into the structure of the coating, which affects its adhesion to the substrate. Although coating adhesion is usually not a primary concern in milling, under the given circumstances the coating needs to retain its multifunctionality in order to enhance its cutting performance. The primary goal of this research work is to perform an in-depth investigation of the micro-mechanical and adhesion properties of the studied coatings, as well as to gain an understanding of their contribution to tool life enhancement during H13 milling. The secondary goal is to develop proper criteria for selecting coated carbide tools best suited for this type of machining process.

### **1.2.2 Research Objective**

To meet the outlined research goals, the main objective of this research is to perform a comprehensive study of micro-mechanical and adhesion properties of physical vapor

deposition (PVD) coated carbide tools for tool life enhancement under severe cutting conditions during the milling of H13 tool steel.

The research study investigated both dry and wet milling conditions and selected cutting parameters which contribute to the high material removal rate. Two aspects were considered for both dry and wet conditions: the incorporation of an interlayer into the



coating architecture and WPC post treatment of the coating. However, previous researchers have concluded that during dry milling, the post-treatment of a multilayer coating failed to enhance tool life and during wet milling, the studied bi-layer coating already possessed an interlayer. With this in mind, the **specific research** objectives are:

- **Estimation of coated carbide tool life through architectural development during dry high-speed milling of H13.**

Variations in the architecture and micro-mechanical properties of the TiAlCrSiYN-based family of PVD coatings, especially in terms of coating adhesion to the substrate, were analyzed to understand their combined effect on machining performance.



- **Optimization of interlayer thickness within the coating structure to enhance coated carbide tool life during the high-speed dry milling of H13.**

TiAlCrSiYN/TiAlCrN multilayer PVD coatings with varied thicknesses of the TiAlCrN interlayer were investigated during H13 milling. Repetitive load wear tests at room temperature were performed to estimate the effect of interlayer thickness variation on overall coating adhesion.

- **A comprehensive study of coated carbide tools following the application of a Wide peening cleaning (WPC) post-treatment during H13 wet milling.**

The tool wear patterns of the (AlCrN-TiAlN) bi-layer PVD coated carbide tools were investigated following WPC post-treatment at various pressures and times. The micro-mechanical and adhesion properties of the studied coatings were evaluated and compared in terms of their effects on machining performance.

## **1.3 Thesis Organization**

### **1.3.1 General technical overview**

A general technical overview of the thesis is presented below.

This study consists of two major phases. The first phase included two objectives.

The **first objective** (Chapter 2), was to adopt a fixed cutting condition for the dry milling of H13 tool steel. The micro-mechanical and adhesion properties of the PVD coating were assessed and discussed in detail.

The **second objective** (Chapter 3), was to examine the variation of interlayer thickness within the multilayer coating structure in order to assess the effect of coating adhesion to the substrate. This was also related to machining performance.

The second phase includes the **third objective** (Chapter 4) of the study. A novel mechanical surface treatment technique, WPC with various process parameters, was implemented on a bilayer coated solid milling tool to enhance tool life during the wet milling of H13.

Each of these chapters, two to four is composed of a journal paper corresponding to the aforementioned subjects. To meet the objectives of this study, further details about the contents of all of the chapters of this thesis are provided below:

### **1.3.2 Chapter contents**

Chapter 1 provides a literature review on the most important aspects of H13 tool steel machining in its hardened state, including relevant tool wear patterns and mechanisms. A comprehensive literature review concerning the selection of PVD cutting tool coatings used for H13 tool steel machining is also provided. Current state-of-the-art mechanical surface post-treatment processes for PVD coatings are described in detail.

Chapter 2 provides the results of a comprehensive study on wear performance of the PVD coated tools through improvement in their architecture during high speed dry milling of H13 tool steel. Chapter 3 intends to explain the effect of interlayer thickness variation on the multilayer coating properties and cutting performance during dry milling of H13. Chapter 4 includes investigations to explain the effect of WPC treatment on the overall coating system's micro-mechanical properties and consequently these properties were

related to machining performance under conditions that arise during wet milling of H13 tool steel. Finally, Chapter 5 includes a general discussion, a summary of the research contributions of the present dissertation along with recommendations for future research.

#### 1.4 Note to the Reader

Since this thesis is a compilation of peer-reviewed published and submitted journal articles, the introduction of each chapter and the background in chapter one may contain some repetition. However, the reader is encouraged to read these introductory sections in each chapter as the material is targeted towards specific aspects of the investigation covered in the corresponding chapters.

#### 1.5 References

1. Beake, B., et al., *Wear performance of different PVD coatings during hard wet end milling of H13 tool steel*. Surface and Coatings Technology, 2015. **279**: p. 118-125.
2. Dolinšek, S. and J. Kopač, *Mechanism and types of tool wear; particularities in advanced cutting materials*. Journal of Achievements in Materials and Manufacturing Engineering, 2006. **19**(1): p. 11-18.
3. Klocke, F. *Manufacturing Processes 1 Cutting Translated by Aaron Kuchle*. in *Germany: Library of Congress Control*. 2011.
4. Löffler, F.H., *Systematic approach to improve the performance of PVD coatings for tool applications*. Surface and Coatings Technology, 1994. **68**: p. 729-740.
5. Biksa, A., *Tribological Characterization of Surface Engineered Tooling for Metal Cutting Applications*. 2010.
6. Zhang, S., T. Ding, and J. Li, *Microstructural alteration and microhardness at near-surface of AISI H13 steel by hard milling*. Machining Science and Technology, 2012. **16**(3): p. 473-486.

7. Roberts, G.A., R. Kennedy, and G. Krauss, *Tool steels*. 1998: ASM international.
8. Ding, H., et al., *Experimental study on machinability improvement of hardened tool steel using two dimensional vibration-assisted micro-end-milling*. International Journal of Machine Tools and Manufacture, 2010. **50**(12): p. 1115-1118.
9. Li, W., Y. Guo, and C. Guo, *Superior surface integrity by sustainable dry hard milling and impact on fatigue*. CIRP Annals, 2013. **62**(1): p. 567-570.
10. Tönshoff, H., C. Arendt, and R.B. Amor, *Cutting of hardened steel*. Cirp Annals, 2000. **49**(2): p. 547-566.
11. Axinte, D. and R. Dewes, *Surface integrity of hot work tool steel after high speed milling-experimental data and empirical models*. Journal of Materials Processing Technology, 2002. **127**(3): p. 325-335.
12. Ribeiro, J.L.S., et al., *Dimensional and geometric deviations induced by milling of annealed and hardened AISI H13 tool steel*. American Journal of Materials Science, 2012. **2**(1): p. 14-21.
13. Dewes, R. and D. Aspinwall, *A review of ultra high speed milling of hardened steels*. Journal of materials processing technology, 1997. **69**(1-3): p. 1-17.
14. Koshy, P., R. Dewes, and D. Aspinwall, *High speed end milling of hardened AISI D2 tool steel (~ 58 HRC)*. Journal of Materials Processing Technology, 2002. **127**(2): p. 266-273.
15. Cui, X., J. Zhao, and X. Tian, *Cutting forces, chip formation, and tool wear in high-speed face milling of AISI H13 steel with CBN tools*. The International Journal of Advanced Manufacturing Technology, 2013. **64**(9-12): p. 1737-1749.
16. Uddeholm, B., *Bohler-Uddeholm H13 tool steel*. 2013.
17. Gu, J., S.C. Tung, and G.C. Barber, *Wear mechanisms of milling inserts: dry and wet cutting*, in *Wear Processes in Manufacturing*. 1998, ASTM International.
18. Ning, L., S. Veldhuis, and K. Yamamoto, *Investigation of wear behavior and chip formation for cutting tools with nano-multilayered TiAlCrN/NbN PVD coating*. International Journal of Machine Tools and Manufacture, 2008. **48**(6): p. 656-665.
19. Gu, J., et al., *Tool life and wear mechanism of uncoated and coated milling inserts*. Wear, 1999. **225**: p. 273-284.

20. Chinchankar, S. and S. Choudhury, *Machining of hardened steel—experimental investigations, performance modeling and cooling techniques: a review*. International Journal of Machine Tools and Manufacture, 2015. **89**: p. 95-109.
21. Fox-Rabinovich, G., et al., *Evolution of self-organization in nano-structured PVD coatings under extreme tribological conditions*. Applied Surface Science, 2014. **297**: p. 22-32.
22. Yamamoto, K., et al., *Properties of (Ti, Cr, Al) N coatings with high Al content deposited by new plasma enhanced arc-cathode*. Surface and Coatings Technology, 2003. **174**: p. 620-626.
23. Toh, C., *Static and dynamic cutting force analysis when high speed rough milling hardened steel*. Materials & design, 2004. **25**(1): p. 41-50.
24. Braghini Jr, A. and R. Coelho, *An investigation of the wear mechanisms of polycrystalline cubic boron nitride (PCBN) tools when end milling hardened steels at low/medium cutting speeds*. The International Journal of Advanced Manufacturing Technology, 2001. **17**(4): p. 244-251.
25. Elbestawi, M., et al., *High-speed milling of dies and molds in their hardened state*. CIRP Annals, 1997. **46**(1): p. 57-62.
26. Chinchankar, S. and S. Choudhury, *Effect of work material hardness and cutting parameters on performance of coated carbide tool when turning hardened steel: An optimization approach*. Measurement, 2013. **46**(4): p. 1572-1584.
27. Hunt, J., *Coated carbide metal cutting tools: development and applications*. PED., 1990. **43**: p. 139-155.
28. Klocke, F. and T. Krieg, *Coated tools for metal cutting—features and applications*. CIRP Annals-Manufacturing Technology, 1999. **48**(2): p. 515-525.
29. Bouzakis, K.-D., et al., *Cutting with coated tools: Coating technologies, characterization methods and performance optimization*. CIRP Annals-Manufacturing Technology, 2012. **61**(2): p. 703-723.
30. Tönshoff, H., et al. *Influence of different grinding processes on coating adhesion on cutting tools*. in *3rd International Conference “THE coatings”*, Nov. 2002.
31. Fox-Rabinovich, G. and G.E. Totten, *Self-organization During Friction: Advanced Surface-engineered Materials and Systems Design*. 2006: CRC Press.

32. PalDey, S. and S. Deevi, *Single layer and multilayer wear resistant coatings of (Ti, Al) N: a review*. Materials Science and Engineering: A, 2003. **342**(1): p. 58-79.
33. Ding, X.-Z. and X. Zeng, *Structural, mechanical and tribological properties of CrAlN coatings deposited by reactive unbalanced magnetron sputtering*. Surface and Coatings Technology, 2005. **200**(5): p. 1372-1376.
34. Donohue, L., et al., *Large-scale fabrication of hard superlattice thin films by combined steered arc evaporation and unbalanced magnetron sputtering*. Surface and Coatings Technology, 1997. **93**(1): p. 69-87.
35. Fox-Rabinovich, G., et al., *Oxidation resistant Ti-Al-Cr alloy for protective coating applications*. Intermetallics, 2006. **14**(2): p. 189-197.
36. Yamamoto, K., S. Kujime, and G. Fox-Rabinovich, *Effect of alloying element (Si, Y) on properties of AIP deposited (Ti, Cr, Al) N coating*. Surface and Coatings Technology, 2008. **203**(5): p. 579-583.
37. Vepřek, S. and S. Reiprich, *A concept for the design of novel superhard coatings*. Thin solid films, 1995. **268**(1-2): p. 64-71.
38. Tanaka, Y., K. Sato, and N. Ichimiya. *paper B5-2-1 presented at the Int. in Conf. Metallurgical Coatings and Thin Films, San Diego*. 2007.
39. Tillmann, W., et al., *Influence of bias voltage on residual stresses and tribological properties of TiAlVN-coatings at elevated temperatures*. Surface and Coatings Technology, 2013. **231**: p. 122-125.
40. Cai, F., et al., *Influence of negative bias voltage on microstructure and property of Al-Ti-N films deposited by multi-arc ion plating*. Ceramics International, 2017. **43**(4): p. 3774-3783.
41. Elmkhah, H., et al., *Surface characteristics for the TiAlN coatings deposited by high power impulse magnetron sputtering technique at the different bias voltages*. Journal of Alloys and Compounds, 2016. **688**: p. 820-827.
42. Ahlgren, M. and H. Blomqvist, *Influence of bias variation on residual stress and texture in TiAlN PVD coatings*. Surface and Coatings Technology, 2005. **200**(1-4): p. 157-160.
43. Chokwatvikul, C., et al., *Effect of nitrogen partial pressure on characteristic and mechanical properties of hard coating TiAlN film*. Journal of Metals, Materials and Minerals, 2011. **21**(1): p. 115-119.

44. Bujak, J., J. Walkowicz, and J. Kusiński, *Influence of the nitrogen pressure on the structure and properties of (Ti, Al) N coatings deposited by cathodic vacuum arc PVD process*. Surface and Coatings Technology, 2004. **180**: p. 150-157.
45. Holleck, H. and Schier, *Multilayer PVD coatings for wear protection*. Surface and Coatings Technology, 1995. **76**: p. 328-336.
46. Zhang, S., et al., *Toughness measurement of thin films: a critical review*. Surface and Coatings Technology, 2005. **198**(1): p. 74-84.
47. Stueber, M., et al., *Concepts for the design of advanced nanoscale PVD multilayer protective thin films*. Journal of Alloys and Compounds, 2009. **483**(1-2): p. 321-333.
48. Suresha, S., et al., *Toughening through multilayering in TiN–AlTiN films*. Philosophical Magazine, 2007. **87**(17): p. 2521-2539.
49. Denkena, B. and B. Breidenstein. *Residual stress gradients in PVD-coated carbide cutting tools*. in *Materials science forum*. 2006. Trans Tech Publ.
50. Bielawski, M., *Residual stress control in TiN/Si coatings deposited by unbalanced magnetron sputtering*. Surface and Coatings Technology, 2006. **200**(12): p. 3987-3995.
51. Fox-Rabinovich, G., et al., *Structure, properties and wear performance of nano-multilayered TiAlCrSiYN/TiAlCrN coatings during machining of Ni-based aerospace superalloys*. Surface and Coatings Technology, 2010. **204**(21): p. 3698-3706.
52. Bouzakis, K.-D., et al., *The effect of substrate pretreatments and HPPMS-deposited adhesive interlayers' materials on the cutting performance of coated cemented carbide inserts*. CIRP annals, 2010. **59**(1): p. 73-76.
53. Bouzakis, K.-D., et al., *Adaption of graded Cr/CrN-interlayer thickness to cemented carbide substrates' roughness for improving the adhesion of HPPMS PVD films and the cutting performance*. Surface and Coatings Technology, 2010. **205**(5): p. 1564-1570.
54. Hong, Y.S., et al., *Effects of Cr interlayer on mechanical and tribological properties of Cr-Al-Si-N nanocomposite coating*. Transactions of Nonferrous Metals Society of China, 2011. **21**: p. s62-s67.

55. Klocke, F., et al., *Adhesive interlayers' effect on the entire structure strength of glass molding tools' Pt-Ir coatings by nano-tests determined*. Surface and Coatings Technology, 2011. **206**(7): p. 1867-1872.
56. Shamsavari, F., et al., *Nanoindentation and nanoscratch behaviors of DLC films growth on different thickness of Cr nanolayers*. Diamond and Related Materials, 2016. **70**: p. 76-82.
57. Cemin, F., et al., *The influence of different silicon adhesion interlayers on the tribological behavior of DLC thin films deposited on steel by EC-PECVD*. Surface and Coatings Technology, 2015. **283**: p. 115-121.
58. Zhang, X., et al., *Hertzian contact response of single-layer, functionally graded and sandwich coatings*. Materials & design, 2007. **28**(1): p. 47-54.
59. Jacob, A., et al., *Influences of micro-blasting as surface treatment technique on properties and performance of AlTiN coated tools*. Journal of Manufacturing Processes, 2017. **29**: p. 407-418.
60. Abusuilik, S.B., *Pre-, intermediate, and post-treatment of hard coatings to improve their performance for forming and cutting tools*. Surface and Coatings Technology, 2015. **284**: p. 384-395.
61. Bouzakis, K.-D., et al., *Influence of dry micro-blasting grain quality on wear behaviour of TiAlN coated tools*. Wear, 2011. **271**(5): p. 783-791.
62. Bouzakis, K.-D., et al., *Effect of PVD films wet micro-blasting by various Al<sub>2</sub>O<sub>3</sub> grain sizes on the wear behaviour of coated tools*. Surface and Coatings Technology, 2011. **205**: p. S128-S132.
63. Bouzakis, K., et al., *Optimization of Wet or Dry Microblasting on PVD Films by Various Al<sub>2</sub>O<sub>3</sub> Grain Sizes for Improving the Coated Tools' Cutting Performance*. Tribology in Industry, 33: 49–56. 2011.
64. Bouzakis, K.-D., et al., *Effect of dry micro-blasting on PVD-film properties, cutting edge geometry and tool life in milling*. Surface and Coatings Technology, 2009. **204**(6-7): p. 1081-1086.



## **Chapter 2. IMPROVEMENT OF WEAR PERFORMANCE OF NANO-MULTILAYER PVD COATINGS UNDER DRY HARD END MILLING CONDITIONS BASED ON THEIR ARCHITECTURAL DEVELOPMENT**

Modified from a paper published in *Coatings* 8(2):59 (2018)

Shahereen Chowdhury, Ben D. Beake, Kenji Yamamoto, Bipasha Bose, Myriam Aguirre, German S. Fox-Rabinovich and Stephen C. Veldhuis

The TiAlCrSiYN-based family of PVD (physical vapor deposition) hard coatings was specially designed for extreme conditions involving the dry ultra-performance machining of hardened tool steels. However, there is a strong potential for further advances in the wear performance of the coatings through improvements in their architecture. A few different coating architectures (monolayer, multilayer, multilayer with interlayer) were studied in relation to cutting-tool life. Comprehensive characterization of the structure and properties of the coatings has been performed using XRD, SEM, TEM, micro-mechanical studies and tool-life evaluation. The wear performance was then related to the ability of the coating layer to exhibit minimal surface damage under operation, which is directly associated with the various micro-mechanical characteristics (such as hardness, elastic modulus and related characteristics; nano-impact; scratch test-based characteristics). The results presented exhibited that a substantial increase in tool life as well as improvement of the mechanical properties could be achieved through the architectural development of the coatings.

### **2.1 Introduction**

It is well known that high hardness, low thermal conductivity and high adhesion to the substrate are the key properties of wear resistant coatings helping them to sustain the heavy loads/high-temperature operating conditions during cutting [1]. This is especially true for severe/extreme frictional conditions associated with dry high-performance machining of hardened steels [2]. High hardness combined with the low thermal conductivity is mandatory for continuous dry cutting conditions associated with hard turning [1]. However, when the cutting environment becomes more complex, as in interrupted cutting conditions

the coating layer must achieve improved multi- functionality [3]. Modern hard PVD (Physical vapor deposition) coatings mostly have a nano- crystalline columnar structure [4]. The introduction of more complex coatings which combine nano- columnar and nano- laminated structures [5] critically improves the multi-functionality of the coating layer [6]. To improve further even more complex architectures must be considered, such as incorporation of interlayer along with multilayer coatings with a potential to improve micro-mechanical characteristics, such as adhesion to substrate [7] and impact fatigue fracture resistance. In general nano-laminates are effective in reducing the brittleness of hard coatings [8]. The brittleness of the hard coating is a very important factor to be addressed under interrupted cutting conditions where poor low cycle fatigue performance is a parameter that limits tool life [2, 3]. This characteristic of the coating could be evaluated through the nano-impact fracture resistance [9]. A unique feature of the nano-laminates is that they can provide simultaneous frictional energy accumulation due to the ability to prevent intensive plastic deformation and dissipation through providing crack deflection under operation [10, 11]. It has been shown elsewhere that an increased number of nano- layers could improve the impact fatigue fracture resistance due to the higher number of nano-layer interfaces which serve as sites for crack deflection [12]. This toughening strategy includes the development of multilayered structures with a high number of interfaces for crack deflection [12]. Additionally, it is very important to achieve a balance between high compressive stress that prevents excessive chipping under operation but could also lead to poor adhesion to the substrate and low residual stress (no crack retardation) [13].

It was also stated in [14] that greater load support (resistance to plastic deformation) that scales with  $H^3/E^2$  ratio can show excellent correlation with the impact fatigue fracture resistance. It minimizes the probability of cracks initiating in the first place (hindering of dislocation movement by the layer interfaces in the nano-multilayer coatings under loading). A larger  $H^3/E^2$  ratio means that a surface layer with better load support remains closer to elastic for longer. Eventually it results in spatial localization of damage. Deformation localization is essential to avoid degradation of the structural and mechanical integrity of the entire surface engineered structure [15]. In general, increased energy dissipation density and damage localization are key challenges for engineered materials, especially those with high brittleness that are prone to radial cracking and catastrophic fracture as a leading failure mechanism. This failure is typical for interrupted cutting conditions.

We also must note that under interrupted cutting conditions exposure to the environment is enhanced within the cutting zone in comparison to continuous cutting. Under such conditions the thermal protection of the cutting tool could be efficiently achieved not only by the coating layer by itself, but also because of the formation of thermal-barrier tribo-ceramic films on the surface through self-organization during friction [16]. The nano-laminated coating with higher number of layers contains bigger amount of lattice defects [16]. Therefore, it possesses a higher non-equilibrium state and has enhanced catalytic features. In this way formation of thermal barrier tribo-films on the friction surface could be accelerated and the wear rate reduced [17]. Consequently, such coatings can exhibit a wider range of multi-functional properties.

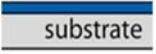

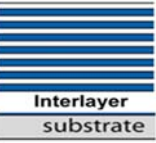
The general idea of the surface engineered layer optimization is to create an architecture that provides adaptive spatio-temporal behavior of the coating [17]. In this way the next generation of coatings could be developed. Such a coating would be able to provide the following: the highest possible adhesion to the substrate; the ability of the coating layer to accumulate and dissipate energy simultaneously, which is typical for nano-laminated structures; high surface protection/lubrication with an additional objective of better wear behavior in a highly loaded contact. Therefore, the goal of this paper is to present the results of investigation on the improvement in the architecture of the TiAlCrSiYN-based PVD coatings in relation to the various mechanical and tribological characteristics that show promise for hard high-speed end milling applications.

## 2.2 Materials and Methods

Table 2.1 exhibits different architectures of TiAlCrSiYN-based coatings investigated in the present study: a) monolayer; b) multilayer; c) multilayer with interlayer, where multilayer thickness was also increased by increasing the number of alternating nano-layers.

Ti<sub>0.2</sub>Al<sub>0.55</sub>Cr<sub>0.2</sub>Si<sub>0.03</sub>Y<sub>0.02</sub> and Ti<sub>0.15</sub>Al<sub>0.6</sub>Cr<sub>0.2</sub>Si<sub>0.03</sub>Y<sub>0.02</sub> targets fabricated by powdered metallurgical process were used for monolayer Ti<sub>0.2</sub>Al<sub>0.55</sub>Cr<sub>0.2</sub>Si<sub>0.03</sub>Y<sub>0.02</sub>N and nano-multilayered Ti<sub>0.2</sub>Al<sub>0.55</sub>Cr<sub>0.2</sub>Si<sub>0.03</sub>Y<sub>0.02</sub>N/Ti<sub>0.25</sub>Al<sub>0.65</sub>Cr<sub>0.1</sub>N coatings deposition.

Table 2.1 Different architectures of TiAlCrSiYN-based coatings

Architecture	Composition	Overall Thickness ( $\mu\text{m}$ )	Schematic
Monolayer	Ti <sub>0.2</sub> Al <sub>0.55</sub> Cr <sub>0.2</sub> Si <sub>0.03</sub> Y <sub>0.02</sub> N	3	
Multilayer	Ti <sub>0.2</sub> Al <sub>0.55</sub> Cr <sub>0.2</sub> Si <sub>0.03</sub> Y <sub>0.02</sub> N/Ti <sub>0.25</sub> Al <sub>0.65</sub> Cr <sub>0.1</sub> N	2	
Multilayer with interlayer	Ti <sub>0.2</sub> Al <sub>0.55</sub> Cr <sub>0.2</sub> Si <sub>0.03</sub> Y <sub>0.02</sub> N/Ti <sub>0.25</sub> Al <sub>0.65</sub> Cr <sub>0.1</sub> N interlayer	2 (100 nm interlayer) 3 (100 nm interlayer)	

Mirror polished cemented carbide WC-Co substrates (SPG 422, SPGN12 03 08) were selected for coating characterization and Mitsubishi C-2SB ball nose end mills (diameter=10 mm, 6 flutes) were chosen for cutting tool life studies. Coatings were deposited in an R&D-type hybrid PVD coater (Kobe Steel Ltd.) using a plasma-enhanced arc source. Samples were heated up to about 500 °C and cleaned through an Ar ion etching process. An Ar–N<sub>2</sub> mixture of gas was fed into the chamber at a pressure of 2.7 Pa with a N<sub>2</sub> partial pressure of 1.3 Pa. The arc source was operated at 100 A for a 100 mm diameter×16 mm thick target. Other deposition parameters were bias voltage 100 V; substrate rotation 5 rpm. The thickness of the coatings studied was adjusted by controlling the coating deposition time.

Full scale comprehensive characterization of the ball nose end mills tool life was performed, according to ISO 8688-2 “Tool life testing in milling. Part 2. End milling”. Cutting conditions are shown in Table 2.2.

Table 2.2 Cutting parameters used for the tool life evaluation.

Machine	Tool	Cutting parameters				
		Speed, m/min	Feed, mm/tooth	axial depth, mm	radial depth, mm	Coolant
Three-axis vertical milling center (Matsuura FX- 5).	Mitsubishi carbide ball nose end mills C-2SB, D = 10 mm.	600	0.06	5	0.6	Dry conditions

The crystal structure and preferred orientation of the coating were determined with X-ray diffraction (XRD, Rigaku ULTIMA-PC) using Cu-K $\alpha$  radiation. The residual stress evaluation was by means of a conventional X-ray diffractometer, using the multiple hkl method [18]. In this method, Cu-K $\alpha$  radiation beam with glancing incidence angle of 1.0 degree was used combined with a parallel beam geometry. Equation (1) indicates a stress-strain relationship of a solid material.

$$\begin{aligned} \varepsilon_{\phi\psi} = & \frac{1}{2} S_2 \sin^2 \psi [\sigma_{11} \cos^2 \phi + \sigma_{12} \sin(2\phi) + \sigma_{22} \sin^2 \phi] \\ & + \frac{1}{2} S_2 [\sigma_{13} \cos \phi \sin(2\psi) + \sigma_{23} \sin \phi \sin(2\psi) + \sigma_{33} \cos^2 \psi] \\ & + S_1 [\sigma_{11} + \sigma_{22} + \sigma_{33}] \end{aligned} \quad (1)$$

$\varepsilon$  is the strain of a crystallographic plane whose direction, i.e. the direction of the diffraction vector is usually described by angles  $\psi$  (angle of inclination of the specimen surface normal about the diffraction vector) and  $\phi$  (the anticlockwise rotation of the specimen around the

specimen surface normal).  $\sigma_{ij}$  ( $i, j=1,2,3$ ) represents a stress tensor and  $S_1$  and  $\frac{1}{2}S_2$  are X-ray elastic constants as defined by Eq. (2).

$$S_1 = -\frac{\nu}{E}, \frac{1}{2}S_2 = -\frac{1+\nu}{E} \quad (2)$$

In the multiple hkl method, stress  $\sigma_{ij}$  can be calculated by measuring changes in lattice spacing  $d$  of multiple planes and resulting strain  $\varepsilon_{\phi\psi}^{hkl}$ , defined as  $\varepsilon_{\phi\psi}^{hkl} = \frac{d_i - d_{i0}}{d_{i0}}$  ( $d_i$  represents measured lattice spacing and  $d_{i0}$  is strain-free lattice spacing of  $d_i$ ). Assuming that the tensor component satisfies,  $\sigma_{33}=0$ ,  $\sigma_{23}=\sigma_{13}=0$ ,  $\sigma_{11}=\sigma_{22}=\sigma$ , then Eq. (1) becomes Eq. (3).

$$\varepsilon_{\phi\psi}^{hkl} = \sigma \left[ \frac{1}{2}S_2^{hkl} \sin^2\psi + 2S_1^{hkl} \right] \quad (3)$$

Stress can be calculated by the slope of  $\varepsilon_{\phi\psi}^{hkl}$  to  $\sin^2\psi$  relationship. In this study, because all coating material exhibits a cubic crystal structure, the elastic constant is assumed to be hkl independent. The value  $d_{i0}$  was calculated by the law of mixture, using a lattice constant of cubic AlN (JCPDS 25-1495,  $a=0.414\text{nm}$ ), CrN (JCPDS 11-65,  $a=0.414\text{nm}$ ), TiN (JCPDS 38-1420  $a=0.424173\text{nm}$ ), hypothetical cubic SiN and YN using ionic radius of Si and Y, being  $a=0.3271\text{nm}$  and  $a=0.4409\text{nm}$  respectively. The micro-mechanical characteristics of the coatings were measured on the WC-Co substrate using a Micro Materials NanoTest system. Nanoindentation was performed in a load-controlled mode with a Berkovich diamond indenter calibrated for load, displacement, frame compliance and indenter shape according to an ISO14577-4 procedure. The area function

for the indenter was determined by indentation into a fused silica reference sample. For the nanoindentation of the coatings, the peak load was 40 mN and 40 indentations were performed for each coating. This load was chosen to minimize any influence of surface roughness on the data whilst ensuring that the indentation contact depth was under 1/10 of the film thickness so that a coating-only (load-invariant) hardness could be measured in combination with coating-dominated elastic modulus. Nano-impact testing was performed with a NanoTest fitted with a cube corner indenter as an impact probe. The indenter was accelerated from 12  $\mu\text{m}$  above the coating surface with 20-30 mN coil force to produce an impact every 4 s for a total test duration of 30-300 s. The coatings' nano-impact fatigue fracture resistance was assessed by the final measured impact depth and confirmed by microscopic analysis of impact craters. Micro-scratch tests were performed to a peak load of 5 N using the NanoTest Scratching Module with a 25  $\mu\text{m}$  radius diamond probe.

Cutting tool life was studied under the conditions mentioned in Table 1. At least three cutting tests were performed for each kind of coating under the corresponding operations. The scatter of the tool life measurements was approximately 10%. Cutting tests have been performed during dry ball-nose end milling (Mitsubishi carbide end mills,  $D=10$  mm) of the hardened AISI H13 tool steel with hardness HRC 53–55 under extreme cutting conditions. The cutting experiments were carried out on a three-axis vertical milling center (Matsuura FX-5). The cutting parameters were as following: speed 600 m/min; feed: 0.06 mm/tooth; axial depth: 5.0 mm; radial depth: 0.6 mm. The coated tool flank wear was measured using an optical microscope (Mitutoyo model TM). A tool dynamometer (9255B, Kistler) was used to measure the cutting forces.



## 2.3 Results and Discussion

### 2.3.1 Structural Analysis

Comparative structural analysis of the monolayer, multilayer and multilayer with interlayer coatings is shown in Figure 2.1. The data shows that monolayer coating has a nano-crystalline columnar structure (Figure 2.1a); nano-multilayered coating also has columnar structure with alternating nano-layers (Figure 2.1b). It was shown previously that these nano-layers are TiAlCrSiYN [19] and TiAlCrN [20]. The thickness of the TiAlCrN interlayer, is approximately 100 nm (Figure 2.1c). X-ray diffractograms of all the coatings studied are presented in Figure 2.2. showing a preferred orientation C (111) for all the coatings.

### 2.3.2 Mechanical properties

#### *Residual stress*

Table 2.3 depicts that the residual stress is highly compressive for all the studied coatings. This range of residual stress is normal for the multilayer PVD coatings deposited under conditions specified in the experimental section [21]. This is beneficial considering the heavy loaded conditions associated with the experiments performed and prevents excessive chipping of the cutting edge under operation. The monolayer TiAlCrN coating has a nano-crystalline structure [19] and the lowest range of compressive residual stress (Table 2.3). The monolayer TiAlCrSiYN coating has a slightly higher compressive residual stress (Table 2.3) which can be related to the grain size refinement and formation

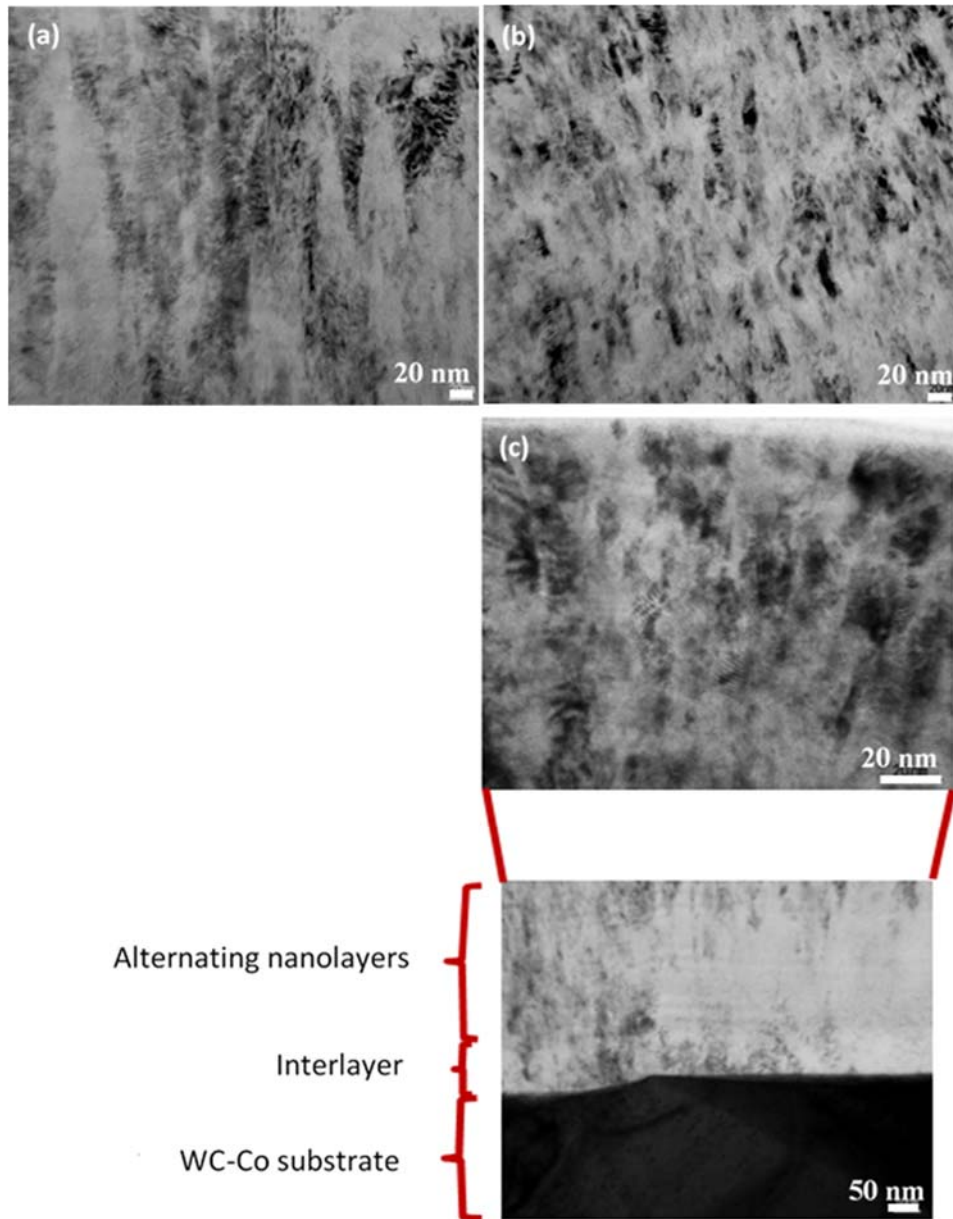


Figure 2.1 TEM (transmission electron microscope, JEOL FS2200, JEO USA, Inc., Peabody, MA, USA) image of FIB cross-section of TiAlCrSiYN-based coatings:(a) monolayer; (b) multilayer; (c) multilayer with interlayer. Thickness of alternating nano-layers in multilayered coatings is 20–40 nm, thickness of TiAlCrN interlayer is 100 nm.

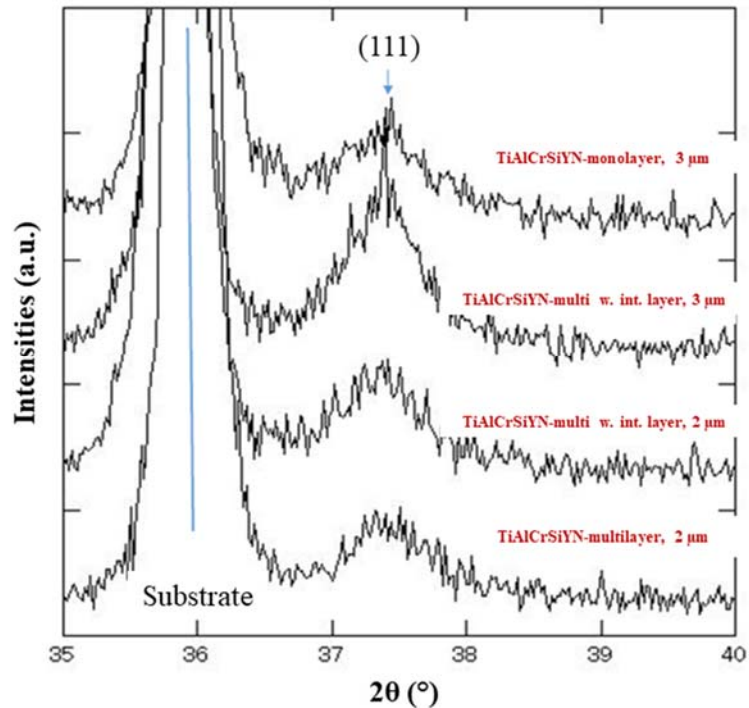


Figure 2.2 X-ray diffractograms of different TiAlCrSiYN-based coating architectures with different thickness.

of ultra-fine nano-crystalline structure in this coating as compared to the TiAlCrN one due to the incorporation of Si into the composition [22]. Grain size refinement is further associated with the higher number of defects on the nano-grain boundaries [23] which ultimately results in residual stress growth. An increase in residual stress is observed for the 2 microns multilayer coating. This is again associated with the further growth of defects at the alternating nano-layer interfaces [16]. However, the incorporation of TiAlCrN interlayer into the multilayer structure resulted in a reduction in the residual stress due to the interlayer having a lower residual stress (Table 2.3). An increase in the overall thickness from 2  $\mu\text{m}$  to 3  $\mu\text{m}$  for the multilayer coating with an interlayer leads to a further reduction of residual stress (Table

2.3). It has been previously shown in [24] that with other parameters being the same, an increase in overall coating thickness can lead to a reduction of compressive residual stress. This consideration can act as a limiting factor for overall thickness of multilayer coating with interlayer to prevent further reduction in the compressive stress that could lead to flaking of the coating off the cutting tool .

Table 2.3 Residual stress values in the studied coatings.

<b>Coating</b>	<b>Residual Stress (GPa)</b>
TiAlCrN monolayer, 3 $\mu\text{m}$	$-5.65 \pm 0.3$
TiAlCrSiYN monolayer, 3 $\mu\text{m}$	$-6.17 \pm 1.2$
TiAlCrN/TiAlCrSiYN multilayer, 2 $\mu\text{m}$	$-7.09 \pm 0.6$
TiAlCrN/TiAlCrSiYN multilayer with TiAlCrN interlayer,	$-6.99 \pm 0.5$
TiAlCrN/TiAlCrSiYN multilayer with TiAlCrN interlayer, 3 $\mu\text{m}$	$-6.50 \pm 0.4$

### ***Micro-mechanical properties***

Micro-mechanical properties of the coatings are summarized in Table 2.4. The hardness of all the coatings is similar. However, multilayer coatings with interlayer have higher hardness and a lower plasticity index. The most pronounced difference is found in the value of  $H^3/E^2$  ratio (Table 2.4) where the highest value is obtained for the 2  $\mu\text{m}$  multilayer coating with interlayer. The 30 s impact test data are summarized in Table 2.5 and corresponding low cycle impact fatigue resistance data is shown in Figure 2.3. SEM (TESCAN VP Scanning Electron Microscope, Nano Images, LLC, Pleasanton, CA, USA) images of the impact craters exhibited a brittle fracture that is more extensive in monolayer

Table 2.4 Micro-mechanical properties of the studied coatings

Coating	Hardness, GPa	Elastic modulus, GPa	P.I★	H/E ratio	H <sup>3</sup> /E <sup>2</sup> Ratio (GPa)
TiAlCrN monolayer (3 μm)	25.9 ± 4.8	430.7	0.49	0.060	0.093
TiAlCrSiYN monolayer (3μm)	29.6±4.5	489.8	0.47	0.060	0.108
TiAlCrN/TiAlCrSiYN multilayer (2μm)	28.4±4.5	429.0	0.46	0.066	0.124
TiAlCrN/TiAlCrSiYN multilayer TiAlCrN interlayer (2μm)	31.6±2.5	432.7	0.43	0.073	0.169
TiAlCrN/TiAlCrSiYN multilayer with TiAlCrN interlayer (3μm)	30.9±2.7	474.6	0.45	0.065	0.131

- P.I stands for plasticity index

coating (TiAlCrSiYN) (Figure 2.3a). Whereas multilayer coatings with interlayer exhibit lower depth of penetration as well as reduced surface damage (Figure 2.3b, c) after 30 s of impact. Although both 2 and 3 μm multilayers with interlayer have higher brittleness (higher  $H/E$  ratio) they have a structural advantage (multilayer with interlayer vs. monolayers/multilayer) that inhibits crack propagation under the given load and results in less dramatic fracture. Additionally, both the aforementioned coatings showed a more gradual increase in the depth of penetration compare to the multilayer and monolayer one

Table 2.5 Penetration depth after 30 s and 300 s during nano impact test (20–30 mN)

Coating	Final depth (mean), microns	
	30 sec	300 sec
TiAlCrSiYN monolayer (3μm)	1.4±0.4	2.2±0.5
TiAlCrN/TiAlCrSiYN multilayer (2μm)	-	1.8±0.3
TiAlCrN/TiAlCrSiYN multilayer; TiAlCrN interlayer (2μm)	0.93±0.3	1.8±0.3
TiAlCrN/TiAlCrSiYN multilayer; TiAlCrN interlayer (3μm)	0.84±0.1	1.4±0.3

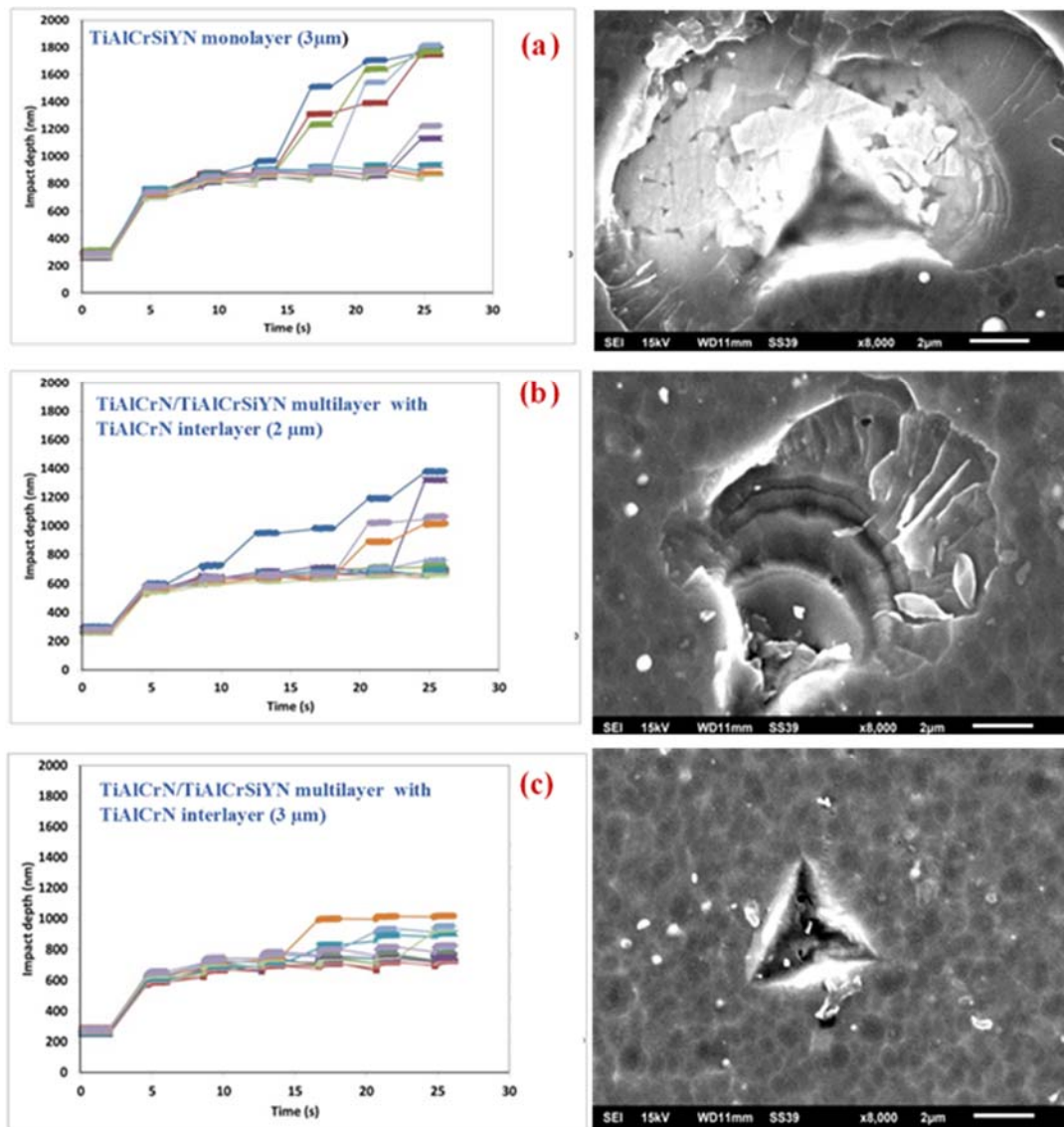


Figure 2.3 30 s impact fatigue fracture resistance data at 20 mN for the studied coatings:  
 (a) TiAlCrSiYN monolayer, 3 μm; TiAlCrN/TiAlCrSiYN multilayer with TiAlCrN interlayer (b) 2 μm, (c) 3 μm.

(Figure 2.4a) under repetitive impacts for 300 s. One explanation might be that most of the impact energy is absorbed inside the coating nanolayers as well as softer interlayer for the coating architecture of multilayer with interlayer during the impact test. Moreover, as

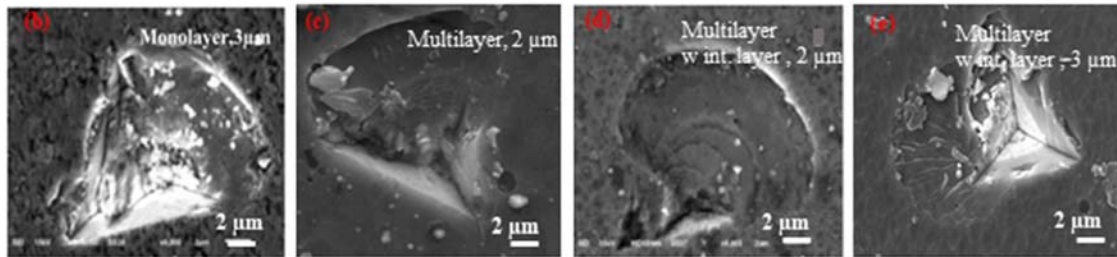
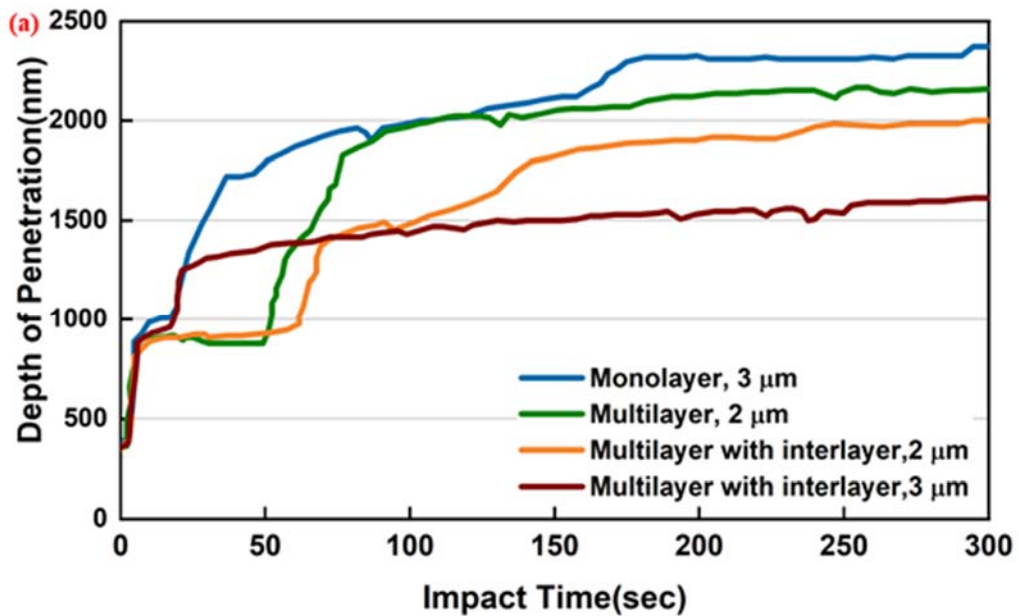


Figure 2.4 (a) Impact fatigue fracture resistance at 25–30 mN, 300 s for the studied coatings, SEM images (b) TiAlCrSiYN monolayer, 3  $\mu\text{m}$ ; (c) TiAlCrN/TiAlCrSiYN multilayer, 2  $\mu\text{m}$  and multilayer with TiAlCrN interlayer (d) 2  $\mu\text{m}$ , (e) 3  $\mu\text{m}$ .

depicted in Figure 2.4a, a sudden increase in depth of penetration develops for 2  $\mu\text{m}$  multilayer coating with interlayer at around 60 s of repetitive impacts and ultimately reaching the coating thickness (2  $\mu\text{m}$ ) after 300 s. Whereas the 3  $\mu\text{m}$  multilayer coating with interlayer shows a gradual impact depth increase vs. time even at a higher impact load of 30 mN. Thus, 3  $\mu\text{m}$  multilayer coating with interlayer exhibits the best fatigue performance with minimal surface damage (Figure 2.3c and Figure 2.4e). The data



indicates that impact behavior depends not only on the combination of load support and micro-structural advantages but also on the overall thickness of the coating.

The fatigue characteristics of the studied coatings correspond well with the fact that coating having a higher  $H^3/E^2$  ratio (Table 2.4) can promote better crack propagation resistance. The 2  $\mu\text{m}$  multilayer coating with interlayer has the highest value of  $H^3/E^2$  ratio but being thinner it provides less load support to the substrate than the 3  $\mu\text{m}$  multilayer one. These characteristics are in good correlation with the wear behavior during milling. The flank and rake wear during the initial running-in stage were higher especially for 2  $\mu\text{m}$  multilayer with interlayer ( Figure 2.7) but due to better fatigue resistance the chipping of the cutting edge occurred at a much later stage compare to the multilayer and monolayer coatings. Also, any fracture on the monolayer coated tool results in more dramatic chipping in the cutting tests.

Table 2.6 Scratch crack propagation resistance of the studied coatings

Coating	CPRs parameter $L_{c1}(L_{c2}-L_{c1}), N^2$ 'Scratch crack propagation resistance'
TiAlCrN monolayer (3 $\mu\text{m}$ )	4.8
TiAlCrSiYN monolayer (3 $\mu\text{m}$ )	1.6
TiAlCrN/TiAlCrSiYN multilayer (2 $\mu\text{m}$ )	1.9
TiAlCrN/TiAlCrSiYN multilayer; TiAlCrN interlayer (2 $\mu\text{m}$ )	5.8
TiAlCrN/TiAlCrSiYN multilayer; TiAlCrN interlayer (3 $\mu\text{m}$ )	3.2

The most significant improvement obtained through architectural development of coatings is in terms of adhesion of coating to the substrate as exhibited in Table 2.6. This property was measured through micro-scratch ramped load test employing crack propagation resistance parameter (CPRs) . A notable enhancement in adhesion property



was obtained for multilayer coatings with interlayer (for both 2 and 3  $\mu\text{m}$  thickness) as compared to the multilayer and monolayer one (Table 2.6). This improvement can be related to the presence of the softer TiAlCrN interlayer providing a cushioning effect under the operational load.

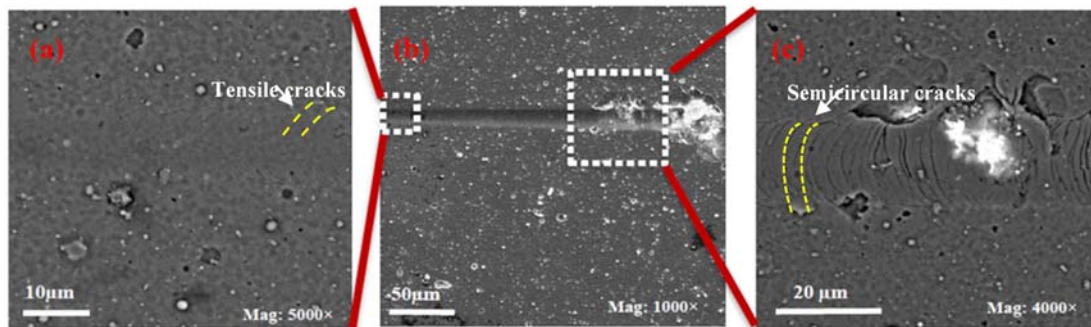


Figure 2.5 SEM images of a micro-scratch test on the 3  $\mu\text{m}$  multilayer with interlayer, with higher magnification images of the deformation at the (a)  $L_{c1}$  and (c)  $L_{c2}$  failures.

Tensile arc cracks were formed in the scratch track clearly visible in optical micrographs (Figure 2.5a). SEM imaging revealed that the cracks start at the periphery of the scratch tracks before extending to produce complete arcs as the load increased (Figure 2.5c). The  $L_{c2}$  failure requires the combination of high tensile stresses at the surface and significant weakening of the interface caused by coating bending and substrate yield. This type of failure mechanism has previously been postulated to explain the failure mechanism of thicker coatings on cemented carbide substrate in scratch tests by Schwarzer and co-workers [25].

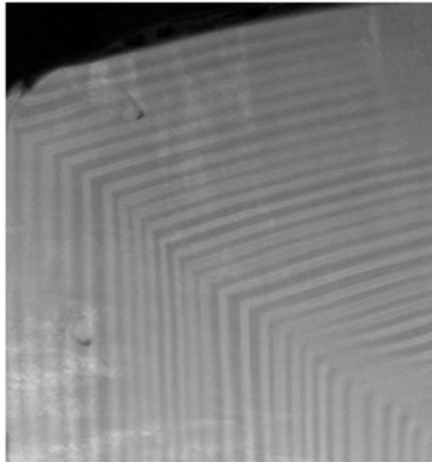


Figure 2.6 FIB cross-section of multilayer TiAlCrSiYN/TiAlCrN coating on the cutting edge.

**Error! Reference source not found.** presents the FIB (Focused Ion Beam) image of the nano-multilayer coating on the very edge of the cutting tool. It could be clearly seen that the nano-layers perfectly follow the shape of the sharp cutting edge. There is no visible damage within the entire coating layer despite significant bending of the nano-layers. It was shown previously [26] that the bending stresses in the individual nano-layers in a multilayer coating are less due to the accommodation of the bending radius that causes fracture in a monolayer coating of similar total thickness.

### 2.3.3 Tool Life and Wear Performance Studies

Tool life of the studied coatings is presented in Figure 2.7. Under extreme cutting conditions considered for dry milling of H13. To the best of our knowledge there are very few data's available in the literature on the wear behavior of multilayer coatings [27, 28] however, there is no literature available on the wear behavior of a multilayer coating

structure with interlayer applied under similar cutting conditions. It was shown previously that under investigated extreme cutting conditions, when the temperature is as high as 1000–1100 °C and stresses are around 1.5–2 GPa in the cutting zone, failure of the cutting tool is due to the flank wear, rake wear (with minimal buildup edge formation) and chipping [29]. To perform comprehensive wear studies of the tools with the investigated coatings all these characteristics have been evaluated.

Flank and rake wear data are shown in Figure 2.7 (a,b) respectively. Chipping resistance is presented in Figure 2.7c. Average cutting forces are shown in Figure 2.7d. The monolayer coating has lower tool-life characteristics. Better wear characteristics and chipping behavior are directly related to its micro-mechanical properties, primarily load support and impact fatigue fracture resistance of the coatings studied. For the given cutting conditions and coating deposition parameters, multilayer 2 µm thick coating achieve a tool life of around 100 m in terms of machining length, whereas the best wear behavior is exhibited by the multilayer coatings with interlayer (i.e., around 60% increase in tool life for 3-micron one comparing to multilayer coating).

The wear evolution is more gradual on the multilayer coatings with interlayer. This relates well to the impact behavior. The combination of low  $L_{c1}$  and high  $L_{c2}$ , i.e., high scratch resistance, on the multilayer coatings with interlayer is consistent with its behavior in the cutting test there is some initial damage that is greater than the other coatings but then it shows good durability.

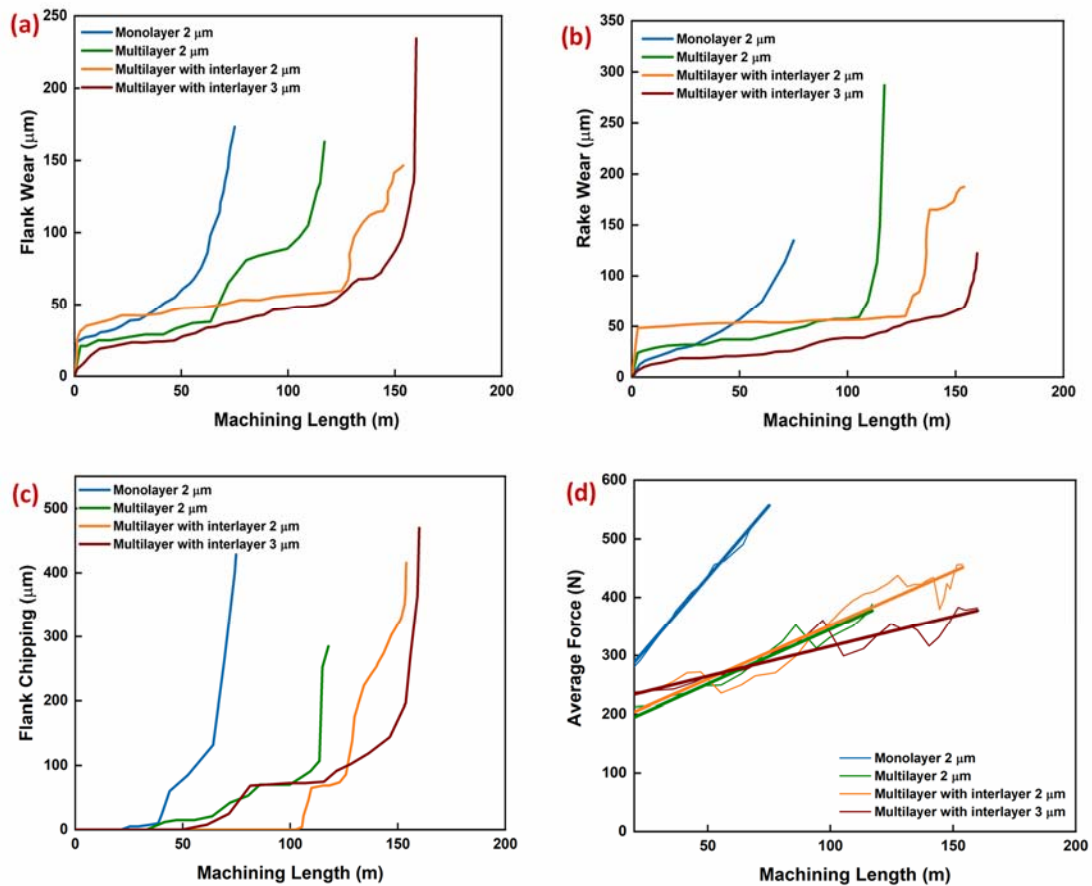


Figure 2.7 Tool-life data of the studied coatings vs. length of cut (m): (a) flank wear; (b) rake wear; (c) chipping intensity; (d) average cutting forces.

Also, 3  $\mu\text{m}$  thick multilayer coating with interlayer has lower cutting forces as well (Figure 2.7d) after the running in stage. This is directly related to the ability of the coating to better protect its surface under operation which is due to the formation of protective tribo-ceramic film layer [17] (Figure 2.8) during the running in stage. It was shown previously that a variety of thermal barrier tribo-films are forming on the surface of the coating under operation [16, 17]. Effective replenishment of these films is strongly related to the surface damage of the coating layer. The coating with lower intensity of surface

damage can be a better environment for the dynamic tribo-films to be formed, worn out and rejuvenated again as a result of friction and interaction with the environment. Consequently, multilayer coatings with interlayer having improved micro-mechanical characteristics, exhibit lower damage of the coating layer and thus show better surface protection (Figure 2.8).

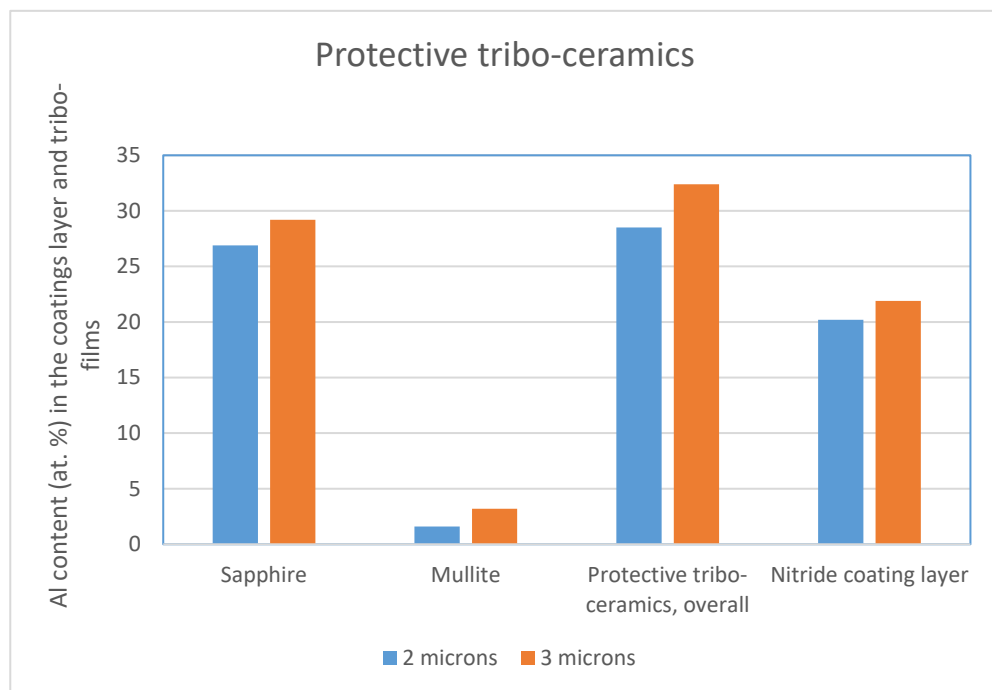


Figure 2.8 XPS (X-ray photoelectron spectroscopy, Physical Electronics (PHI) Quantera II spectrometer, Physical Electronics, Inc, Chanhassen, MN, USA) data for tribo-films formed on the worn surface of TiAlCrSiYN/TiAlCrN multilayer with interlayer coatings of different thickness (of 2 and 3  $\mu\text{m}$ ) during running-in stage (after machining of 30 m).

The mechanical behavior outlined above affects the ability of the coating layer to self-protect its surface under operation through the formation of protective tribo-ceramic films on the friction surface (Figure 2.8). The surface that undergoes less damage under operation has the ability to form a higher amount of thermal barrier ceramic tribo-films

(Figure 2.8), such as sapphire [16] and mullite [16]. This critically improves the wear performance of the coating layer. Therefore, the tool with better protection of surface has a higher tool life (Figure 2.7). As was shown previously [17] non-protective  $\text{TiO}_x$  and lubricious  $\text{CrO}_x$  tribo-films also form but their amount is below 10% and therefore they are believed to be less critical to the overall tool life than the sapphire and mullite tribo-films.

## 2.4 Conclusion

Detailed studies of the structure and properties of a number of different TiAlCrSiYN-based coatings (a) monolayer; b) multilayer; c) multilayer with interlayer, where multilayer thickness was also increased by increasing the number of alternating nano-layers) have been performed. The wear performance of the TiAlCrSiYN-based coating was improved through optimization of their architecture. The relationship between the coatings' structure characterized by different methods such as XRD, SEM, TEM and micro-mechanical characteristics (hardness, elastic modulus and their ratios; nano-impact, scratch characteristics) and their tool life was established. It was shown by XPS analysis that the coating layer with lower intensity of surface damage is a better environment for the formation of the dynamic nanoscale tribo-films on the friction surface that result in improved surface protection under extreme conditions. It could be concluded that a noticeable improvement in the wear behavior could be achieved during high-performance dry machining of hardened tool steels through the incorporation of interlayer in multilayer coating architectures with a realization of better micro-mechanical characteristics of the coatings.

**Author Contributions:** Shahereen Chowdhury designed and performed experiments on machining and micro-mechanical characterization; Ben D. Beake performed experiments and modeling on micro-mechanical characterization; Kenji Yamamoto designed the coatings and made XRD characterizations; Bipasha Bose performed micro-mechanical characterization and assisted with evaluating the results; Myrian Aguirre performed TEM characterization; German S. Fox-Rabinovich analyzed, discussed the results and co-wrote the paper; and Stephen C. Veldhuis served as the supervisor.

## 2.5 References

1. Bouzakis, K.-D., et al., *Cutting with coated tools: Coating technologies, characterization methods and performance optimization*. CIRP Annals-Manufacturing Technology, 2012. **61**(2): p. 703-723.
2. Fox-Rabinovich, G., et al., *Emergent behavior of nano-multilayered coatings during dry high-speed machining of hardened tool steels*. Surface and Coatings Technology, 2010. **204**(21): p. 3425-3435.
3. Fox-Rabinovich, G.S., et al., *Hierarchical adaptive nanostructured PVD coatings for extreme tribological applications: the quest for nonequilibrium states and emergent behavior*. Science and technology of advanced materials, 2012. **13**(4): p. 043001.
4. Fox-Rabinovich, G., et al., *Mechanism of adaptability for the nano-structured TiAlCrSiYN-based hard physical vapor deposition coatings under extreme frictional conditions*. Journal of Applied Physics, 2012. **111**(6): p. 064306.
5. Fox-Rabinovich, G., et al., *Structure, properties and wear performance of nano-multilayered TiAlCrSiYN/TiAlCrN coatings during machining of Ni-based aerospace superalloys*. Surface and Coatings Technology, 2010. **204**(21): p. 3698-3706.
6. Beake, B.D., et al., *Why can TiAlCrSiYN-based adaptive coatings deliver exceptional performance under extreme frictional conditions?* Faraday discussions, 2012. **156**(1): p. 267-277.
7. Bouzakis, K.-D., et al., *Adaption of graded Cr/CrN-interlayer thickness to cemented carbide substrates' roughness for improving the adhesion of HPPMS PVD films and the cutting performance*. Surface and Coatings Technology, 2010. **205**(5): p. 1564-1570.

8. Voevodin, A.A., J.S. Zabinski, and C. Muratore, *Recent advances in hard, tough, and low friction nanocomposite coatings*. Tsinghua Science and Technology, 2005. **10**(6): p. 665-679.
9. Skordaris, G., et al., *Brittleness and fatigue effect of mono-and multi-layer PVD films on the cutting performance of coated cemented carbide inserts*. CIRP Annals-Manufacturing Technology, 2014. **63**(1): p. 93-96.
10. Chan, K., M. He, and J. Hutchinson, *Cracking and stress redistribution in ceramic layered composites*. Materials Science and Engineering: A, 1993. **167**(1-2): p. 57-64.
11. He, M.Y., A.G. Evans, and J.W. Hutchinson, *Crack deflection at an interface between dissimilar elastic materials: role of residual stresses*. International Journal of Solids and Structures, 1994. **31**(24): p. 3443-3455.
12. Chen, J., H. Li, and B.D. Beake, *Load sensitivity in repetitive nano-impact testing of TiN and AlTiN coatings*. Surface and Coatings Technology, 2016. **308**: p. 289-297.
13. Astakhov, V.P. and J.P. Davim, *Tools (geometry and material) and tool wear*, in *Machining*. 2008, Springer. p. 29-57.
14. Hassani, S., et al., *Predictive tools for the design of erosion resistant coatings*. Surface and Coatings Technology, 2008. **203**(3): p. 204-210.
15. Bruet, B.J., et al., *Materials design principles of ancient fish armour*. Nature materials, 2008. **7**(9): p. 748.
16. Fox-Rabinovich, G., et al., *Evolution of self-organization in nano-structured PVD coatings under extreme tribological conditions*. Applied Surface Science, 2014. **297**: p. 22-32.
17. Fox-Rabinovich, G., et al., *Spatio-temporal behaviour of atomic-scale tribo-ceramic films in adaptive surface engineered nano-materials*. Scientific reports, 2015. **5**: p. 8780.
18. Welzel, U., et al., *Stress analysis of polycrystalline thin films and surface regions by X-ray diffraction*. Journal of Applied Crystallography, 2005. **38**(1): p. 1-29.
19. Yamamoto, K., S. Kujime, and G. Fox-Rabinovich, *Effect of alloying element (Si, Y) on properties of AIP deposited (Ti, Cr, Al) N coating*. Surface and Coatings Technology, 2008. **203**(5): p. 579-583.



20. Yamamoto, K., et al., *Properties of (Ti, Cr, Al) N coatings with high Al content deposited by new plasma enhanced arc-cathode*. Surface and Coatings Technology, 2003. **174**: p. 620-626.
21. Carvalho, N., et al., *Stress analysis and microstructure of PVD monolayer TiN and multilayer TiN/(Ti, Al) N coatings*. Thin Solid Films, 2003. **429**(1-2): p. 179-189.
22. Fox-Rabinovich, G., et al., *Nanocrystalline coating design for extreme applications based on the concept of complex adaptive behavior*. Journal of Applied Physics, 2008. **103**(8): p. 083510.
23. Mayrhofer, P.H., et al., *Microstructural design of hard coatings*. Progress in Materials Science, 2006. **51**(8): p. 1032-1114.
24. Bielawski, M., *Residual stress control in TiN/Si coatings deposited by unbalanced magnetron sputtering*. Surface and Coatings Technology, 2006. **200**(12): p. 3987-3995.
25. Schwarzer, N., et al., *Optimization of the Scratch Test for specific coating designs*. Surface and Coatings Technology, 2011. **206**(6): p. 1327-1335.
26. Matthews, A., R. Jones, and S. Dowey, *Modelling the deformation behaviour of multilayer coatings*. Tribology Letters, 2001. **11**(2): p. 103-106.
27. Hovsepian, P.E., C. Reinhard, and A. Ehiasarian, *CrAlYN/CrN superlattice coatings deposited by the combined high power impulse magnetron sputtering/unbalanced magnetron sputtering technique*. Surface and Coatings Technology, 2006. **201**(7): p. 4105-4110.
28. Veprek, S. and M.J. Veprek-Heijman, *Industrial applications of superhard nanocomposite coatings*. Surface and Coatings Technology, 2008. **202**(21): p. 5063-5073.
29. Trent, E.M. and P.K. Wright, *Metal cutting*. 2000: Butterworth-Heinemann.

### **Chapter 3. EFFECT OF INTERLAYER THICKNESS ON NANO-MULTILAYER COATING PERFORMANCE DURING HIGH SPEED DRY MILLING OF H13 TOOL STEEL**

Manuscript published in Coatings 9(11):737 (2019)

Shahereen Chowdhury, Bipasha Bose, Kenji Yamamoto and Stephen C. Veldhuis

The TiAlCrSiYN-based family of physical vapor deposition (PVD) coatings were systematically designed through the incorporation of TiAlCrN interlayer to increase coating adhesion and consequently the tool life for extreme conditions that arise during dry high-speed milling of hardened tool steels. The investigation in the present paper intends to explain the effect of TiAlCrN interlayer thickness on the overall coating properties and cutting performance. A comprehensive characterization of the structure and properties of the coatings has been performed using focused ion beam (FIB), scanning electron microscope (SEM), X-ray powder diffraction (XRD), nanoindentation, ramped load scratch test, repetitive load wear test, and nano-impact test. The wear test at a subcritical load of 1.5 N showed that there was a gradual improvement in coating adhesion to the substrate as the interlayer thickness increased from 100 to 500 nm. However, the wear performance, being related to the ability of the coating layer to exhibit minimal surface damage under operation, was found to be associated with micro-mechanical characteristics (such as hardness, elastic modulus). Around a 40% increase in the cutting performance with 300 nm interlayer exhibited that a substantial increase in tool life can be achieved through interlayer thickness variation, by obtaining a balance between mechanical and tribological properties of the studied coatings.

#### **3.1 Introduction**

Over the years, concepts such as high-speed machining [1] have been considered in an attempt to expand the application of milling of H13 tool steel (HRC 45-55) in their hardened state for dies and molds. This process benefits material removal rates, lead times, cutting forces, part precision, and surface finishes [2] during machining. However, excessive tool wear poses a major concern [3, 4] due to poor low cycle fatigue performance [4, 5] at these heavy loads/high temperatures during dry interrupted cutting [6]. Therefore,

significant emphasis is put upon determining the best tool materials [3], machining strategies [7], and operating parameters [5] during H13 machining. An alternative approach is recommended to handle the corresponding situation by applying different physical vapor deposition (PVD) [8] coatings on the cutting tools.

In recent years, advancements in coating deposition techniques [9] enabled widespread usage of nano crystalline PVD coatings such as TiAlN and AlTiN for the surface engineering of carbide tools used in alloy steel machining (42 HRC and over) [6]. This in turn enhances the protection of cutting tools from thermal and mechanical loads on the cutting zone. However, in a complex cutting environment such as interrupted cutting, the coating layer must achieve improved multi-functionality [10]. Thus, complex coatings with nano-columnar and nano-laminated structures (i.e., multilayer coatings) [11] were introduced to significantly improve the multi-functionality of the coating layer. This is accomplished by reducing the brittleness of hard coatings [12], and at the same time providing simultaneous frictional energy accumulation from the resistance to severe plastic deformation and dissipation via crack deflection [13, 14]. In their work, Hovsepian et al. [15] have shown that CrAlYN/CrN nano-scale multilayer coated end mills outperform a range of TiAlN based PVD coatings during dry high-speed machining of hardened steel. In addition, previous investigations showed that the increased number of nano-layer interfaces which serve as sites for crack deflection [16] could consequently improve the impact fatigue resistance of coatings evaluated through nano-impact fracture resistance [17]. At the same time, it is very important to obtain a balance in optimum compressive residual stress to prevent excessive chipping under operating conditions [18].

Furthermore, coating architecture could be improved by incorporating an interlayer [19] with a potential to improve the coating's adhesion to the substrate. The high plasma density during the coating deposition process results in high energy ions which could lead to a superficial deterioration of cemented carbide substrate properties during deposition [20]. As a result, local adhesion could diminish. Conversely, deposition of these high kinetic energy ions favors their superficial diffusion into the Co rich binding materials, thus promoting better adhesion. Therefore, an interlayer is considered to benefit the coating structure if the combined effect improves coating adhesion. Previous works found in literature [21, 22] largely focus on improving monolayer coating adhesion through the incorporation of an interlayer. However, introducing an interlayer into a multilayer coating [23] can make the whole system very complex. For instance, according to the result of a previous work displayed in Figure 3.1, the TiAlCrSiYN/TiAlCrN multilayer coating with a TiAlCrN interlayer was shown to have improved adhesion than the multilayer coating [23]. This property was successfully determined by a micro-scratch test in terms of crack propagation resistance (CPRs) [24].

Moreover, recent research has shown that the thickness of the interlayer is equally crucial in achieving an overall coating structure strength and adhesion when adapted to the substrate roughness [25]. This could assure that the improved multifunctionality of the coating better serves the purpose of H13 dry milling. However, two opposing phenomena play an important role in deciding the thickness of the interlayer in a coating structure [22]. In the case of a very thin interlayer uncoated substrate regions may occur due to restricted

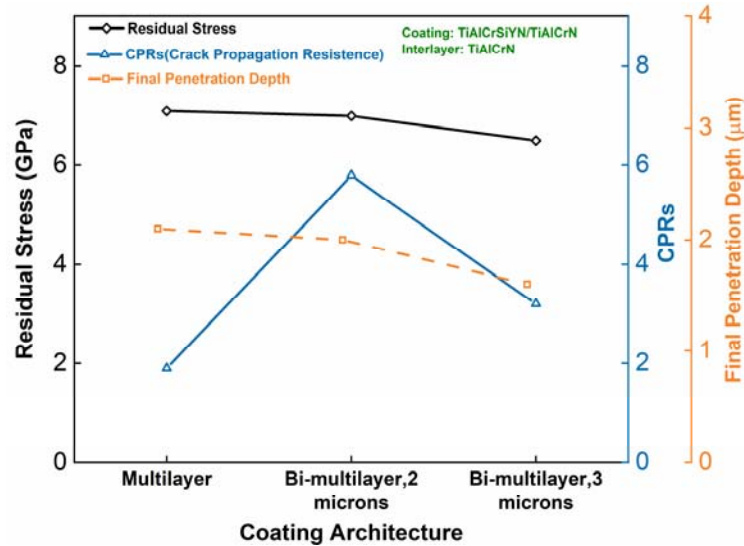


Figure 3.1 Comparison of micro-mechanical properties of a TiAlCrSiYN/TiAlCrN multilayer coating with a TiAlCrN interlayer [23].

substrate exposure to plasma flux caused by the reduction in deposition time as well as plasma flux shadowing effect. Thus, the coating deposited in these regions may possess a deteriorated adhesion as shown in Figure 3.2a. When the thickness of the interlayer is kept in the range of the substrate roughness  $R_t$  (Figure 3.2b), the average shear strain on the reference plane for an applied load is lower in comparison to the corresponding plane of a thicker interlayer. This is due to the fact that the reference plane in the first case includes both the coating and the substrate materials (Figure 3.2b), and thus contributes to a better shear stiffness on that plane. Again, as the adhesive interlayer thickness increases (Figure 3.2c), an interlayer fracture may develop due to the shear stress during operational load owing to the reduced mechanical properties of the interlayer.

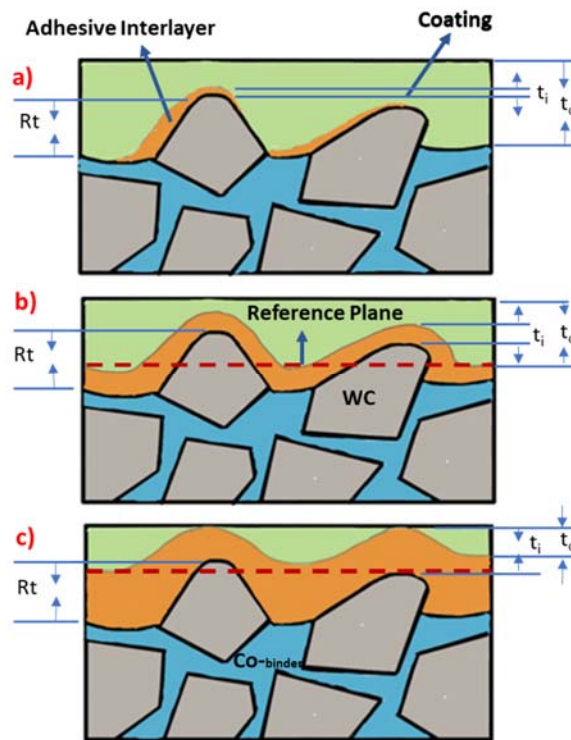


Figure 3.2 Schematic diagram of interlayer thickness effect on the coating substrate adhesion (a), and on the entire coating structure shear strength in a reference plane (b,c), with the same roughness of cemented carbide substrate [22];  $t_i$  and  $t_c$  represent interlayer and coating thicknesses respectively.

Considering the aforementioned dependencies, the selection of nano-interlayer thickness has to be appropriate with regard to the substrate topography as well as the coatings' overall mechanical and tribological properties. Therefore, the effect of TiAlCrN interlayer thickness on the overall coating properties was studied in this paper to optimize the coating performance in terms of its end application for high-speed H13 dry milling.

## 3.2 Experimental Details

### 3.2.1 Substrate Specification

In this study, solid cemented carbide Mitsubishi ball nose end mill (type: C-2SB, 10 mm diameter and two flute) was chosen as the tool substrate. In Figure 3.3a, an SEM image with back-scattered electron (BSE) at 12,000x magnification exhibits the microstructure of the tool substrate (hardness HV 1950–2000) [26] with an average WC grain diameter  $d_g$  (0.45  $\mu\text{m}$ ). Additionally, Figure 3.3b represents the surface profile of the tool substrate in terms of  $R_t$  (total height of the roughness profile) and  $R_a$  (arithmetical mean roughness value), which was measured by Alicona infinite focus at a roughness sampling length of 250  $\mu\text{m}$ .

### 3.2.2 Coating Deposition

The interlayer (TiAlCrN) was included into nano multilayered TiAlCrSiYN/TiAlCrN coating that has an architecture with modulating chemical composition but similar crystal structure. The initial thickness of the interlayer [21] was selected to be less than one third of WC grains' average diameter in the cemented carbide substrate. A further variation in interlayer thickness was considered by varying the duration of coating deposition to understand its effect on machining. Different interlayer thickness within TiAlCrSiYN-based multilayer coatings investigated in this study are presented in Table 3.1.

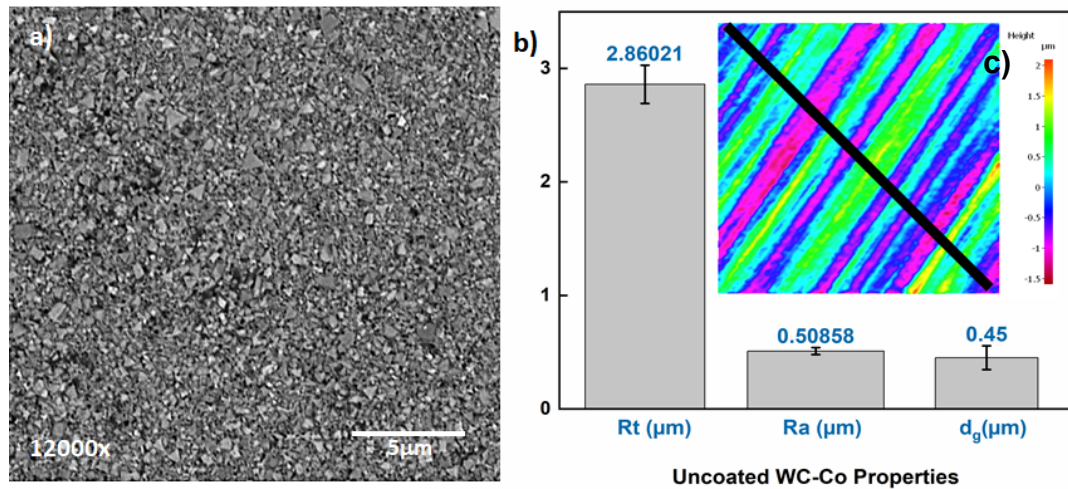


Figure 3.3 (a) Microstructure with back-scattered electron (BSE) at 12,000x magnification; (b) surface profile ( $R_t$  and  $R_a$ ) at a roughness sampling length of 250  $\mu\text{m}$  and average WC grain diameter  $d_g$  of the tool substrate; (c) surface profile of the substrate.

$\text{Ti}_{0.2}\text{Al}_{0.55}\text{Cr}_{0.2}\text{Si}_{0.03}\text{Y}_{0.02}$  and  $\text{Ti}_{0.25}\text{Al}_{0.65}\text{Cr}_{0.1}$  targets fabricated by a powdered metallurgical process were used for the deposition of a nano-multilayer  $\text{Ti}_{0.2}\text{Al}_{0.55}\text{Cr}_{0.2}\text{Si}_{0.03}\text{Y}_{0.02}\text{N}/\text{Ti}_{0.25}\text{Al}_{0.65}\text{Cr}_{0.1}\text{N}$  coating and an interlayer  $\text{Ti}_{0.25}\text{Al}_{0.65}\text{Cr}_{0.1}\text{N}$  of different thickness using a cathodic arc source. Coatings were deposited in an R&D-type hybrid PVD coater (AIP-SS002, Kobe Steel Ltd., Kobe, Japan) where samples were heated up to about 500  $^{\circ}\text{C}$  and cleaned through an Ar ion etching process at a pressure of 1.33 Pa and a bias of 400 V for 7.5 min.  $\text{N}_2$  gas was fed into the chamber at a pressure of 4 Pa. The arc source was operated at 150 A for a 100 mm diameter  $\times$  16 mm thick target. The rotation speed of the substrate holder was 5 rpm and the substrate bias was fixed at 150 V for all the depositions.



Table 3.1 Coatings studied for tool life and micro-mechanical property evaluation.

<b>Overall Thickness</b>	<b>Interlayer Thickness</b>	<b>Deposition Time (Interlayer)</b>
2 $\mu\text{m}$	100 nm	1 min
2 $\mu\text{m}$	300 nm	3 min
2 $\mu\text{m}$	500 nm	5 min

### 3.2.3 Determination of Micro-Mechanical Properties of Coatings

The crystal structure and preferred orientation of the coatings were determined with X-ray diffraction (XRD, Rigaku ULTIMA-PC, Rigaku, Tokyo, Japan) using Cu K $\alpha$  radiation. The residual stress was assessed by means of a conventional X-ray diffractometer, using the multiple *hkl* method [27, 28]. In this method, Cu K $\alpha$  radiation beam with glancing incidence angle of 5.0° was used, combined with a parallel beam geometry.

Nano-indentations on coatings were performed using a P-3 Micro Materials NanoTest system (Platform-3, Micro Materials Ltd., Wrexham, UK) in a load-controlled mode with a Berkovich diamond indenter. Initially a multiple load cycle experiment (depth profiling) with an increasing load from 5 to 100 mN was carried out to evaluate the depth dependent hardness variation within the studied coatings as well as to determine the appropriate load that ensures the indentation contact depth to be less than 1/10 of the film thickness during static indentation. Thus, a coating-only (load-invariant) hardness could be measured in combination with coating-dominated elastic modulus. Five depth profiles with 20 cycles in each sample were conducted at a loading rate of 25 mN/s with 50% unloading at each cycle of a particular indentation. Following this step, 40 indentation tests were performed on each coating at a peak load of 40 mN to diminish any effect of surface roughness on the data.

Ramped load micro-scratch testing to a peak load of 5 N was performed with an Anton Paar Revetest Micro Scratch Tester (Anton Paar, Peseux, Switzerland) using a 3-scan procedure with a 20  $\mu\text{m}$  radius diamond probe to increase the sensitivity of the test to interfacial adhesion [29]. Three sequential scans were involved in this procedure, topography-scratch-topography at 0.78 mm/min: (i) a pre scan at low load (0.5 N) over a 500  $\mu\text{m}$  track; (ii) a progressive load scratch: the load was ramped at a constant rate of 7.02 N/min until 5 N was reached just before the end of the scan; and (iii) a post-scan, at the same low load as the pre-scan. The scans were performed in the same direction and at least 3 scratch tests were carried out on each sample, with neighboring tracks separated by 200  $\mu\text{m}$ . Depending on the results obtained from the ramped load scratch tests, a subcritical load of 1.5 N (explained in Section 3.2) was selected for multi-pass constant load repetitive wear tests on a track of 1000  $\mu\text{m}$ . In these 15-scan tests, the progression of wear was assessed by changes in the depth measured under load (the on-load wear depth).

The fatigue properties of the desired coatings were encountered through nano-impact testing at an ambient temperature with a cube corner indenter serving as an impact probe. The indenter was accelerated from 12  $\mu\text{m}$  above the coating surface with 25 mN coil force corresponding to the impact energy of 300 nJ to produce an impact every 4 s for a total test duration of 400 s. Ten repeat tests were performed at different locations on each sample. The coatings' nano-impact fatigue fracture resistance was assessed by the final measured impact depth and confirmed by microscopic analysis of impact craters.

### 3.2.4 Cutting Performance of Coated Tools

Cutting-tool life was studied under the conditions outlined in Table 3.2. At least three cutting tests were performed for each kind of coating under the corresponding conditions on a three-axis vertical milling center (Matsuura FX-5, Matsuura Machinery Corporation 1-1, Fukui-City, Japan) to ensure repeatability. The scatter of the tool-life measurements was approximately 10%. Cutting tests were carried out on hardened AISI H13 tool steel workpiece having a hardness of HRC 53–55. The coated tool wear was measured using an optical microscope (Mitutoyo model TM, Mitutoyo Corporation, Kawasaki, Japan). Additionally, a tool dynamometer (9255B, Kistler, Winterthur, Switzerland) was used to measure the cutting forces.

Table 3.2 Cutting parameters used for the tool-life evaluation.

Cutting parameters				
Speed, m/min	Feed, mm/tooth	Axial Depth, mm	Radial Depth, mm	Coolant
600	0.06	5	0.6	Dry condition

## 3.3 Results and Discussion

### 3.3.1 Structural Analysis

Comparative structural analysis of the nano-multilayer coatings with different interlayer thickness is presented in Figure 3.4. All nano-multilayered coatings have a columnar structure with alternating nano-layers of 20–40 nm [23] and the interlayer thicknesses are 100 nm (Figure 3.4a), 300 nm (Figure 3.4b), and 500 nm (Figure 3.4c). It was previously shown that the alternating nano-layers are TiAlCrSiYN and TiAlCrN [23].

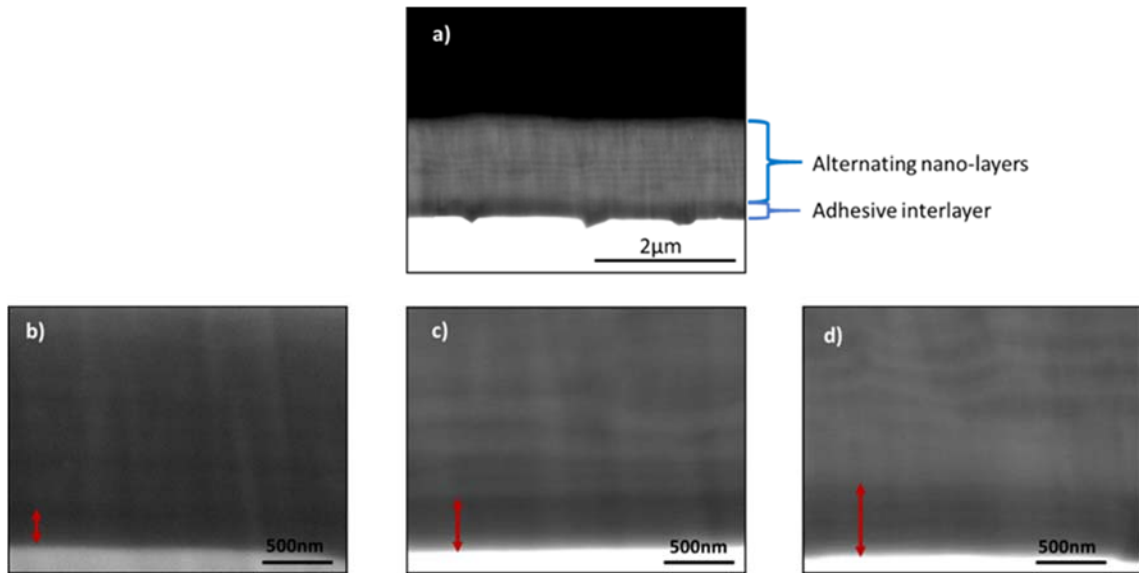


Figure 3.4 SEM images of the focused ion beam (FIB) cross-section showing (a) alternating nano-layers, the interlayer in the studied multilayer coatings, and the variation of interlayer thickness (b) ( $100 \pm 30$  nm), (c) ( $300 \pm 30$  nm), and (d) ( $500 \pm 30$  nm).

X-ray diffractograms of all the coatings studied are presented in Figure 3.5. It can be seen that all coatings exhibit a B1 crystal structure with the preferred orientation being C(200), which is a strong function of the substrate bias during coating deposition [30]. As previously seen, the introduction of TiAlCrN interlayer did not result in any evidence of microstructure changes such as peak position shifting and broadening [23]. No effect of the interlayer thickness on the diffraction peak intensity is observed in this study. Thus, the result indicates that the effect of TiAlCrN interlayer thickness variation on the microstructure of TiCrAlSiYN- based multilayer coatings is negligible. A similar kind of result was also observed elsewhere [19].

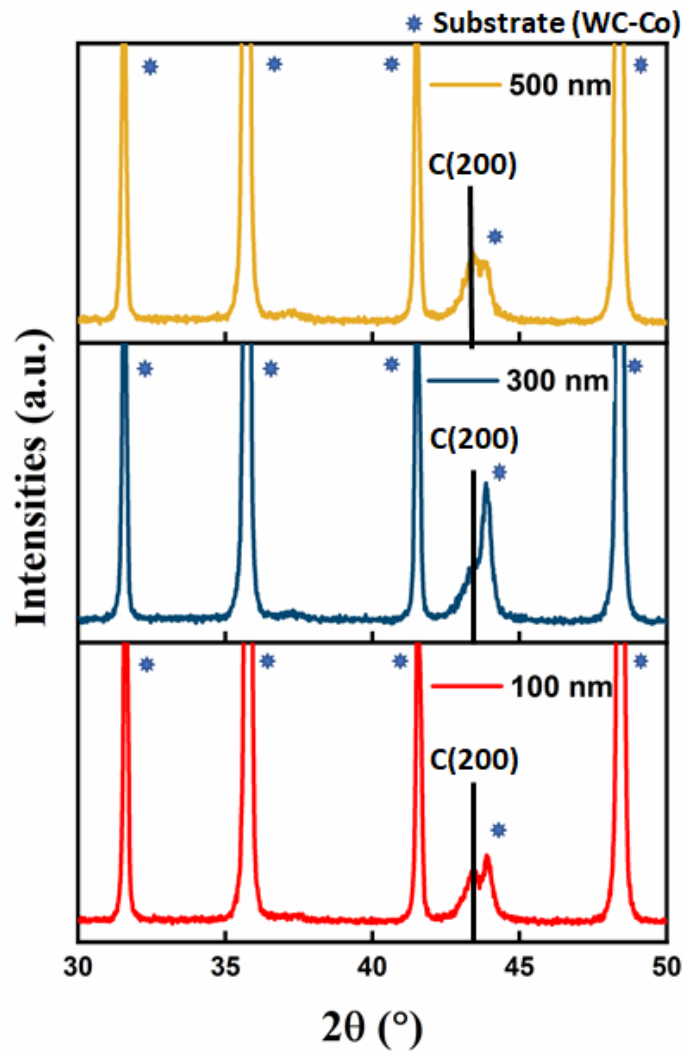


Figure 3.5 X-ray diffraction patterns of TiAlCrSiYN-based coatings with different interlayer thickness from 100 to 500 nm. Mark C represents the cubic (B1) phase.

### 3.3.2 Micro-Mechanical Property Analysis

The residual stress in all the coatings are highly compressive as depicted in Table 3.3. For the coatings deposited under specified conditions, a similar range of residual stresses was observed elsewhere [31]. This high compressive residual stress is beneficial for avoiding

excessive chipping of the cutting edge during the heavy loaded and high temperature conditions associated with dry milling.

Table 3.3 Residual stress in the studied coatings when  $E$  is 500 GPa for all crystal axis.

Coating	TiAlCrN Interlayer Thickness (nm)	Residual Stress (GPa)
TiAlCrSiYN/TiAlCrN Multilayer	100	$-8.21 \pm 1.39$
	300	$-8.64 \pm 1.65$
	500	$-8.71 \pm 1.47$

The inclusion of Si and Y in TiAlCrN (Residual stress  $-5.65 \pm 0.3$  [23]) coating results in grain size refinement [32] and thus higher residual stress. Grain size refinement is also associated with the higher number of defects at the alternating nano-layer interface [33]. Hence, all multilayer coatings in this study possess a high compressive residual stress. It was previously observed that the incorporation of an interlayer within the coating [23] as well as an increase in overall coating thickness [34] can result in decreased compressive residual stress. The variation of residual stress with the coating thickness is related to the deposition time during the coating deposition process. Two opposing phenomenon decides the type and quantity of residual stress in the coating as such annealing at the temperature of the deposition process allows increase diffusion of atoms and thus relaxation of internal stress. On the other hand, the ion bombardment during the same process creates defects that diminish the diffusion kinetics and contribute to the internal stress. Thus, the factor playing the dominant role during coating deposition decides the type and quantity of residual stress.

It is evident in the present study that the variation of interlayer thickness has a negligible effect on the overall residual stress of the coatings.

The depth dependent hardness of TiAlCrSiYN/TiAlCrN multilayer coatings with varying TiAlCrN interlayer thickness is shown in Figure 3.6a. Although the hardness of the coating systems at a lower penetration depth is similar, the multilayer coating with a 500 nm interlayer shows a steep decrease in its hardness value compared to the other two coatings at a penetration depth range of 200–300 nm. Static indentation hardness data in Figure 3.6b showed that the multilayer coating with a 500 nm interlayer has the lowest hardness of  $(31.99 \pm 1.588)$  GPa. This gradual decrease in the hardness value, alongside increasing TiAlCrN interlayer thickness can be attributed to the crucial role of the relatively

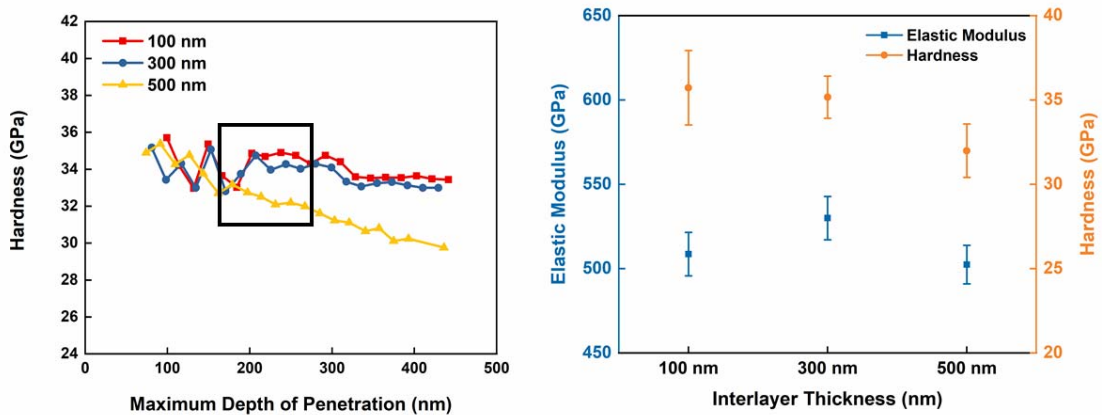


Figure 3.6 (a) Depth dependent hardness variation at a load range of 5–100 mN; (b) mechanical properties of the studied coatings obtained through nano-indentation tests (elasticity obtained by taking the Poisson's ratio of all coatings to be 0.25).

soft TiAlCrN interlayer ( $25.9 \pm 4.8$  GPa [23]), in energy dissipation and cushioning, which accommodates plastic deformation during indentation testing. Hence, more significant

cushioning activity is observed as the thickness of the TiAlCrN interlayer increases and the hardness of the coatings consequently decreases. In addition, a decrease in the hardness of multilayer coatings with similar elastic moduli (Figure 3.6b) resulted in the reduction of  $H^3/E^2$  as TiAlCrN interlayer thickness increased, as shown in Table 3.4.  $H^3/E^2$  parameter scales with greater load support (resistance to plastic deformation) [35], which indicates that a surface layer with better load support tends to be elastic for a longer period of time. The accompanying spatial localization of damage consequently mitigates the degradation of the structural and mechanical integrity of the entire surface engineered structure [36].

Table 3.4 Variation of dimensionless parameter  $H^3/E^2$  and  $H/E$  with the interlayer thickness.

<b>Coating</b>	<b>Multilayer</b>	<b>Multilayer</b>	<b>Multilayer</b>
Interlayer Thickness	100 nm	300 nm	500 nm
$H^3/E^2$ (Resistance to Plastic Deformation) (GPa)	0.17	0.15	0.12
$H/E$	0.07	0.066	0.063

The ramped load micro-scratch test signifies two important characteristics: as load is increased to  $L_{c1}$  there is an onset of cracking within the coating and a further increase of the load to  $L_{c2}$  causes a well-defined failure event that represents coating detachment in front of the probe. It is shown in Figure 3.7 (a,b) that the multilayer coating with a 300 nm interlayer has a slightly higher value of  $L_{c1}$ , whereas the coating with the 500 nm interlayer displays crack initiation at the lowest load of around 1.5 N among the coatings studied. Nonetheless, the load  $L_{c2}$  at which the coatings undergo adhesive failure, shows an increasing trend from the 100 nm interlayer to the 500 nm interlayer. This kind of critical load data from ramped load micro-scratch tests have been previously reported elsewhere



[37]. Additionally, Figure 3.8 (a–c) presents the microscopic images of the scratch track, which is the same for all the coatings studied, suggesting a brittle fracture dominated process. In the process, arc tensile cracks opening in the direction of the scratch (Figure 3.8a), are formed behind the scratch probe. These tensile cracks are then followed by coating chipping that extends laterally from the edges of the scratch groove. This kind of failure has been previously observed for hard coatings (Figure 3.8b) on a hard substrate (cemented carbide) [38].

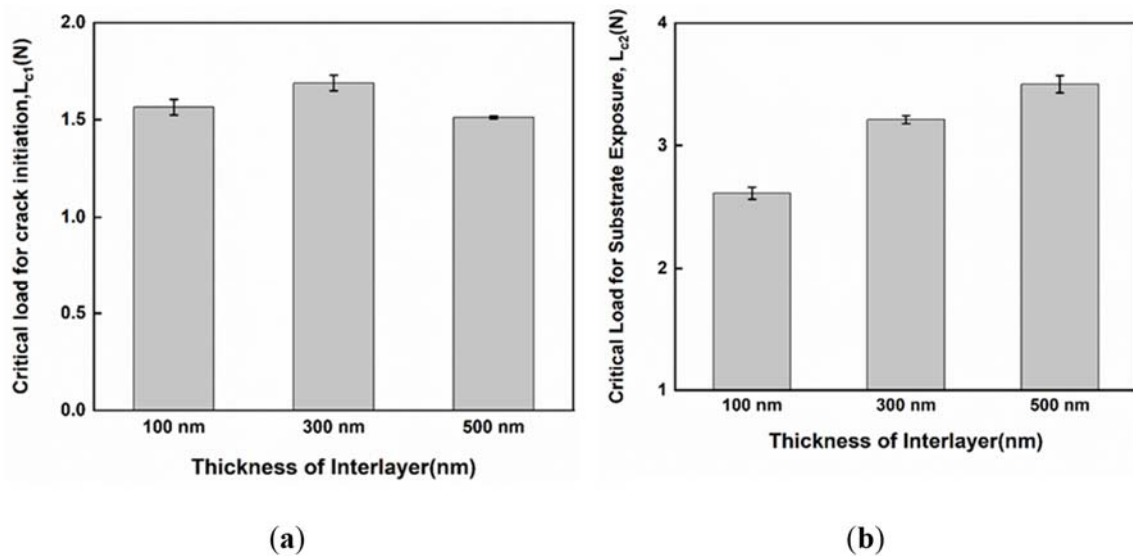


Figure 3.7 Comparison of (a) critical load for crack initiation in coating,  $L_{c1}$  and (b) critical load for coating failure,  $L_{c2}$  due to the variation of interlayer thickness within the multilayer coatings.

Previous works have shown that there is a correlation between the scratch test critical load  $L_{c2}$  and the mechanical properties of the coatings, essentially hardness and the ratio of hardness to elasticity ( $H/E$ ) [39, 40]. The nano-indentation data in Figure 3.6b, shows that at room temperature, the multilayer coating with a 500 nm interlayer has the

lowest hardness with elastic modulus of  $(502.35 \pm 11.42092)$  GPa, which results in the lowest  $H/E$  ratio for this coating. Hence, in the case of brittle fracture failure of the coating in the scratch test, multilayer coating with the 500 nm interlayer having lower  $H/E$  (Table 3.4) can function better due to improved ductility with increased critical load  $L_{c2}$ .

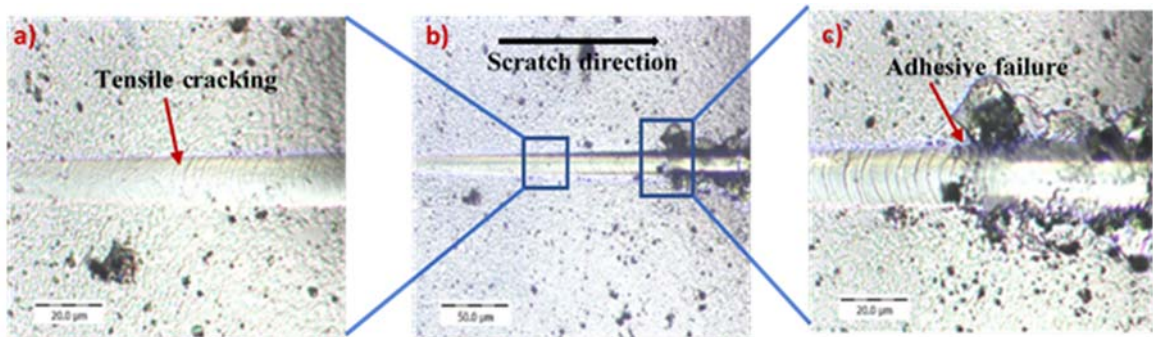


Figure 3.8 (a–c) Microscopic images of the ramped load scratch test track showing the cohesive (a) and adhesive (c) failure within the studied coating (same failure mechanism for all the studied coatings).

Furthermore, repetitive scratch tests performed at a subcritical load of 1.5 N (when all the studied coatings undergo crack initiation) are more sensitive to adhesion differences than the ramped load scratch test [41, 42]. Hertzian analysis was applied on the ramped load test data for each coating and the position of maximum von Mises stress was found to occur at a depth of  $\sim 1.5 \mu\text{m}$  below the free surface in the vicinity of the coating surface interface at a load of 1.5 N. Thus, observations from the repetitive scratch test at this load are more predominantly influenced by the coating layer than the deformation of the substrate. The repetitive scratch on load depth along with the relative performance of the coatings is illustrated in Figure 3.9 (a–d). For simplicity, only the passes where a significant change in depth was observed among the coatings are presented. The on-load scratch depth,

which combines both plastic and the elastic deformation is sufficient to interpret the wear progression with each consecutive pass. This is because the elastic contribution is

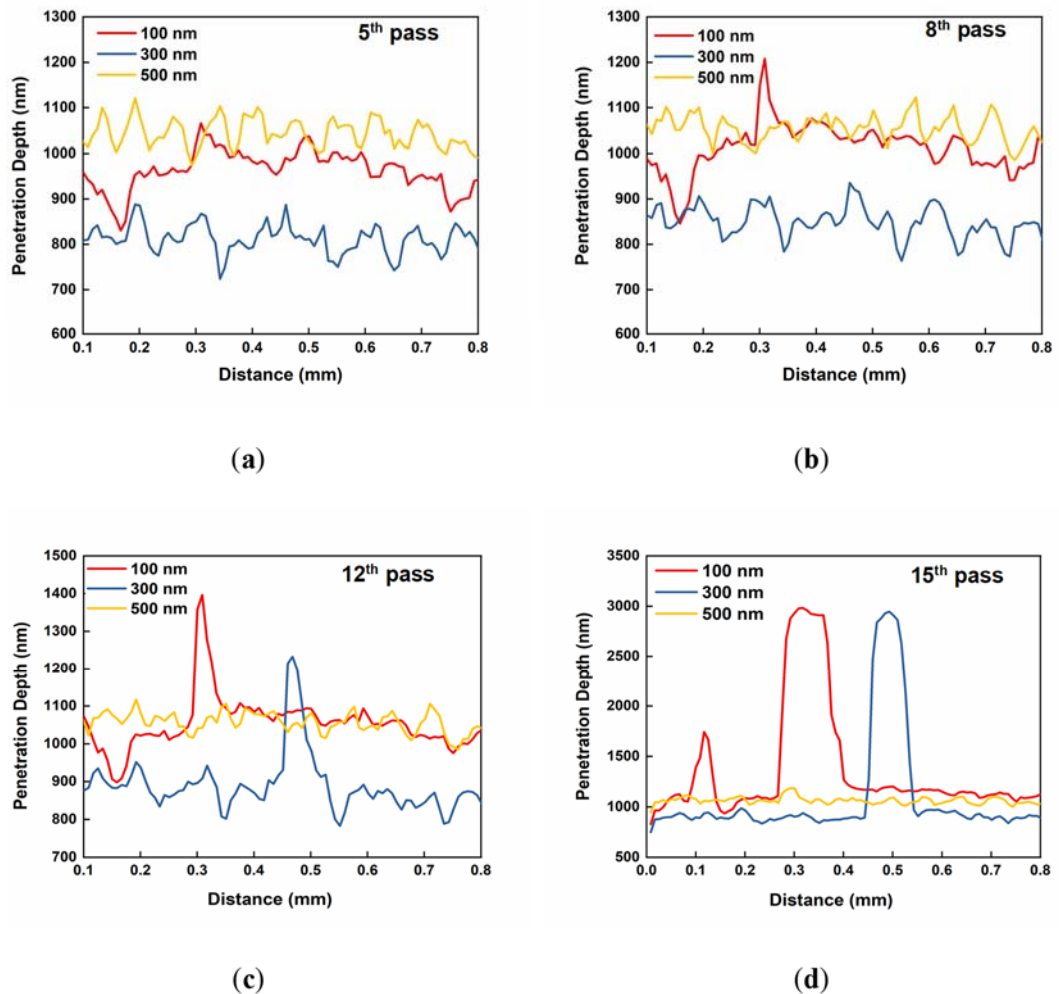


Figure 3.9 (a–d) Evolution of penetration depth at different passes during repetitive wear test at 1.5 N.

anticipated to be relatively constant during the tests. As depicted in Figure 3.9a, the penetration depth of the coating with a 300 nm interlayer is the lowest (around 800 nm) at the fifth pass, and highest for the one with a 500 nm interlayer (around 1050 nm). However,

after the next few passes, there is no significant change in the penetration depth for the coating with a 500 nm interlayer. The coating with a 100 nm interlayer shows the first sign of cohesive failure within the coating at the eighth pass (Figure 3.9b) in two of the three repeats. Evidence of cohesive failure in the coating with a 300 nm interlayer is found at the 11th pass (Figure 3.9c). At the 15th pass both coatings with the 100 and 300 nm interlayers exhibit adhesive failure at a scratch depth that exceeds the coating thickness, but with no noticeable change in the scratch depth for the coating with the 500 nm interlayer (only tensile cracks on the scratch track). Illustration of the scratch tracks of the studied coatings after the 15th pass is shown in Figure 3.10(a–c). It can be observed that by the end of the 15th pass, the multilayer coating with 100 nm interlayer has a mixture of low wear areas and total coating failure at several positions within the track, whereas the coating with a 500 nm interlayer shows no sign of fracture for the given load along the scratch track.

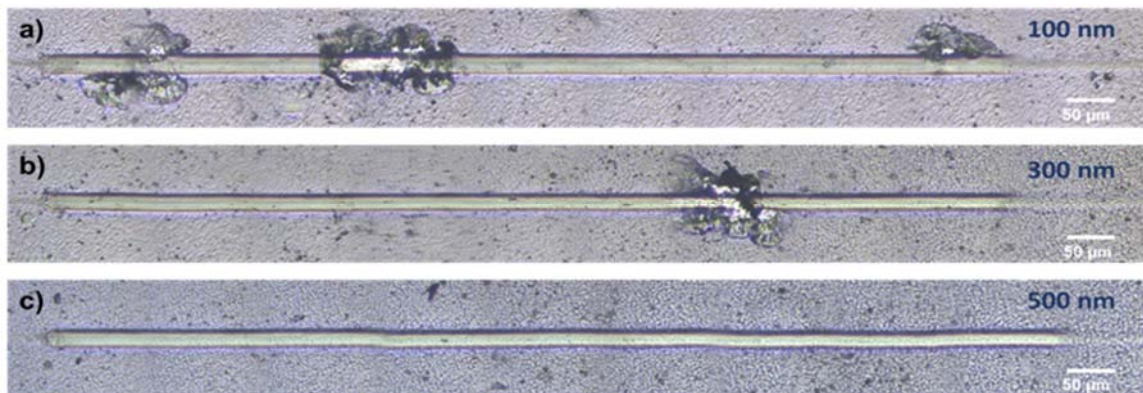


Figure 3.10 Microscopic images of the wear track after 15th pass at a repetitive load of 1.5 N, for coatings with interlayer thickness (a) 100 nm, (b) 300 nm, and (c) 500 nm.

The difference in wear resistance of the coating with a 500 nm interlayer that shows the highest initial penetration (consistent with its low near surface  $H/E$  and low  $L_{c1}$  in the

scratch test) but without failing after 15 cycles at 1.5 N can better explained in terms of the substrate roughness,  $R_t$ . It was previously observed [22] that a 50 nm Cr adhesive interlayer performed better than the 15 nm interlayer in the Pt–Ir coating on a cemented carbide substrate (precision glass molding tool material) of surface roughness  $R_t$  ( $60.1 \pm 8$ ) nm. Given the high surface roughness (Figure 3.1b) of cemented carbide substrate in the current study, the intense coating removal at an interlayer thickness of 100 nm (Figure 3.10a) compared to the 300 nm thick one (Figure 3.10b) can be explained by the non-uniform distribution of adhesive interlayer thickness on the substrate. The improvement of the coating's adhesion with the 300 nm interlayer, (which is even further improved in the 500 nm one) can be attributed to the increase in shear stiffness of the reference plane passing through the soft TiAlCrN interlayer as well as the TiAlCrSiYN/TiAlCrN coating itself (Figure 3.2b). However, a further increase in interlayer thickness can lead to adhesion deterioration when the reference plane only passes through softer interlayer.

The nano-impact test performed at 25 mN is presented in Figure 3.11a in terms of fracture probability variation with final probe penetration depth. Fracture probability was predicted by ranking the final depth of penetration to fracture events in order of increasing fatigue resistance and then assigning a probability of fracture  $P(f) = n/(N + 1)$  to the  $n$ -ranked fracture event in a total sample size of  $N (=10)$ , as was done previously [43]. It can be seen that both multilayer coatings with a 100 and 300 nm interlayer with better load support (higher  $H^3/E^2$  ratio) demonstrate the lowest final depths and only cohesive fractures. In addition, the spallation is more extensive in the 100 nm interlayer and much deeper ( $2.8 \pm 0.2 \mu\text{m}$ ) in the 500 nm interlayer (Figure 3.11e) than the multilayer coating with an

interlayer thickness of 300 nm ( $2.1 \pm 0.18 \mu\text{m}$ ). It can be said that in the nano-impact test, the 300 nm works more effectively to stop the total coating failure and substrate exposure. A combination of multilayer structure and interlayer thickness prevent cracks from

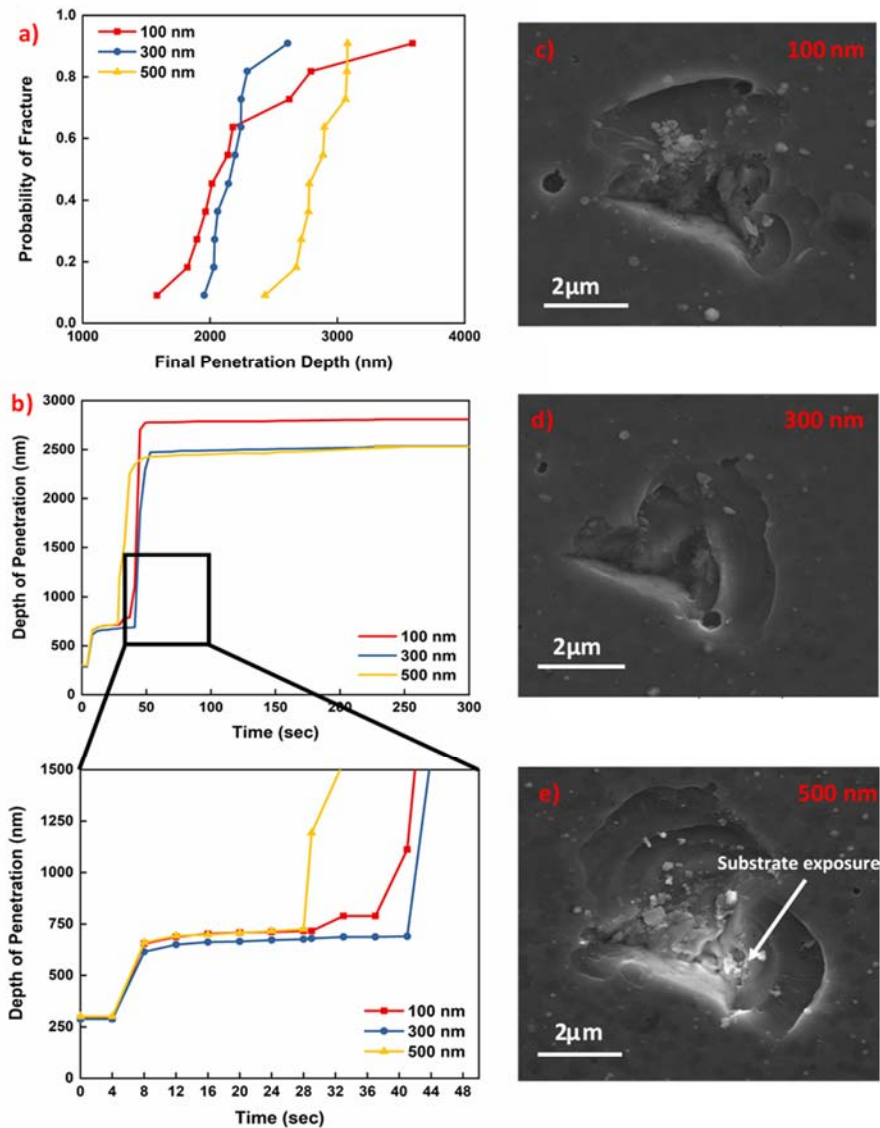


Figure 3.11 Nano-impact testing, (a) probability distribution vs final penetration depth; (b) penetration depth at a load of 25 mN; SEM image of the impact site for the coating with (c) 100 nm, (d) 300 nm, and (e) 500 nm interlayer.



propagating to the substrate. A similar phenomenon was previously observed [21] in a TiAlN coating with a 200 nm Cr/CrN graded interlayer that sustained repetitive impact loads more competently than corresponding interlayers of 50 and 600 nm under an inclined impact test.

Furthermore, as shown in Figure 3.11b all the studied coatings exhibit abrupt fracture at the given load where the multilayer coating with a 500 nm interlayer fails sooner than the other two coatings. This can be related to the fact that both multilayer coatings with a 100 and 300 nm interlayer have better load support (higher  $H^3/E^2$  ratio). Musil et al. [44] reported in a previous work that  $H^3/E^2$  ratio and coating thickness are both determining factors for crack resistance in micro indentation with a Vickers indenter where thicker and higher  $H^3/E^2$  ratio coatings have greater resistance. Additionally, data reported by Pei and co [45] shows that the onset critical load for indentation-induced radial cracking with a cube corner indenter correlates well with the  $H^3/E^2$  ratio at a range of 1.5  $\mu\text{m}$  nc-TiC/a-C:H film, ensuring that impact resistance of the coating is a combination of microstructural advantages as well as load support.

### 3.3.3 Tool Life Analysis

Tool life of the studied coatings investigated under extreme cutting conditions is presented in Figure 3.12. It can be observed that failure of the coated cutting tool is caused by flank wear (Figure 3.12a), rake wear (Figure 3.12b) (with minimal buildup edge formation), and predominantly, flank chipping (Figure 3.12c). This type of wear phenomenon was previously reported [11] under these severe cutting conditions where the machining

temperature can reach as high as 1000–1100 °C with stresses around 1.5–2 GPa [46]. A more gradual wear evolution is exhibited by the multilayer coating with a 300 nm interlayer. A 40% and 50% increase in tool life is observed in comparison to the 100 and 500 nm interlayer, respectively. Resultant cutting forces are presented in Figure 3.12d. Both multilayer coatings with a 100 and 500 nm interlayer have higher resultant forces than the 300 nm interlayer due to the high force contribution in the feed direction (in the 500 nm interlayer) and high force perpendicular to it (in the 100 nm interlayer).

Better wear characteristics and chipping behavior are a combination of both tribological and micromechanical properties of the coatings. The ramped load scratch tests and more significantly, the wear tests outlined above, demonstrated that the multilayer coating with a 100 nm interlayer has the worst performance in terms of adhesion of the coating to the substrate. This confirms that the coating undergoes a briefer machining length prior to tool failure than the multilayer coating with a 300 nm interlayer. The superior performance of the multilayer coating with a 500 nm interlayer in terms of adhesion is not consistent with its behavior in the cutting test. Therefore, the importance of micromechanical properties come into play. A better load support achieved through high  $H^3/E^2$  ratio for the multilayer coatings with 100 and 300 nm interlayer plays a crucial role in damage localization observed in nano-impact tests. This is more substantial for coatings with high brittleness as they are susceptible to radial cracking and catastrophic fracture as a leading failure mechanism typically seen in interrupted cutting conditions [47]. Thus, the multilayer coating with a 300 nm interlayer having improved micro-mechanical characteristics ensures lower intensity of surface damage compare to the 500 nm interlayer



and a better surface protection [48, 49]. Another important aspect to consider is the state of high temperatures during the milling process. Previous nanoindentation tests at temperature ranges between 25–600 °C on a TiAlCrSiYN/TiAlCrN multilayer coating [50] demonstrate that a drop-in hardness with no significant change in elastic modulus causes a steeper

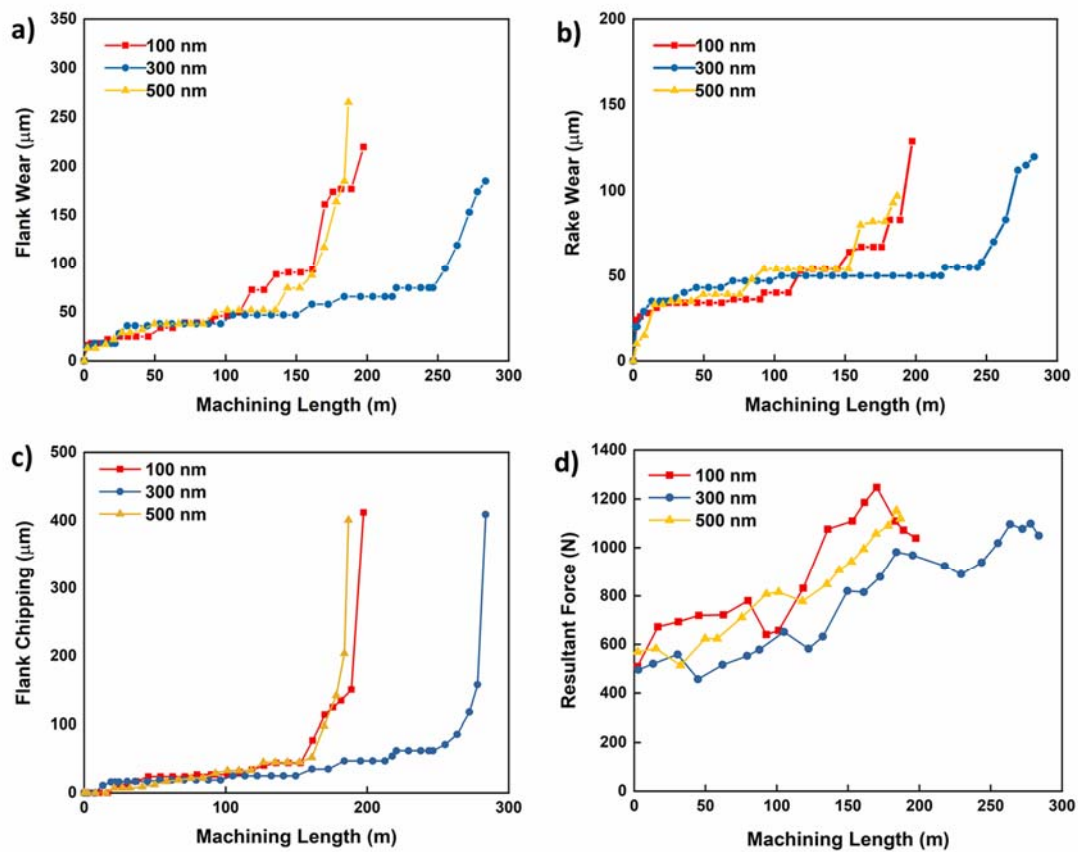


Figure 3.12 Tool-life data of the studied coatings vs. machining length (m): (a) flank wear; (b) rake wear; (c) chipping intensity; (d) resultant cutting forces.

decrease in the  $H^3/E^2$  ratio at a higher temperature. Additionally, Guiliani et al. reported a similarly significant hardness drop from 25 to 15 GPa occurring over a temperature range of 25–500 °C in AlN/CrN multilayered coatings on M2 tool steel, although the elastic

modulus was virtually unchanged [51]. Cross-sectional TEM of the indentations showed that the drop in measured hardness with temperature was due to the softening of CrN layers and/or changes in residual stress with temperature causing substrate and coating deformation. A similar phenomenon may occur in the studied TiAlCrSiYN/TiAlCrN multilayer coating, especially with a 500 nm TiAlCrN interlayer, which is already softer than the 100 and 300 nm interlayer at room temperature. The absence of yttrium in the composition of the interlayer hinders grain coarsening at the elevated temperature [52] and probably increases phase stability [53], possibly resulting in further softening of the coating with a 500 nm (the thickest) interlayer. Therefore, increasing plastic deformation causes a decrease in hardness as well as  $H^3/E^2$  ratio (already lowest at room temperature), which if too great, can be damaging to tool life.

### 3.4 Conclusions

In this paper, TiAlCrSiYN based multilayer coatings with varying interlayer thicknesses were systematically studied in terms of microstructure and micromechanical properties. A significant improvement in the wear performance of the TiAlCrSiYN-based coatings was achieved through the proper selection of the interlayer thickness within the multilayer coating structure. This result is attributed to the combination of the coating's micro-mechanical and tribological characteristics that control the tool life under extreme cutting conditions during high speed dry milling of hardened tool steel. The multilayer coating with a 300 nm interlayer has a better repetitive wear resistance resulting in better adherence to the substrate considering its high roughness. The coating also has better load support,

which can contribute to the localization of damage. This paper also suggests that a coating with good adhesion (500 nm interlayer) at room temperature can behave differently at a higher temperature during machining in terms of load support, which carries a significant importance during milling.

**Author Contributions:** “conceptualization, S.C.; methodology, S.C.; validation, S.C., B.B. and K.Y.; investigation, S.C., K.Y. ; resources, B.B, K.Y. and S.C.V.; data curation, S.C. , K.Y.; writing—original draft preparation, S.C.; writing—review and editing, B.B.; visualization, S.C.; supervision, B.B., S.C.V.; project and student supervision”

### 3.5 References

1. Fallböhmer, P., et al., *High-speed machining of cast iron and alloy steels for die and mold manufacturing*. Journal of Materials Processing Technology, 2000. **98**(1): p. 104-115.
2. Tönshoff, H., W. Bussmann, and C. Stanske. *Requirements on tools and machines when machining hard materials*. in *Proceedings of the Twenty-Sixth International Machine Tool Design and Research Conference*. 1986. Springer.
3. Nelson, S., J. Schueller, and J. Tlustý, *Tool wear in milling hardened die steel*. Journal of manufacturing science and engineering, 1998. **120**(4): p. 669-673.
4. Cui, X., J. Zhao, and X. Tian, *Cutting forces, chip formation, and tool wear in high-speed face milling of AISI H13 steel with CBN tools*. The International Journal of Advanced Manufacturing Technology, 2013. **64**(9-12): p. 1737-1749.
5. Elbestawi, M., et al., *High-speed milling of dies and molds in their hardened state*. CIRP Annals, 1997. **46**(1): p. 57-62.
6. Beake, B., et al., *Wear performance of different PVD coatings during hard wet end milling of H13 tool steel*. Surface and Coatings Technology, 2015. **279**: p. 118-125.
7. Chinchankar, S. and S. Choudhury, *Machining of hardened steel—experimental investigations, performance modeling and cooling techniques: a review*. International Journal of Machine Tools and Manufacture, 2015. **89**: p. 95-109.
8. Mativenga, P. and K. Hon, *A study of cutting forces and surface finish in high-speed machining of AISI H13 tool steel using carbide tools with TiAlN based coatings*.

- Proceedings of the Institution of Mechanical Engineers, Part B: Journal of Engineering Manufacture, 2003. **217**(2): p. 143-151.
9. Bouzakis, K.-D., et al., *Cutting with coated tools: Coating technologies, characterization methods and performance optimization*. CIRP Annals-Manufacturing Technology, 2012. **61**(2): p. 703-723.
  10. Fox-Rabinovich, G.S., et al., *Hierarchical adaptive nanostructured PVD coatings for extreme tribological applications: the quest for nonequilibrium states and emergent behavior*. Science and technology of advanced materials, 2012. **13**(4): p. 043001.
  11. Fox-Rabinovich, G., et al., *Structure, properties and wear performance of nanomultilayered TiAlCrSiYN/TiAlCrN coatings during machining of Ni-based aerospace superalloys*. Surface and Coatings Technology, 2010. **204**(21): p. 3698-3706.
  12. Voevodin, A.A., J.S. Zabinski, and C. Muratore, *Recent advances in hard, tough, and low friction nanocomposite coatings*. Tsinghua Science and Technology, 2005. **10**(6): p. 665-679.
  13. Chan, K., M. He, and J. Hutchinson, *Cracking and stress redistribution in ceramic layered composites*. Materials Science and Engineering: A, 1993. **167**(1-2): p. 57-64.
  14. He, M.Y., A.G. Evans, and J.W. Hutchinson, *Crack deflection at an interface between dissimilar elastic materials: role of residual stresses*. International Journal of Solids and Structures, 1994. **31**(24): p. 3443-3455.
  15. Hovsepian, P.E., C. Reinhard, and A. Ehiasarian, *CrAlYN/CrN superlattice coatings deposited by the combined high power impulse magnetron sputtering/unbalanced magnetron sputtering technique*. Surface and Coatings Technology, 2006. **201**(7): p. 4105-4110.
  16. Skordaris, G., et al., *Brittleness and fatigue effect of mono-and multi-layer PVD films on the cutting performance of coated cemented carbide inserts*. CIRP Annals-Manufacturing Technology, 2014. **63**(1): p. 93-96.
  17. Chen, J., H. Li, and B.D. Beake, *Load sensitivity in repetitive nano-impact testing of TiN and AlTiN coatings*. Surface and Coatings Technology, 2016. **308**: p. 289-297.
  18. Davim, J.P., *Machining: fundamentals and recent advances*. 2008: Springer Science & Business Media.

19. Hong, Y.S., et al., *Effects of Cr interlayer on mechanical and tribological properties of Cr-Al-Si-N nanocomposite coating*. Transactions of Nonferrous Metals Society of China, 2011. **21**: p. s62-s67.
20. Fernandes, C., et al., *Carbide phases formed in WC-M (M= Fe/Ni/Cr) systems*. Ceramics International, 2009. **35**(1): p. 369-372.
21. Bouzakis, K.-D., et al., *Adaption of graded Cr/CrN-interlayer thickness to cemented carbide substrates' roughness for improving the adhesion of HPPMS PVD films and the cutting performance*. Surface and Coatings Technology, 2010. **205**(5): p. 1564-1570.
22. Klocke, F., et al., *Adhesive interlayers' effect on the entire structure strength of glass molding tools' Pt-Ir coatings by nano-tests determined*. Surface and Coatings Technology, 2011. **206**(7): p. 1867-1872.
23. Chowdhury, S., et al., *Improvement of wear performance of nano-multilayer PVD coatings under dry hard end milling conditions based on their architectural development*. Coatings, 2018. **8**(2): p. 59.
24. Bull, S. and E. Berasetegui, *An overview of the potential of quantitative coating adhesion measurement by scratch testing*. Tribology International, 2006. **39**(2): p. 99-114.
25. Bouzakis, K.-D., et al., *The effect of substrate pretreatments and HPPMS-deposited adhesive interlayers' materials on the cutting performance of coated cemented carbide inserts*. CIRP annals, 2010. **59**(1): p. 73-76.
26. Ning, L., S. Veldhuis, and K. Yamamoto, *Investigation of wear behavior and chip formation for cutting tools with nano-multilayered TiAlCrN/NbN PVD coating*. International Journal of Machine Tools and Manufacture, 2008. **48**(6): p. 656-665.
27. Welzel, U., et al., *Stress analysis of polycrystalline thin films and surface regions by X-ray diffraction*. Journal of Applied Crystallography, 2005. **38**(1): p. 1-29.
28. Vermeulen, A.C., *Accurate absolute peak positions for multiple {hkl} residual stress analysis by means of misalignment corrections*. Z. Kristallogr., Suppl, 2006. **23**: p. 49-54.
29. Schwarzer, N., et al., *Optimization of the Scratch Test for specific coating designs*. Surface and Coatings Technology, 2011. **206**(6): p. 1327-1335.

30. Yamamoto, K., et al., *Properties of (Ti, Cr, Al) N coatings with high Al content deposited by new plasma enhanced arc-cathode*. Surface and Coatings Technology, 2003. **174**: p. 620-626.
31. Carvalho, N., et al., *Stress analysis and microstructure of PVD monolayer TiN and multilayer TiN/(Ti, Al) N coatings*. Thin Solid Films, 2003. **429**(1): p. 179-189.
32. Yamamoto, K., S. Kujime, and G. Fox-Rabinovich, *Effect of alloying element (Si, Y) on properties of AIP deposited (Ti, Cr, Al) N coating*. Surface and Coatings Technology, 2008. **203**(5): p. 579-583.
33. Mayrhofer, P.H., et al., *Microstructural design of hard coatings*. Progress in Materials Science, 2006. **51**(8): p. 1032-1114.
34. Bielawski, M., *Residual stress control in TiN/Si coatings deposited by unbalanced magnetron sputtering*. Surface and Coatings Technology, 2006. **200**(12): p. 3987-3995.
35. Hassani, S., et al., *Predictive tools for the design of erosion resistant coatings*. Surface and Coatings Technology, 2008. **203**(3): p. 204-210.
36. Bruet, B.J., et al., *Materials design principles of ancient fish armour*. Nature materials, 2008. **7**(9): p. 748.
37. Fox-Rabinovich, G., et al., *Effect of mechanical properties measured at room and elevated temperatures on the wear resistance of cutting tools with TiAlN and AlCrN coatings*. Surface and coatings technology, 2006. **200**(20-21): p. 5738-5742.
38. Bull, S., *Failure mode maps in the thin film scratch adhesion test*. Tribology international, 1997. **30**(7): p. 491-498.
39. Zeng, X., et al., *Comparison of three types of carbon composite coatings with exceptional load-bearing capacity and high wear resistance*. Thin Solid Films, 2002. **420**: p. 366-370.
40. Beake, B., V. Vishnyakov, and A. Harris, *Nano-scratch testing of (Ti, Fe) Nx thin films on silicon*. Surface and Coatings Technology, 2017. **309**: p. 671-679.
41. Beake, B., B. Shi, and J. Sullivan, *Nanoscratch and nanowear testing of TiN coatings on M42 steel*. Tribology-Materials, Surfaces & Interfaces, 2011. **5**(4): p. 141-147.

42. Beake, B., et al., *Elevated temperature repetitive micro-scratch testing of AlCrN, TiAlN and AlTiN PVD coatings*. International Journal of Refractory Metals and Hard Materials, 2017. **69**: p. 215-226.
43. Beake, B.D. and J.F. Smith, *Nano-impact testing—an effective tool for assessing the resistance of advanced wear-resistant coatings to fatigue failure and delamination*. Surface and Coatings Technology, 2004. **188**: p. 594-598.
44. Musil, J. and M. Jirout, *Toughness of hard nanostructured ceramic thin films*. Surface and Coatings Technology, 2007. **201**(9-11): p. 5148-5152.
45. Pei, Y., D. Galvan, and J.T.M. De Hosson, *Nanostructure and properties of TiC/aC: H composite coatings*. Acta materialia, 2005. **53**(17): p. 4505-4521.
46. Trent, E.M. and P.K. Wright, *Metal cutting*. 2000: Butterworth-Heinemann.
47. Fox-Rabinovich, G., et al., *Emergent behavior of nano-multilayered coatings during dry high-speed machining of hardened tool steels*. Surface and Coatings Technology, 2010. **204**(21): p. 3425-3435.
48. Fox-Rabinovich, G., et al., *Evolution of self-organization in nano-structured PVD coatings under extreme tribological conditions*. Applied Surface Science, 2014. **297**: p. 22-32.
49. Fox-Rabinovich, G., et al., *Spatio-temporal behaviour of atomic-scale tribo-ceramic films in adaptive surface engineered nano-materials*. Scientific reports, 2015. **5**: p. 8780.
50. Fox-Rabinovich, G., et al., *Mechanism of adaptability for the nano-structured TiAlCrSiYN-based hard physical vapor deposition coatings under extreme frictional conditions*. Journal of Applied Physics, 2012. **111**(6): p. 064306.
51. Giuliani, F., et al. *Indentation of AlN/CrN Multilayers from Room Temperature to 400 C*. in *Materials Science Forum*. 2005. Trans Tech Publ.
52. Fox-Rabinovich, G., et al., *Nanocrystalline coating design for extreme applications based on the concept of complex adaptive behavior*. Journal of Applied Physics, 2008. **103**(8): p. 083510.
53. Rovere, F., et al., *Experimental and computational study on the effect of yttrium on the phase stability of sputtered Cr–Al–Y–N hard coatings*. Acta Materialia, 2010. **58**(7): p. 2708-2715.



## **Chapter 4. IMPROVEMENT IN COATED CARBIDE TOOL LIFE FOLLOWING THE APPLICATION OF SURFACE TREATMENT TECHNIQUE-WIDE PEENING CLEANING (WPC) WHILE WET MILLING OF H13 TOOL STEEL**

Manuscript submitted for peer review

Shahereen Chowdhury, Bipasha Bose, Abul Fazal M. Arif and Stephen C. Veldhuis

The (AlCrN-TiAlN) bi-layer PVD (physical vapor deposition) coating was post-treated by a wide peening cleaning (WPC) process at various pressures and times. The micro-mechanical and adhesion properties of the studied coatings were evaluated in terms of their effects on machining performance during the wet milling of H13 tool steel. A comprehensive characterization of the cutting-edge geometry was performed by infinite focus microscope and EDX micro-analyses. Micro-mechanical and adhesion properties of the studied coatings were analyzed by nanoindentation, a nano impact test, ramped load scratch test, a repetitive load wear test and SEM. The wear performance was found to be associated with the fatigue resistance, which was improved by micro-mechanical characteristics, such as,  $H^3/E^2$  ratio and yield stress. Coating adhesion deteriorated as WPC pressure increased. The data of critical load for crack initiation ( $L_{c1}$ ) and the wear evolution at a subcritical load of 1 N demonstrated this gradual deterioration in coating adhesion. However, the tool life was improved by 35% at a pressure of 0.2 MPa due to the superior balance found between fatigue resistance and coating adhesion.

### **4.1 Introduction**

AISI H13 hardened steel is widely used as hot work dies and molds due to the combined properties of high hot hardness and toughness [1]. It also possesses high-temperature strength and wear resistance [2]. A traditional die/mold manufacturing process comprises of conventional machining of H13 in the annealed (soft) state followed by electro-discharge machining (EDM) and manual polish/finish grinding. Considering the low material removal rate of EDM and the formation of surface damaged layer by both methods [3], in recent times, direct milling of H13 (HRC 45-48) in its hardened state has become



widespread for competitive finish and semi-finish process [4-6]. Also, the selection of high feed rate during milling can assure high material removal rate and reduction in lead time. Moreover, recent development in tool materials has also enabled direct milling of H13 process with an advantage of elimination of part distortion caused by heat treatment [7]. Nevertheless, excessive tool wear [8, 9] mostly dominated by flank, crater and edge chipping [10] due to poor low cycle fatigue performance [9, 11] is a major concern during interrupted cutting of H13. This is more crucial in wet milling where thermal fatigue limits the tool performance [12]. Henceforth, much importance has been given to determine the best tool materials [8], machining strategies [13] and operating parameters [11] while milling of H13.

Recent progress in coating deposition techniques [14] offered a widespread use of nano-crystalline PVD (physical vapor deposition) coatings such as AlTiN [15] with high fatigue fracture resistance [16, 17], AlCrN-based coatings [18, 19] with improved micro-mechanical properties [20, 21] and AlCrN-TiAlN bi-layer coating with better adhesion [22] for surface engineering of carbide tools during milling of H13 (42 HRC and over) [22]. Consequent protection from thermal and mechanical loads is the cutting tool is achieved [12]. However, lower compressive residual stress or tensile stress in the coating layer could lead to the formation of surface cracks and delamination of a coating from the substrate [23]. More importantly this has a detrimental effect on the fatigue life of the coated cutting tools during milling. However, compressive residual stress induced into the coating can be used to strengthen it, because more energy would then be needed to initiate a crack.

At the present, the mechanical surface treatment of a coating is one of many ways to induce surface compressive residual stress into the coating system [24, 25]. Recent developments in mechanical surface treatments of coated tools demonstrate that most of the research works focused on micro-blasting of coated tools for milling operation [26-29]. This confirms that mechanical surface treatment can enhance tool life during milling where low cycle fatigue resistance of tools plays an important role. Furthermore, an elaborate analysis of various process parameters associated with micro-blasting exhibited the influence of type [26] and size of shot particle [27], the medium of shot particle delivery [28], process pressure and process duration [29] upon surface integrity, microstructure, micro-mechanical properties and cutting performance of coated tools. Moreover, some surface treatment techniques such as micro shot peening [30], laser ablation [31], fine particle bombarding [32] were also used for treatment on uncoated tools.

However, the wear mechanisms and the tool wear patterns of the post treated coating are seldom explored in literature for milling of H13. No previous investigation was found with regards to the coating's substrate adhesive properties following a post treatment process which involved inducing compressive residual stress to strengthen the surface. Under the given circumstances, adhesion becomes a key property in predicting the performance of the post-treated coated tool.

The present work involves WPC (wide peening cleaning), a fairly new technique in the branch of mechanical surface treatment [Japan Patent No. 1594395] with better control of the process parameters where peening particles impact the surface at a much higher velocity compared to the regular peening. As a result, a near surface compressive residual

stress is induced [33] where the depth of residual stress can be altered by careful selection of the diameter of the shots. The peening pressure which controls the velocity of the peening particles with carrier air flow speed also controls the degree of deformation of the peened surface. Another factor is process duration, in which smaller particles produce more impacts per pound, thereby requiring less exposure time. Therefore, this technique with little previous research, which too is limited to the bulk materials [33], can provide an alternative to other mechanical surface treatment processes for coated cutting tool.

The goal of this paper is twofold: 1) to identify tool wear patterns for coated end mills following the application of WPC post treatment and 2) to investigate the effect of micro-mechanical and adhesion properties of WPC post treated tools on the wear behaviour during wet milling of hardened H13 tool steel.

## **4.2 Experimental Details**

### **4.2.1 Coating deposition**

The hard coating investigated in this research was synthesized using Oerlikon Balzers Rapid Coating System (RCS) in the cathodic arc ion plating mode [30]. The AlCrN–TiAlN bilayer coating deposited on the cemented carbide substrate (WC-6%Co) has an AlCrN functional layer deposited on the TiAlN supporting layer. TiAlN layer endures good adhesion and mechanical strength whereas AlCrN layer exhibits good oxidation resistance, hot hardness and low thermal conductivity [33]. A pure reactive nitrogen atmosphere was used during the deposition of the coating. The pressure during deposition was 3.5 Pa and the substrate temperature was held at 450 °C. The DC-substrate bias voltage was held at

–40 V during the deposition and targets were operated with ~3.5 kW. The thickness of the coating is  $1.8 \pm 0.2 \mu\text{m}$ .

#### 4.2.2 Post-treatment process

After deposition, the coating was subjected to wide peening cleaning (WPC) treatment performed using an injector-type system. In the described investigations spherical steel beads with average grain diameter of  $15 \mu\text{m}$  were used to conduct peening on AlCrN–TiAlN bilayer coating. The distance between the nozzle and substrate was set to 50 mm. As presented in Table 4.1, the air pressure was varied from 0.2 MPa up to 0.4 MPa, in steps of 0.1 MPa for a process duration of 4 seconds. Again, a variation in process duration of 2 seconds, 4 seconds and 8 seconds was achieved for an air pressure of 0.2MPa.

Table 4.1 WPC conditions applied on coatings studied for tool life and micro-mechanical property evaluation

Process time sec	Process pressure MPa	Process pressure MPa	Process time sec
	0.2		2
4	0.3	0.2	4
	0.4		8

#### 4.2.3 Determination of micro-mechanical properties of coatings

Nanoindentation on coatings was performed by Micro Materials NanoTest Platform 3 system (Micro Materials Ltd., Wrexham, UK) in a load-controlled mode with a Berkovich diamond indenter calibrated for load, displacement, frame compliance and diamond area function by indentation into a fused silica reference sample. A multiple load cycle

experiment (depth profiling) with increasing load from 5 mN to 100 mN was carried out in order to evaluate the depth dependent hardness variation within the studied coatings. 10 indentations with 20 cycles in each sample were accomplished at a loading rate of 25 mN/s with a 50% unloading at each cycle of an indentation.

The yield property of the studied coatings was evaluated with Anton Paar NHT<sup>3</sup> Nanoindentation tester (Anton Paar, Switzerland) using the sinus mode at a set frequency of 5 Hz. A spherical indenter with a radius of 20  $\mu\text{m}$  which allows progressive transition from elastic to elastic-plastic regime was employed at a load of 400 mN to derive the yield stress values. To obtain information on the statistical errors of these quantities, the underlying measurement was repeated ten times for the given load at a loading and unloading rate of 800 mN/min.

The fatigue properties of the desired coatings were encountered through nano-impact testing at an ambient temperature with a cube corner indenter as an impact probe. The same Micro-Materials Nano-Test system mentioned above was used for these tests. The indenter was accelerated from 12  $\mu\text{m}$  above the coating surface with 15 mN coil force corresponding to impact energy of 180 nJ to produce an impact every 4 s for a total test duration of 300 s. Five repeat tests were performed at different locations on each sample. The coatings' nano-impact fatigue fracture resistance was assessed by the final measured impact depth. Ramped load micro-scratch testing to a peak load of 5 N was performed with Anton Paar MST<sup>3</sup> Micro Scratch Tester (Anton Paar, Switzerland) using a 3-scan procedure with a 20  $\mu\text{m}$  radius diamond probe to increase the sensitivity of the test to interfacial adhesion. 3 sequential scans were involved in this procedure, topography-scratch-

topography, at 0.78 mm/min. These were (i) pre scan: scanning at low load (0.5 N) over a 500  $\mu\text{m}$  track (ii) progressive load scratch: the load is ramping at a constant rate of 7.02 N/min to reach 5 N just before the end of the scan (iii) post-scan, at the same low load as the pre-scan. The scans were performed in the same direction and at least 3 scratch tests were carried out on each sample, with neighboring tracks separated by 200  $\mu\text{m}$ . Depending on the results obtained from the ramped load scratch tests, a subcritical load of 1 N was selected for constant load repetitive micro scratch tests (micro-wear) on a track of 1000  $\mu\text{m}$ . In these 15-scans no. of passes required for the system to fail adhesively was pursued by changes in the depth measured under load (the on-load wear depth).

#### **4.2.4 Cutting performance**

Cutting tests with Kennametal carbide high feed end mills KMDA 1000A6ANA,  $D = 10$  mm were performed according to the requirements of the ISO 8688. Machining parameters used are shown in Table 4.2. At least three cutting tests were performed under the corresponding conditions on a three-axis vertical milling center (Matsuura FX-5, Matsuura Machinery Corporation 1-1, Fukui-City, Japan) to ensure repeatability. Comprehensive data on wear performance including flank wear, rake wear, average cutting forces and chipping intensity was reported. The post-treated coated tool wear and chipping was measured using a Mitutoyo optical microscope and a magnification of 30x. The accuracy of measurement was  $\pm 5$  microns.

Table 4.2 Cutting parameters used for the tool-life evaluation.

Cutting Parameter				
Speed, m/min	Feed, mm/min	Depth of cut, mm	Width of cut, mm	Coolant
160	15275	0.3	4	Wet condition

### 4.3 Results and Discussion

#### 4.3.1 Effect on cutting-edge geometry and coating roughness

To investigate the effect of WPC process pressure on the cutting-edge SEM, EDS (Figure 4.1) and infinite focus microscope scanning (Figure 4.3a) along the edges of variously post treated cutting tools were conducted. Corresponding investigations were also conducted to study the effect of WPC process time on the cutting edge as exhibited in Figure 4.2 and Figure 4.3b. It can be observed that the effect of WPC conditions on the cutting-edge is more intense, as pressure grows. Related result in Figure 4.1c shows that at a pressure of 0.4 MPa a local substrate revelation occurs on the cutting edge. The EDX microanalyses verify local coating removal at the pressure of 0.4 MPa, since the substrate chemical elements W and Co were intensified.

Also, there is an insignificant change in the cutting-edge radius with process pressure variation (Figure 4.3a) with only factor to take into consideration is that for the process pressure of 0.4 MPa cutting edge radius value is little less than that of the as deposited coating. This event can be a consequence of cutting-edge radius measurement points being at the position of local substrate revelation at this pressure. Similar data was previously observed for micro-blasting of TiAlN coating (3  $\mu\text{m}$  thick) [29] where up to the process

pressure of 0.4 MPa there was no significant change in cutting edge radius whereas further increase in pressure to 0.6 MPa during micro-blasting process, lead to a cutting edge geometry change as well as substrate revelation.

Variation of WPC process time has a minimal effect on the cutting-edge geometry at a constant process pressure of 0.2 MPa. Although for all the given process time cutting edge radius is slightly increased compared to the as deposited coating as shown in Figure 4.3b. Also, characteristics results from SEM images do not show any sign of substrate exposure with increasing process time as illustrated in Figure 4.2.

Roughness on the cutting tools measured for both WPC pressure and time variations are presented in Table 4.3 in terms of  $Ra$  (arithmetical mean roughness value) and  $Rt$  (total height of the roughness profile) value. It was measured by Alicona infinite focus microscope at a roughness sampling length of 250  $\mu\text{m}$ . Roughness increases with increasing process pressure and time ( in terms of  $Rt$  value) for the treated coatings, a pattern that has been previously observed elsewhere [34].

#### **4.3.2 Analysis of Micro-mechanical properties**

The depth dependence of hardness (multi-load cycle test) of WPC treated coatings at various process pressures are displayed in Figure 4.4a. Corresponding investigations were also conducted for process time variation as exhibited in Figure 4.4b. The selection of process parameters follow the similar trend obtained from the literature [29]. It is apparent that WPC post treatment on coatings results in an improved superficial hardness. This can



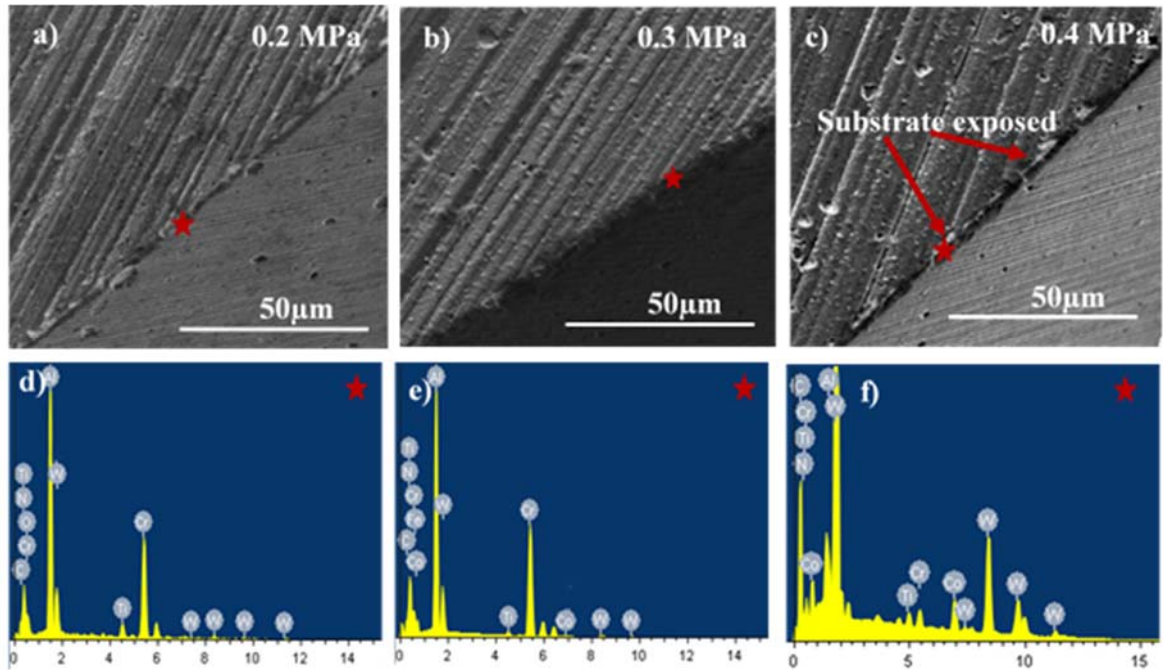


Figure 4.1 SEM image and corresponding point EDS on the cutting edges for variation of WPC pressure of (a, d) 0.2 MPa; (b, e) 0.3 MPa; (c, f) 0.4 MPa.

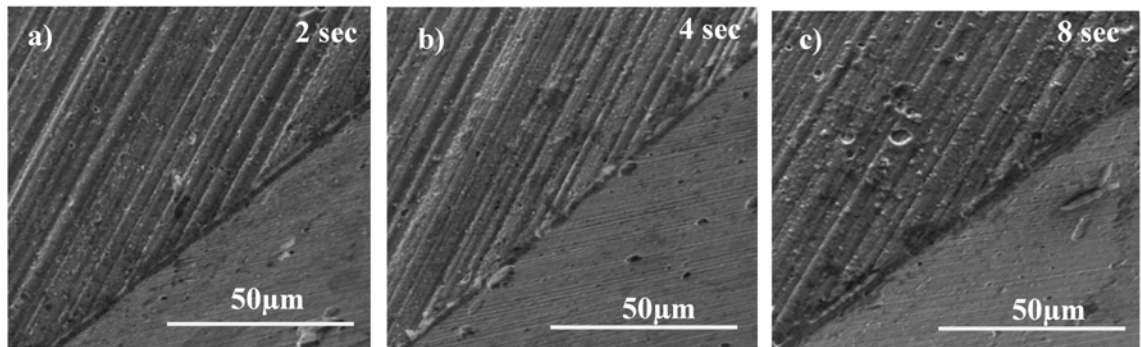


Figure 4.2 SEM image of the cutting edges for variation of WPC time of (a) 2 s; (b) 4 s; (c) 8 s.

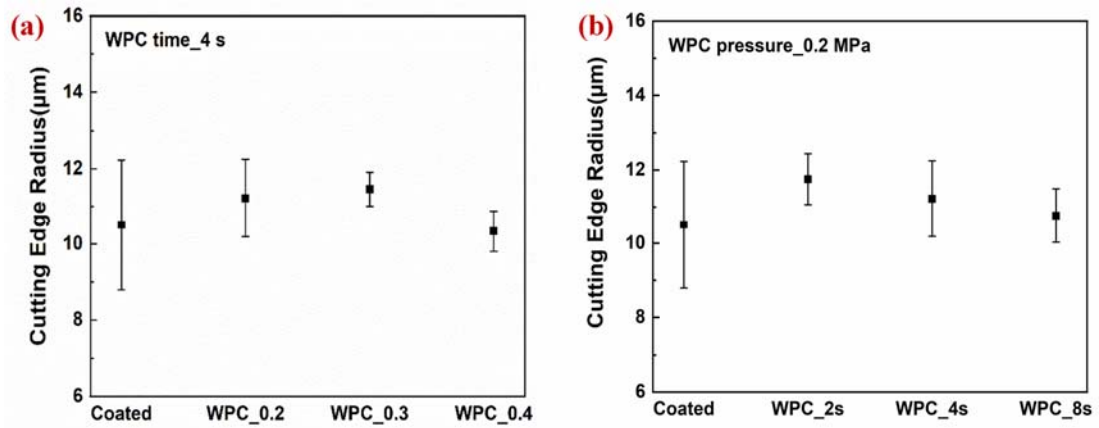


Figure 4.3 Cutting edge radius for (a) WPC process pressure variation for a process time of 4 s; (b) WPC process time variation for a process pressure of 0.2 MPa.

Table 4.3 Surface profile ( $Ra$  and  $Rt$ ) at a roughness sampling length of 250 μm due to the variation of WPC conditions

Coating		WPC time_4 sec					
		0.2 MPa		0.3 MPa		0.4 MPa	
$Ra(\mu\text{m})$	$Rt(\mu\text{m})$	$Ra(\mu\text{m})$	$Rt(\mu\text{m})$	$Ra(\mu\text{m})$	$Rt(\mu\text{m})$	$Ra(\mu\text{m})$	$Rt(\mu\text{m})$
		0.05	$0.68\pm 0.1$	0.06	$0.9\pm 0.1$	0.06	$1.01\pm 0.1$
0.05		WPC pressure_0.2 MPa					
		2 sec		4 sec		8 sec	
$Ra(\mu\text{m})$	$Rt(\mu\text{m})$	$Ra(\mu\text{m})$	$Rt(\mu\text{m})$	$Ra(\mu\text{m})$	$Rt(\mu\text{m})$	$Ra(\mu\text{m})$	$Rt(\mu\text{m})$
	$0.61\pm 0.1$	0.06	$1.1\pm 0.1$	0.05	$0.68\pm 0.1$	0.05	$0.82\pm 0.1$

be due to the compressive residual stress induced in the coating by peening particles during the treatment process [27]. The elastic modulus ( $E \approx 500$  GPa) was obtained from the nano-indentation test at 30 mN load. The value of elastic modulus is similar for both as deposited and treated coatings. Previous work [35] has demonstrated that there was no significant change in elastic modulus value of TiAlN coating following the application of dry micro-blasting post treatment.

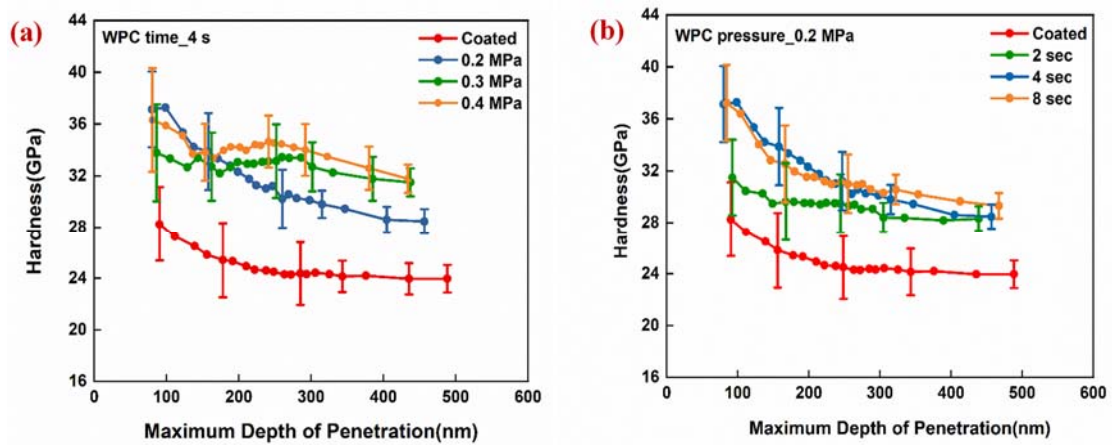


Figure 4.4 Depth dependent hardness variation at a load range of 5–100 mN (a) WPC process pressure variation for a process time of 4 s; (b) WPC process time variation for a process pressure of 0.2 MPa.

As illustrated in Figure 4.4 a, hardness of the treated coatings at a lower penetration depth is similar, yet a higher value of hardness at penetration depth over 300 nm is observed when WPC pressure increases to 0.3 MPa and above. This can be associated with a higher degree of deformation along the depth of the coating as WPC pressure increases. On the contrary, there is no consequential variation in hardness along the penetration depth when WPC process time is varied for a constant pressure of 0.2 MPa (Figure 4.4b).

In addition, increase in hardness with similar elastic modulus resulted in an increase of both  $H^3/E^2$  (Figure 4.5a) and  $H/E$  (Figure 4.5b) ratios along the penetration depth following the coating post treatment at various process pressures.  $H^3/E^2$  parameter scales with greater load support (resistance to plastic deformation) [36], an indication of surface layer being elastic for a longer period of time when a load is applied. This results in a spatial localization of damage and consequently mitigates the degradation of the structural and

mechanical integrity of the entire surface engineered structure [37]. Likewise,  $H/E$  ratio is a measure of brittleness of coatings [20, 38].

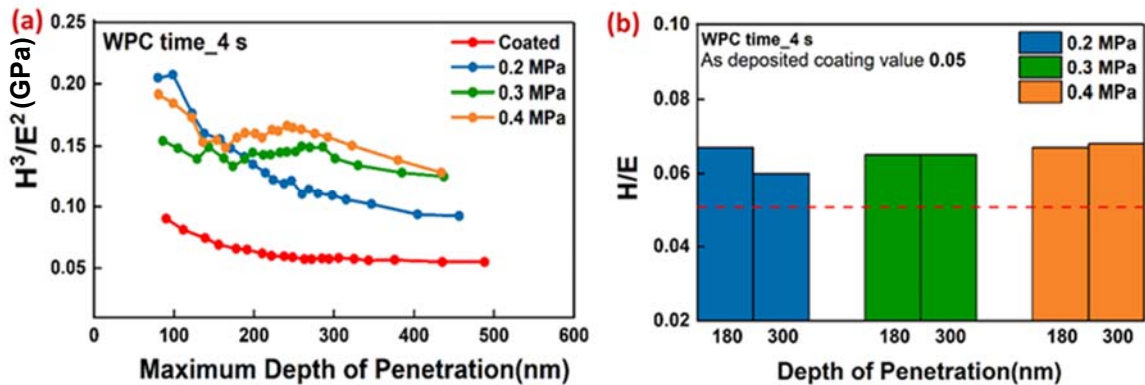


Figure 4.5 Depth dependent value of (a)  $H^3/E^2$  and (b)  $H/E$  ratio for WPC process pressure variation at a process time of 4 s. ( $E \sim 500$  GPa).

Table 4.4 Value of  $H^3/E^2$  and  $H/E$  ratio at a depth of penetration of 180 nm for WPC process time variation at a process pressure of 0.2 MPa ( $E \sim 500$  GPa)

Process Time	Treated Coating at WPC pressure_0.2 MPa			As Deposited
	2 sec	4 sec	8 sec	
$H^3/E^2$ (GPa)	0.104	0.155	0.141	0.065
$H/E$	0.058	0.067	0.065	0.05

Table 4.4 demonstrates the value of above-mentioned ratios (Figure 4.5) at a penetration depth of 180 nm (10% of the coating thickness) for process time variation. Post treatment of coatings at various process times resulted in a higher value of the same ratios compare to the as deposited one. However, the effect of process time variation on these values is minimal.

The load–penetration depth curve in Figure 4-6a was obtained by indenting the studied coatings with a 20- $\mu\text{m}$  diamond spherical indenter at 400 mN load. The indentation curve

exhibits an elastic recovery of around 70%-75% for all the studied coatings. It must be pointed out that the maximum indentation depth (400-550 nm) clearly surpasses 10%–15% of the coating thickness. However, a higher indentation load was selected to explain the behaviour of the studied coatings at a penetration depth range of 300-500 nm where a significant change in their hardness values is observed (Figure 4.4a). Furthermore, it was previously explained [38] that the existence of residual stress in a target material can cause a shift in the load-displacement curve compared to the stress-free state (reference state). In the present study, as deposited coating is the reference although it already possesses a pre-existing compressive residual stress [39]. From Figure 4-6a it can be depicted that coating treated at 0.4 MPa requires a greater indentation load ( $L_c$ ) to attain the same penetration depth of the as deposited one ( $L_o$ ). This is a consequence of a further increase in compressive residual stress due to the post treatment of coatings.

The stress-strain curves illustrated in Figure 4.6b. was also obtained using spherical indentation.

The representative strain is usually expressed as the ratio of contact radius  $a$  ( $\approx \sqrt{2Rh_c}$ ) and indenter radius  $R$ ;

$$\varepsilon_{\text{rep}} = 0.2 \left( \frac{a}{R} \right) \quad (1)$$

where  $h_c$  is the contact depth obtained during the indentation process and 0.2 is the yield factor. The representative stress can be calculated from mean contact pressure,

$$p_m \left( = \frac{P}{\pi a^2} \right) \text{ as}$$

$$\sigma_{\text{rep}} = \frac{P_m}{C} \quad (2)$$

where  $C$  is the plastic constrain factor. According to the previous work [40] the plastically deformed zone is small for hard materials ( $E/H < 40$ ) and surrounded by a relatively large elastic region. Thus, the elastic-plastic property of the given material affects the stress value. To characterize this property,  $E/H$  [40] parameter has been used and the value of this parameter is low ( $\approx 38$ ) for all coatings in the present study. Thus, a constrain factor of 1.5 (1.2 consider for DLC coatings) [41] was used to calculate the representative stress values in Figure 4.6b. However,  $E/Y$  parameter can only be used to categorize and compare materials if the indentation geometry remains constant, which in this study is attained by using a spherical indenter. The representative stress–strain curve illustrated in Figure 4.6b confirms that the applied mean pressure was high enough to cause the initial stages of yielding of the coatings. Thus, the point of curve slope change was denoted as the yield stress value for the studied coatings as shown in Figure 4.6(c, d). According to the results in Figure 4.6c, the yield stress of the as deposited coating is increased following the post treatment at various process pressure. Furthermore, the increase in process pressure also lead to an increasing yield stress for the treated coatings. A similar behavior was previously reported for wet micro-blasting of coatings at various process pressure [42]. However, yield stress of the treated coatings is practically unaffected (Figure 4.6d) by the process time variation.

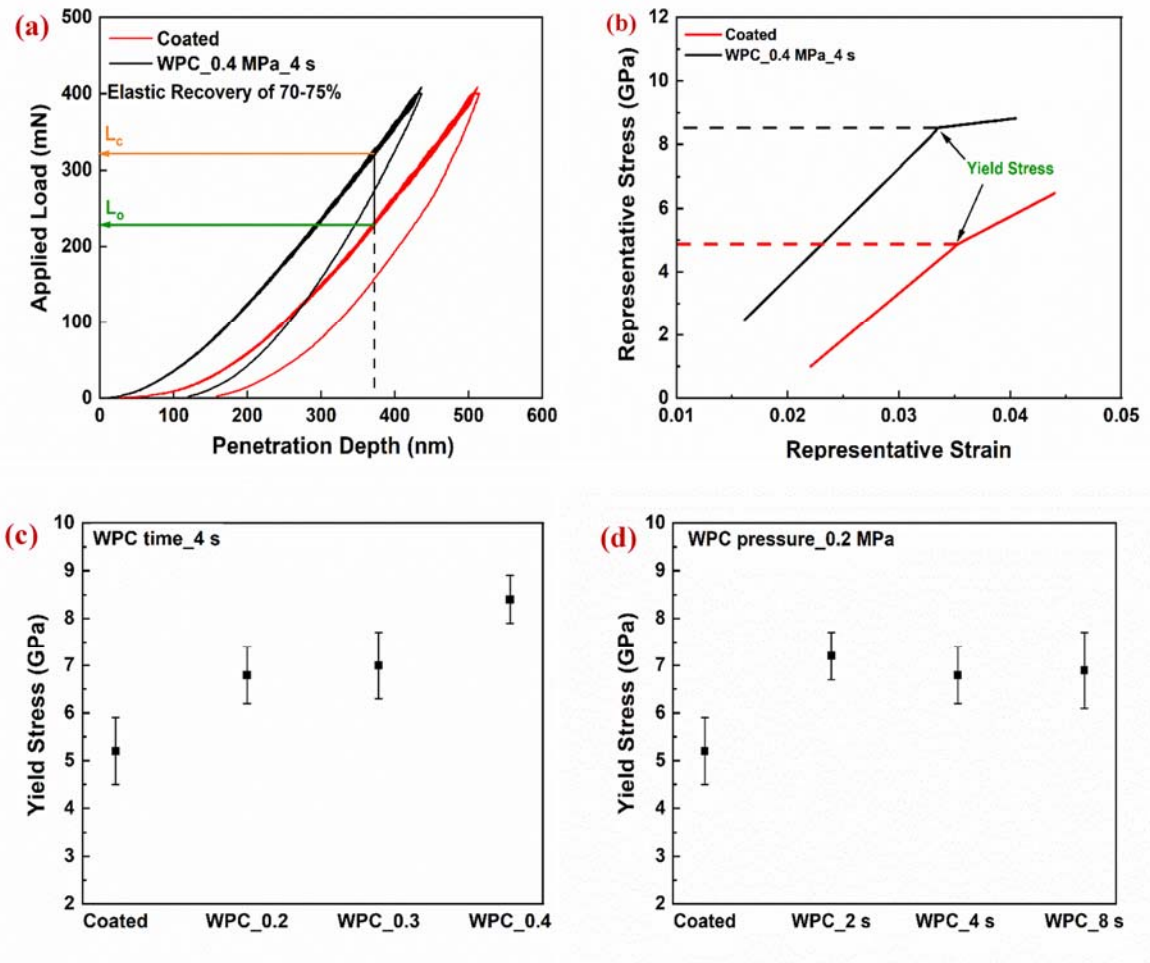


Figure 4.6 (a) load-depth penetration curve; (b) Representative stress vs strain , for as deposited coating and treated coating at a pressure of 0.4 MPa for 4 s; Comparison of yield stress for (c) WPC process pressure variation s; (d) WPC process time variation.

The nano impact test performed at 15 mN load allows repetitive impacts at the same spot on the sample surface at a set (0.25 Hz) frequency and continuous monitoring of the evolution of impact depth due to the progressing coating damage through an appropriate automation process[43]. The test data presented as final depth of penetration after 300 s of impact is considered as the measure of fatigue resistance [44] for both WPC pressure (Figure 4.7a) and time (Figure 4.7c) variation. Also, a difference between the final and



initial depth of penetration illustrated in Figure 4.7(b, d) can interpret coating behavior under subsequent impacts during the test. WPC treatment on coatings resulted in an improved fatigue resistance and the increase in depth due to repetitive impact (i.e. final depth–depth after initial impact) is also smaller compared to the as deposited one. Furthermore, a gradual decrease in final penetration depth is observed when both WPC pressure (Figure 4.7a) and time (Figure 4.7c) is increased. A similar trend is found in Figure 4.7 (b, d) for (final-initial) depth of penetration data. Additionally, it is depicted from Figure 4.7(b, d) inset that for as deposited coating the probe depth after a single impact is higher (around 1.5  $\mu\text{m}$ ) compare to the treated ones ( an average depth of 1.1  $\mu\text{m}$  except for treated coating at 0.2 MPa for 2 s). Coatings retain a better load support (higher  $H^3/E^2$  ratio) following the WPC treatment at various pressure (Figure 4.5a) and time (Table 4.4), hence relates well with the fatigue behaviour during the nano-impact test. Consequence resistance to an initial impact as well as damage tolerance under dynamic contact load is achieved by preventing cracks from forming in the first place. Musil et. al. [45] reported in a previous work that  $H^3/E^2$  ratio is a determining factor for crack resistance in micro indentation with a Vickers indenter where higher  $H^3/E^2$  ratio coatings have greater resistance to crack initiation. Also, data reported by Pei and co [46] shows that the onset critical load for indentation-induced radial cracking with a cube corner indenter correlates well with the  $H^3/E^2$  ratio at a range of 1.5  $\mu\text{m}$  nc-TiC/a-C: H film, ensuring that impact resistance of the coating is a combination of microstructural advantages as well as load support.



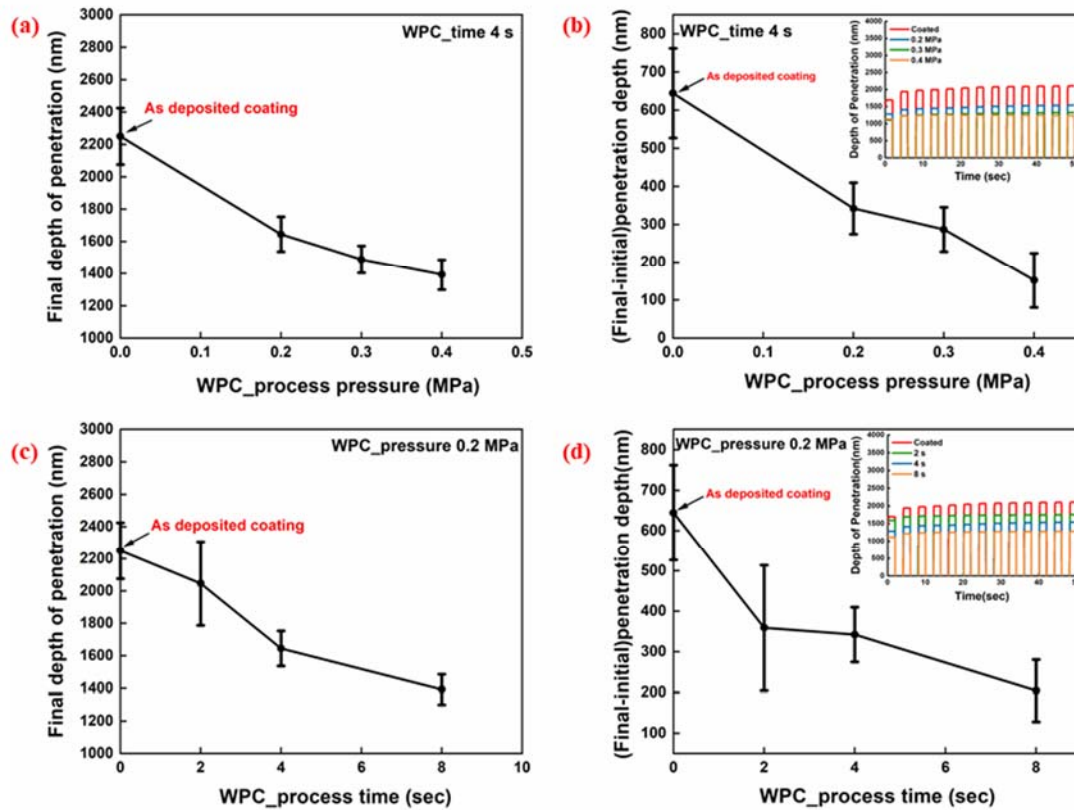


Figure 4.7 Nano-impact testing, (a) final depth after 300 s of impacting ; (b) (final-initial); (b inset) first 50 s depth of penetration for WPC process pressure variation, (c) final depth after 300 s of impacting; (d) (final-initial); (d inset) first 50 s depth of penetration for WPC process time variation at a load of 15 mN.

### 4.3.3 Coating adhesion and tool life analysis

The understanding of coating adhesion during scratch test can interpret coatings' performance during the milling operation. Ramped load micro-scratch test was performed to investigate the adhesion of coating to the substrate following the WPC treatment at various process parameters. The test signifies two important characteristics: as load is increased to  $L_{c1}$  there is an onset of cracking within the coating and a further increase of the load to  $L_{c2}$  causes a well-defined failure event that represents coating detachment from

the substrate. As depicted in Figure 4.8(a, b) the load for crack initiation is higher ( $L_{c1} \approx 2$  N) for as deposited coatings than the treated ones. Also, the load  $L_{c2}$  ( $L_{c2} \approx 2.4$  N) at which as deposited coating undergoes adhesive failure is very close to that of the load  $L_{c1}$ . However, for treated coatings, angular cracks develop in the scratch track at a much lower load when WPC process pressure is varied. Thus, a decreasing trend in  $L_{c1}$  value is observed as WPC pressure increases (Figure 4.8a) along with a lower  $L_{c2}$  value compared to the as deposited coating (Figure 4.8b).

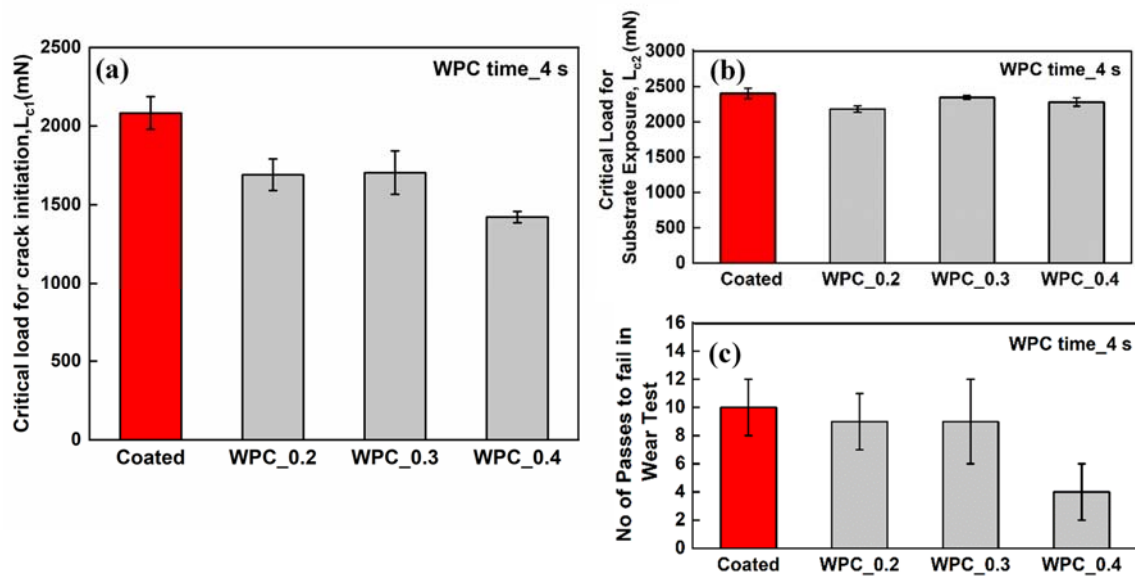


Figure 4.8 Comparison of (a) critical load for crack initiation,  $L_{c1}$  and (b) critical load for coating failure,  $L_{c2}$  (c) wear test data for the variation of WPC pressure.

It has been previously observed that, low critical load is largely a consequence of high compressive residual stress which acts as a pre-load on the coating/substrate interface [47].

Thus, treatment on coated tools lead to lower critical load values.

Previous works have also shown that there is a correlation between the scratch test critical load  $L_{c1}$ ,  $L_{c2}$  and the mechanical properties of the coatings, essentially hardness and the ratio of hardness to elasticity ( $H/E$ ). As deposited coating has the lowest value of  $H/E$  as illustrated in Figure 4.5b. Consequently, for brittle fracture failure of the coatings under the effect of scratch load (effect of both normal and transverse load), as deposited coating having lower  $H/E$  ratio undergoes less cracking (higher  $L_{c1}$  value) and function better due to improved ductility. This kind of critical load data from ramped load micro-scratch tests have been previously reported elsewhere [21]. Furthermore, repetitive load wear test, more sensitive to adhesion differences compare to the ramped load scratch test [48, 49], was performed at a subcritical load of 1 N. Number of passes to an adhesive failure in the wear test is presented in Figure 4.8c and treated coating at 0.4 MPa survives lower number of passes before failing adhesively.

Table 4.5 Comparison of ramped load scratch test and wear test data for the variation of WPC process time at a WPC pressure of 0.2 MPa

WPC_time(s)	Critical load for crack initiation, $L_{c1}$	Critical load for coating failure, $L_{c2}$	No of passes to fail in wear test
2	1660 ± 45	2157 ± 10	9 ± 3
4	1691 ± 100	2181 ± 45	9 ± 2
8	1571 ± 23	2047 ± 73	8 ± 2

However, coating adhesion to the substrate due to WPC process time variation is insignificant in terms of both  $L_{c1}$  and  $L_{c2}$  values as well as the number of passes to fail in the wear test as illustrated in Table 4.5.

As can be seen in the SEM images of the scratch track, angular cracks form in the direction of the scratch (Figure 4.9a) , further evolving into semicircular cracks (Figure 4.9b) that propagate from outward to the center line of the scratch track. Figure 4.9 c demonstrates small interface delamination spots at certain intervals. These are compressive (wedge) spallation present in the scratch track once the studied coatings reach their  $L_{c2}$  value. The coating becomes too stiff to buckle once a critical thickness is reached and instead sloping shear cracks form through the thickness of the coating prior to interfacial failure[50]. Continuous forward motion of the scratch probe further strains the coating and drives wedges of the adjacent coating layer underneath the section confined by the shear cracks. This results in coating delamination. Coating spallation and the frequency of the formed wedges occurs due to the combination of residual stress in the coating at room temperature and stress introduced by the scratch probe [51]. Compressive residual stress plays a predominant role in the given coating under the same experimental conditions. The EDS microanalysis of the scratch tracks is illustrated in terms of Ti-Ka1 and W-La1 in Figure 4.9(d-i) for both as deposited and treated coatings (for process pressure of 0.2 MPa and 0.4 MPa). A gradual increase in the frequency of wedge spallation is observed from as deposited coating illustrated in Figure 4.9 (d, g) to the treated one at 0.2 MPa and 0.4 MPa illustrated in Figure 4.9 (e, g) and Figure 4.9 (f, i) respectively to frequently minimize the elastic energy stored by large compressive stress ahead of the indenter. However, the

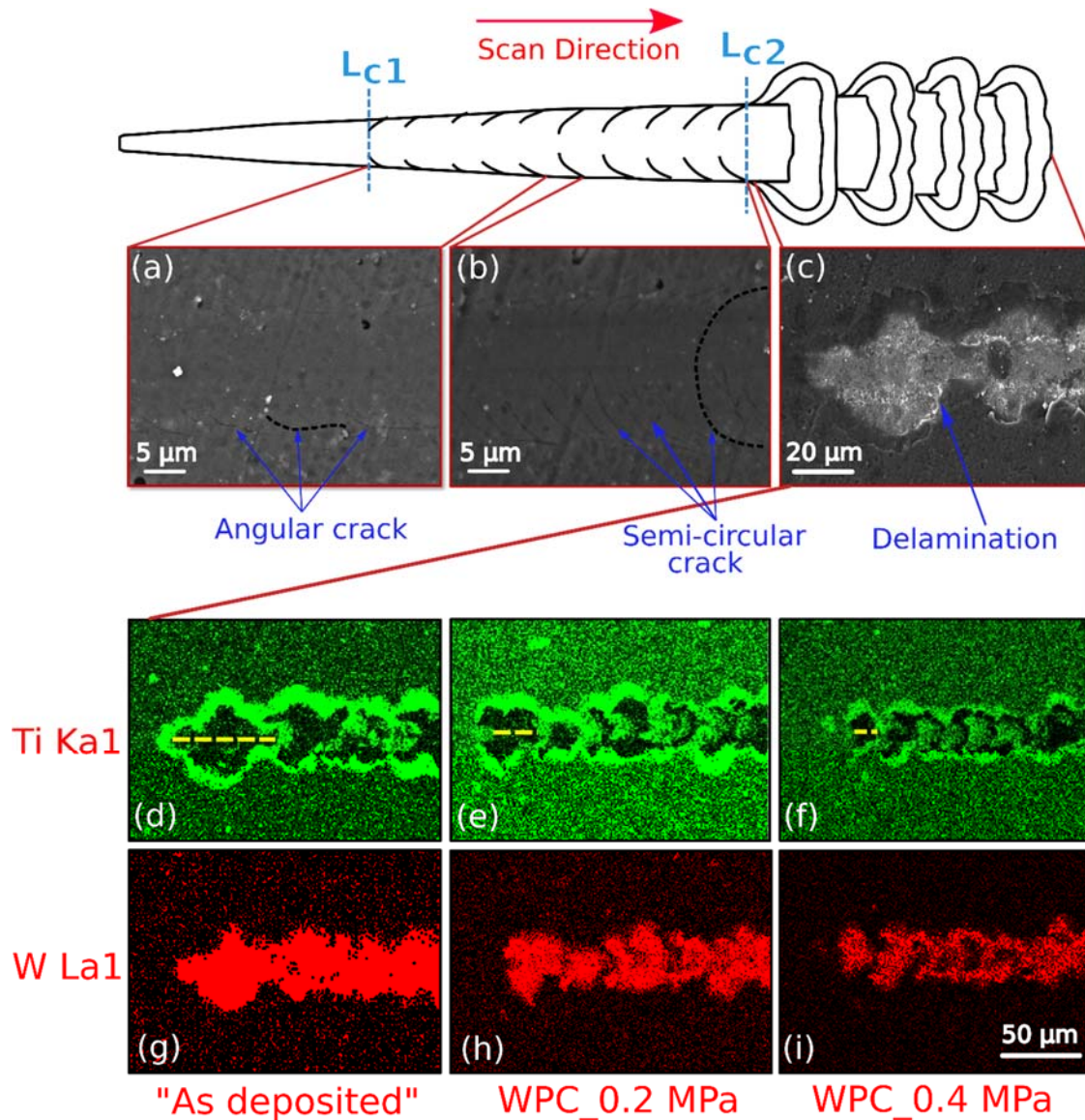


Figure 4.9 SEM images of the ramped load scratch test track showing the (a) cohesive; (b) semicircular cracks and (c) adhesive failure (same failure mechanism for all the studied coatings-including the as deposited one); EDS of the delaminated part of the scratch track (d, e, f) Ti- Ka 1, (g, h, i) W La 1 for the variation of WPC process pressure.

susceptibility of the coating-substrate system to wedge spallation is reduced in as deposited coating due to lower brittleness ( lower  $H/E$ ) which prevents shear crack propagation and ensures that interfacial crack propagation actually occurs in a ductile fashion [52].

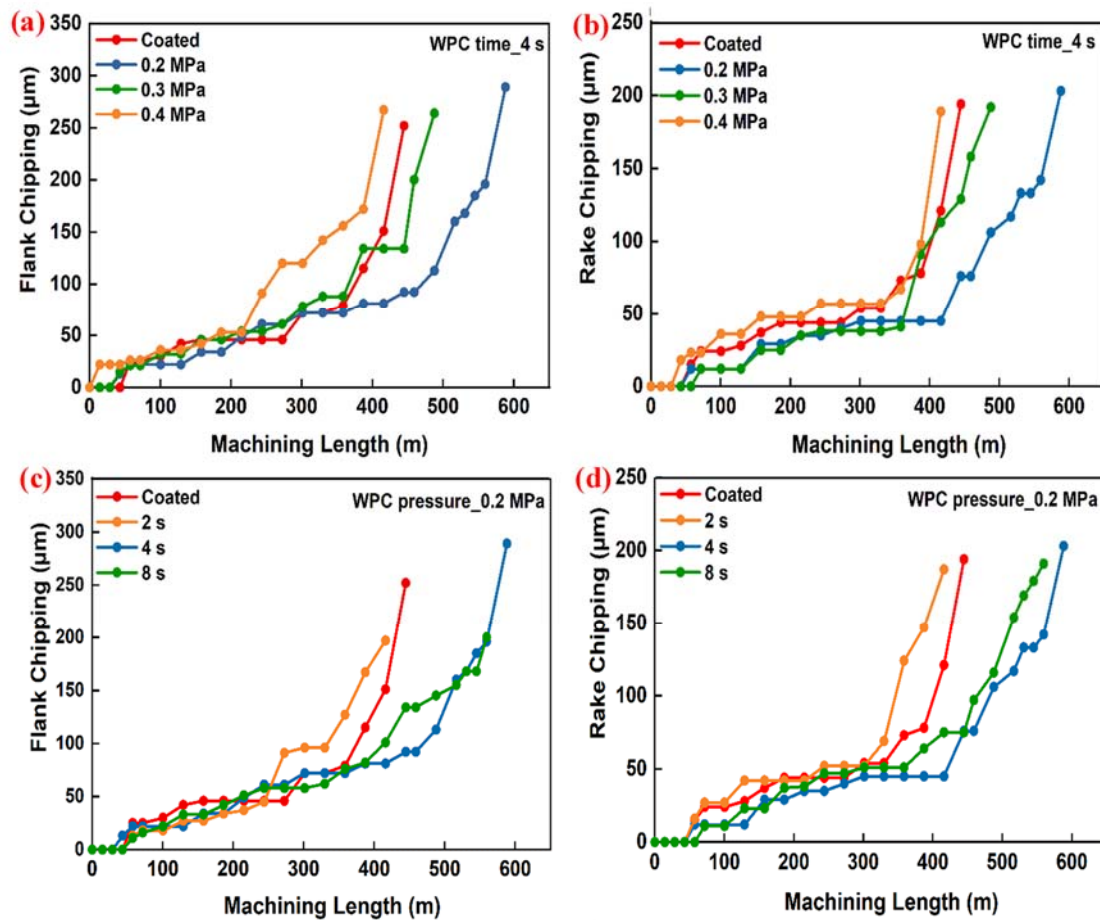


Figure 4.10 Tool-life data of the studied coatings vs. machining length (m); (a,b) flank and rake chipping intensity with WPC pressure variation; (c,d) flank and rake chipping intensity with WPC time variation.

To investigate the effect of WPC conditions on cutting tool life wet milling was performed for the given cutting parameters (Table 4.2) as presented in Figure 4.10. Tool wear pattern of the coated cutting tool was predominantly, flank (Figure 4.11a) and rake chipping (Figure 4.11c) [12] at the position of depth of cut. The mechanical load under the given cutting conditions is large enough to cause the cutting edge to undergo micro chipping which tend to change the geometry of the cutting edge. The micro chipping stage usually



leads to macro chipping to cause the failure of the tool. Conversely, micro-chipping occurs at multiple locations other than the depth of cut in the treated coated tool (Figure 4.11(b, d)) during the running in stage of machining. Micro-chipping occurring at multiple zones along the depth-of-cut during milling can be attributed to the increased frequency of spallation of the treated coatings from the wedge during the delamination process, as shown by the ramped load scratch test. The emergence of micro-chipping at multiple locations ensured the stable development of a microcrack network at the depth-of-cut at the given strain rate, enabling the material to tolerate large strains without tool fracture. The WPC treated cutting tool exhibited the best cutting performance and an around 35% increase in tool life at a pressure of 0.2 MPa and time of 4 s. Tool life was slightly reduced at a pressure of 0.2 MPa and time of 8 s. The worst cutting performance was obtained at a WPC pressure of 0.4 MPa (approximately 10% less compared to the as deposited coating).

One of the crucial ways a cutting tool fail during wet milling is through fatigue caused by high mechanical and thermal loads on the cutting edge under operating conditions [10]. This is due to the cyclic stresses that arise during the intermittent milling process. It has been demonstrated that the coated tool following the application of WPC post-treatment can attain better micro-mechanical properties. For instance, an augmentation in hardness (Figure 4.4(a, b)) as well as  $H^3/E^2$  ratio (Figure 4.5a) is possible to achieve along the depth of penetration for the treated coated tools. Also, the increase in yield stress (Figure 4.6(c, d)) due to the treatment process justifies the fact that treated

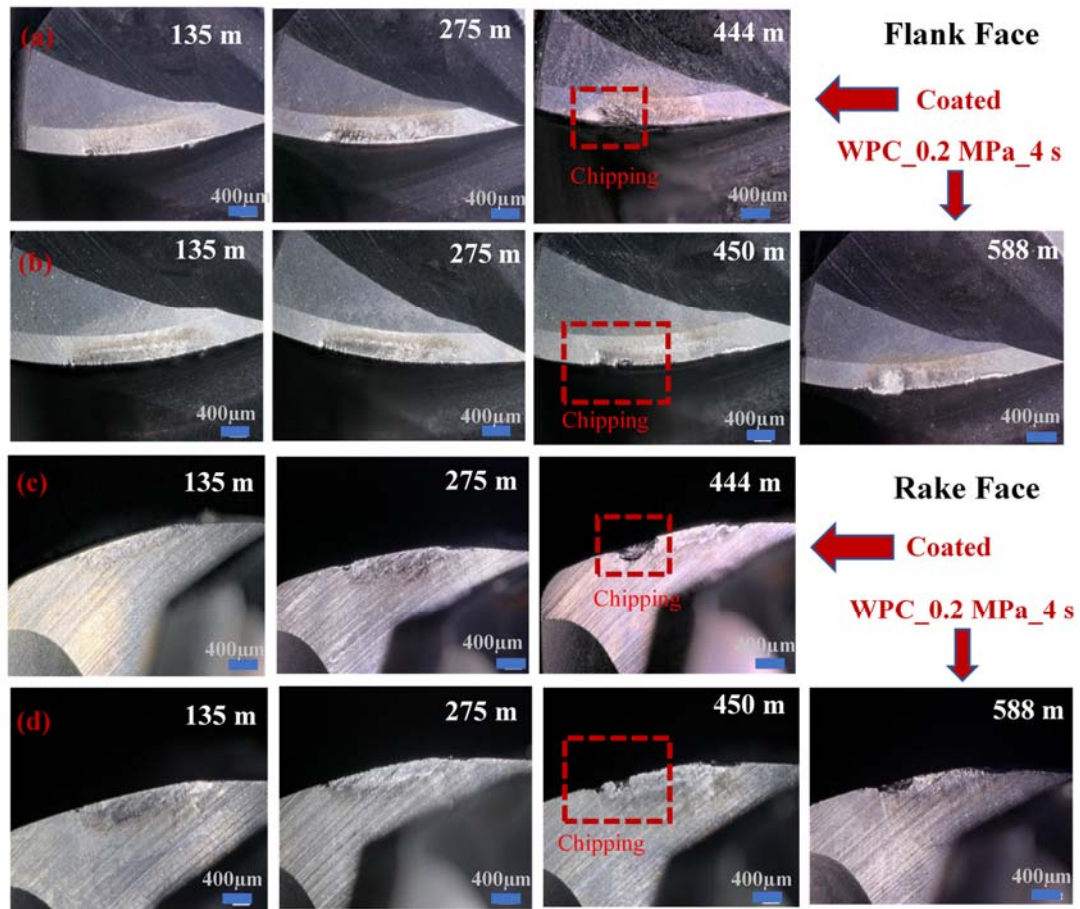


Figure 4.11 Wear evolution vs machining length (m); (a, c) flank and rake face for as deposited coating; (b, d) flank and rake face for treated coating at 0.2 MPa and 4 s.

coated tools with higher value of  $H^3/E^2$  ratio tends to be more elastic under a given load compare to the as deposited one. These micro-mechanical properties contributed to the improved low cycle fatigue resistance of the treated coatings and consequently reduced cutting tool failure by fatigue [44]. Additionally, the increase in yield stress value (Figure 4.6c) can be a qualitative depiction of increased compressive residual stress with the increase in WPC process pressure [38]. The brittleness enhancement (increase in  $H/E$  ratio) is also a consequence of the treatment on the coated tool. Nevertheless, increase in



brittleness with increased WPC pressure specifically at higher penetration depth (at 300nm) (Figure 4.5b) imposes a negative effect on the adhesion property. This aspect of coating adhesion to the substrate is well evident from the ramped load scratch test (Figure 4.8(a, b)) and wear test (Figure 4.8c) data. Therefore, the best tool life achieved for 0.2 MPa pressure is due to the achieved balance between the micro-mechanical and adhesion properties of the coating system. Also, maintaining an integrity of the cutting edge is an important factor to consider for successful application of WPC treatment on the coated tool which to an extent depends on the combination of process pressure and thickness of the as deposited coating [29]. In the present study, the effect of process parameter (Figure 4.3(a, b)) on the tool cutting edge radius was found negligible. However, an incident of local substrate exposure (Figure 4.1c) was observed at a pressure of 0.4 MPa. This occurrence in various literature [29, 42] has been related to a simultaneous film thickness decrease in individual micro-regions on rake and flank face of the cutting edge. This decrease in film thickness was aggravated further by high rough surface (in terms of  $Rt$  value) to cause the worst machining performance during the wet milling of H13 tool steel.

#### **4.4 Conclusion**

This research work introduced WPC for the first time as a post treatment process of coatings to improve cutting performance while wet milling of H13 tool steel. In the present study, the effect of WPC process pressure and time on coated tool cutting edge geometry, micro-mechanical properties and cutting performance during milling was investigated. The effect of the process parameters on the tool's cutting-edge roundness was insignificant. However,

local substrate exposure occurred at a pressure of 0.4 MPa. Thus, the pressure of the process was limited by the integrity of the cutting edge for the given coating thickness. Additionally, an increase in WPC pressure lead to superficial coating strength properties enhancement (in terms of hardness,  $H^3/E^2$  ratio). Also, an increase in yield stress caused by the WPC treatment confirmed that the treated coatings with a higher  $H^3/E^2$  ratio tend to be more elastic under the given load compared to the “as deposited” one. Moreover, WPC treatment of the coatings improved their fatigue resistance and reduced the depth-of-penetration under repetitive impact tests. The post-treatment of the coated tools also increased their brittleness, which hindered coating adhesion with increased process pressure. This trend in adhesion of the coating system to the substrate was verified by the ramped load scratch test and the wear test. An analysis of the tool wear pattern of a post treated coated tool during milling was performed and a relationship with the coating failure mode during the ramped load scratch test was established. A 35% increase in tool life at a pressure of 0.2 MPa was achieved in the WPC treated coating compared to the “as deposited” coating through a balance between the micromechanical and adhesion properties.

**Author Contributions.** “conceptualization, S.C.; methodology, S.C.; validation, S.C., B.B. ; investigation, S.C. ; resources, B.B, A.F.M.A. and S.C.V.; data curation, S.C. ; writing—original draft preparation, S.C.; writing—review and editing, B.B., A.F.M.A. ; visualization, S.C.; supervision, B.B., A.F.M.A., S.C.V.; student and project supervision S.C.V.”

## 4.5 References

1. Zhang, S., T. Ding, and J. Li, *Microstructural alteration and microhardness at near-surface of AISI H13 steel by hard milling*. Machining Science and Technology, 2012. **16**(3): p. 473-486.

2. Roberts, G.A., R. Kennedy, and G. Krauss, *Tool steels*. 1998: ASM international.
3. Ding, H., et al., *Experimental study on machinability improvement of hardened tool steel using two dimensional vibration-assisted micro-end-milling*. International Journal of Machine Tools and Manufacture, 2010. **50**(12): p. 1115-1118.
4. Li, W., Y. Guo, and C. Guo, *Superior surface integrity by sustainable dry hard milling and impact on fatigue*. CIRP Annals, 2013. **62**(1): p. 567-570.
5. Tönshoff, H., C. Arendt, and R.B. Amor, *Cutting of hardened steel*. Cirp Annals, 2000. **49**(2): p. 547-566.
6. Axinte, D. and R. Dewes, *Surface integrity of hot work tool steel after high speed milling-experimental data and empirical models*. Journal of Materials Processing Technology, 2002. **127**(3): p. 325-335.
7. Ribeiro, J.L.S., et al., *Dimensional and geometric deviations induced by milling of annealed and hardened AISI H13 tool steel*. American Journal of Materials Science, 2012. **2**(1): p. 14-21.
8. Nelson, S., J. Schueller, and J. Tlustý, *Tool wear in milling hardened die steel*. Journal of manufacturing science and engineering, 1998. **120**(4): p. 669-673.
9. Cui, X., J. Zhao, and X. Tian, *Cutting forces, chip formation, and tool wear in high-speed face milling of AISI H13 steel with CBN tools*. The International Journal of Advanced Manufacturing Technology, 2013. **64**(9-12): p. 1737-1749.
10. Gu, J., S.C. Tung, and G.C. Barber, *Wear mechanisms of milling inserts: dry and wet cutting*, in *Wear Processes in Manufacturing*. 1998, ASTM International.
11. Elbestawi, M., et al., *High-speed milling of dies and molds in their hardened state*. CIRP Annals, 1997. **46**(1): p. 57-62.
12. Gu, J., et al., *Tool life and wear mechanism of uncoated and coated milling inserts*. Wear, 1999. **225**: p. 273-284.

13. Chinchanikar, S. and S. Choudhury, *Machining of hardened steel—experimental investigations, performance modeling and cooling techniques: a review*. International Journal of Machine Tools and Manufacture, 2015. **89**: p. 95-109.
14. Bouzakis, K.-D., et al., *Cutting with coated tools: Coating technologies, characterization methods and performance optimization*. CIRP Annals-Manufacturing Technology, 2012. **61**(2): p. 703-723.
15. Endrino, J., G. Fox-Rabinovich, and C. Gey, *Hard AlTiN, AlCrN PVD coatings for machining of austenitic stainless steel*. Surface and Coatings Technology, 2006. **200**(24): p. 6840-6845.
16. Beake, B. and G. Fox-Rabinovich, *Advanced nanomechanical testing for high speed machining of hard-to-cut aerospace alloys*. International Heat Treatment and Surface Engineering, 2011. **5**(1): p. 17-20.
17. Beake, B., et al., *Investigating the correlation between nano-impact fracture resistance and hardness/modulus ratio from nanoindentation at 25–500° C and the fracture resistance and lifetime of cutting tools with Ti 1– x Al x N (x= 0.5 and 0.67) PVD coatings in milling operations*. Surface and Coatings Technology, 2007. **201**(8): p. 4585-4593.
18. Kalss, W., et al., *Modern coatings in high performance cutting applications*. International Journal of Refractory Metals and Hard Materials, 2006. **24**(5): p. 399-404.
19. Soldán, J., et al., *Structure–property relations of arc-evaporated Al–Cr–Si–N coatings*. Surface and Coatings Technology, 2008. **202**(15): p. 3555-3562.
20. Beake, B.D., et al., *Coating optimisation for high speed machining with advanced nanomechanical test methods*. Surface and Coatings Technology, 2009. **203**(13): p. 1919-1925.
21. Fox-Rabinovich, G., et al., *Effect of mechanical properties measured at room and elevated temperatures on the wear resistance of cutting tools with TiAlN and AlCrN coatings*. Surface and coatings technology, 2006. **200**(20-21): p. 5738-5742.

22. Beake, B., et al., *Wear performance of different PVD coatings during hard wet end milling of H13 tool steel*. Surface and Coatings Technology, 2015. **279**: p. 118-125.
23. Zhang, X., et al., *Hertzian contact response of single-layer, functionally graded and sandwich coatings*. Materials & design, 2007. **28**(1): p. 47-54.
24. Abusuilik, S.B., *Pre-, intermediate, and post-treatment of hard coatings to improve their performance for forming and cutting tools*. Surface and Coatings Technology, 2015. **284**: p. 384-395.
25. Jacob, A., et al., *Influences of micro-blasting as surface treatment technique on properties and performance of AlTiN coated tools*. Journal of Manufacturing Processes, 2017. **29**: p. 407-418.
26. Bouzakis, K.-D., et al., *Influence of dry micro-blasting grain quality on wear behaviour of TiAlN coated tools*. Wear, 2011. **271**(5): p. 783-791.
27. Bouzakis, K.-D., et al., *Effect of PVD films wet micro-blasting by various Al<sub>2</sub>O<sub>3</sub> grain sizes on the wear behaviour of coated tools*. Surface and Coatings Technology, 2011. **205**: p. S128-S132.
28. Bouzakis, K., et al., *Optimization of Wet or Dry Microblasting on PVD Films by Various Al<sub>2</sub>O<sub>3</sub> Grain Sizes for Improving the Coated Tools' Cutting Performance*. Tribology in Industry, 33: 49–56. 2011.
29. Bouzakis, K.-D., et al., *Effect of dry micro-blasting on PVD-film properties, cutting edge geometry and tool life in milling*. Surface and Coatings Technology, 2009. **204**(6-7): p. 1081-1086.
30. Harada, Y., K. Fukauara, and S. Kohamada, *Effects of microshot peening on surface characteristics of high-speed tool steel*. Journal of Materials Processing Technology, 2008. **201**(1-3): p. 319-324.
31. Denkena, B., et al., *Influence of shot peening and laser ablation on residual stress state and phase composition of cemented carbide cutting inserts*. International Journal of Refractory Metals and Hard Materials, 2013. **36**: p. 85-89.

32. Morita, T., S. Noda, and C. Kagaya, *Influence of hardness of substrates on properties of surface layer formed by fine particle bombarding*. Materials Science and Engineering: A, 2013. **574**: p. 197-204.
33. Yonekura, D., et al. *Effect of residual stress on fatigue strength of steel modified by WPC process*. in *ICF10, Honolulu (USA) 2001*.
34. Adoberg, E., et al., *The effect of surface pre-treatment and coating post-treatment to the properties of TiN coatings*. Estonian Journal of Engineering, 2012. **18**(3): p. 185.
35. Bouzakis, K.-D., et al., *Micro-blasting of PVD films, an effective way to increase the cutting performance of coated cemented carbide tools*. CIRP annals, 2005. **54**(1): p. 95-98.
36. Hassani, S., et al., *Predictive tools for the design of erosion resistant coatings*. Surface and Coatings Technology, 2008. **203**(3): p. 204-210.
37. Bruet, B.J., et al., *Materials design principles of ancient fish armour*. Nature materials, 2008. **7**(9): p. 748.
38. Kim, Y.-C., et al., *Quantitative Characterization of Mechanical Properties using Instrumented Indentation*. Procedia Engineering, 2011. **10**: p. 3162-3172.
39. Oettel, H. and R. Wiedemann, *Residual stresses in PVD hard coatings*. Surface and coatings technology, 1995. **76**: p. 265-273.
40. MENČÍK, J., *Opportunities and problems in nanoindentation with spherical indenters*. Chem. Listy, 2011. **105**: p. s680-s683.
41. Clausner, A. and F. Richter, *Determination of yield stress from nano-indentation experiments*. European Journal of Mechanics-A/Solids, 2015. **51**: p. 11-20.
42. Bouzakis, K.-D., et al., *Optimization of wet micro-blasting on PVD films with various grain materials for improving the coated tools' cutting performance*. CIRP annals, 2011. **60**(1): p. 587-590.

43. Beake, B.D. and J.F. Smith, *Nano-impact testing—an effective tool for assessing the resistance of advanced wear-resistant coatings to fatigue failure and delamination*. Surface and Coatings Technology, 2004. **188**: p. 594-598.
44. Beake, B., V. Vishnyakov, and J. Colligon, *Nano-impact testing of TiFeN and TiFeMoN films for dynamic toughness evaluation*. Journal of Physics D: Applied Physics, 2011. **44**(8): p. 085301.
45. Musil, J. and M. Jirout, *Toughness of hard nanostructured ceramic thin films*. Surface and Coatings Technology, 2007. **201**(9-11): p. 5148-5152.
46. Pei, Y., D. Galvan, and J.T.M. De Hosson, *Nanostructure and properties of TiC/aC: H composite coatings*. Acta materialia, 2005. **53**(17): p. 4505-4521.
47. Nordin, M., M. Larsson, and S. Hogmark, *Mechanical and tribological properties of multilayered PVD TiN/CrN, TiN/MoN, TiN/NbN and TiN/TaN coatings on cemented carbide*. Surface and coatings technology, 1998. **106**(2-3): p. 234-241.
48. Beake, B., B. Shi, and J. Sullivan, *Nanoscratch and nanowear testing of TiN coatings on M42 steel*. Tribology-Materials, Surfaces & Interfaces, 2011. **5**(4): p. 141-147.
49. Beake, B., et al., *Elevated temperature repetitive micro-scratch testing of AlCrN, TiAlN and AlTiN PVD coatings*. International Journal of Refractory Metals and Hard Materials, 2017. **69**: p. 215-226.
50. Bull, S. and E. Berasetegui, *An overview of the potential of quantitative coating adhesion measurement by scratch testing*. Tribology International, 2006. **39**(2): p. 99-114.
51. Li, J. and W. Beres, *Scratch test for coating/substrate systems—A literature review*. Canadian Metallurgical Quarterly, 2007. **46**(2): p. 155-173.
52. Bull, S., *Failure mode maps in the thin film scratch adhesion test*. Tribology international, 1997. **30**(7): p. 491-498.

## Chapter 5. CONCLUSIONS AND FUTURE WORKS

This dissertation is the first demonstration of approaches like multilayer coating combined with an interlayer and WPC treatment on coatings to improve a coatings' micro-mechanical and adhesion properties during milling. The primary goal of this thesis is to advance the PVD coating architecture and WPC treatment for conditions relevant to dry and wet milling of H13 tool steel. The first logical step towards this objective was to validate these approaches in terms of tool life enhancement for heavy loaded/high temperature conditions during milling of H13. Furthermore, accounting for the micro-mechanical and adhesion properties of coatings that can relate the applicability of such approaches to extreme cutting conditions.

### 5.1 General Conclusions

Three TiAlCrSiYN-based coating architectures deposited at a negative substrate bias of 100V were investigated: i) monolayer; ii) multilayer; iii) multilayer with an interlayer. A 100 nm thick interlayer (TiAlCrN) was included in the nano multilayered TiAlCrSiYN/TiAlCrN coating. X-ray diffraction using Cu-K $\alpha$  radiation beam exhibited a B1 crystal structure with the preferred orientation of C (111) in all the coatings. Moreover, the incorporation of an interlayer into the multilayer structure reduced the compressive residual stress. A significant increase of the  $H^3/E^2$  and  $H/E$  ratio was observed when an interlayer was present in the multilayer structure. Despite their higher brittleness (higher  $H/E$  ratio), the multilayer coatings with an interlayer exhibited a more gradual increase in the



depth of penetration in the nano-impact test, primarily due to their structural advantage as compared to coatings with traditional multilayers or monolayers. The most promising feature provided by the incorporation of an interlayer into the multilayer coating was the improvement in adhesion as measured in the ramped load micro-scratch test. The von Mises, tensile and shear stresses during the micro-scratch test were evaluated using the Scratch Stress Analyzer. It was found that the area over which the substrate yields at the load of coating adhesive failure ( $L_{c2}$ ), depends more on the coatings thickness rather than its architecture. Wear evolution during the dry high-speed milling of H13 was more gradual for the multilayer coating with the interlayer which related well to the impact behavior. Although its low  $L_{c1}$  value resulted in high initial damage during the cutting test, a 50% increase in tool life was reported due to the superior load support (higher  $H^3/E^2$  value) and high CPRs value compared with those of the multilayer coating.

A second set of experiments was carried out where the TiAlCrN interlayer thickness was varied (100 nm, 300 nm and 500 nm) within the multilayer coating structure. The coating was deposited at a negative substrate bias of 150 V at an overall thickness of 2  $\mu\text{m}$ . X-ray diffraction patterns showed that all studied coatings had a B1 crystal structure and its preferred orientation was C (200). However, the shift in the preferred orientation from the previous study was due to the change in negative substrate bias from 100V to 150 V during the deposition process. The variation of interlayer thickness had no observable effect on the diffraction peak intensity. Moreover, the variation in deposition time only affected interlayer thickness and had a negligible effect on the overall residual stress of the coating layer.

The indentation hardness data showed that the multilayer coating with a 500 nm interlayer has the lowest hardness. Thus, a decrease in hardness with similar elastic modulus reduced the  $H^3/E^2$  ratio as the thickness of the TiAlCrN interlayer increased. The  $H^3/E^2$  ratio tends to further decrease at a high temperature during the milling process. This can be attributed to the absence of Yttrium in the interlayer, causing grain coarsening at an elevated temperature and consequently further softening of the coating when a 500 nm (the thickest) interlayer was used. Moreover, an increase in the final penetration depth after 300 s of impact was observed with increasing interlayer thickness. Thus, the coating with a 500 nm interlayer had a poor low cycle fatigue resistance compared with the coatings that had 100 and 300 nm interlayers. However, spallation was more extensive in the coating with the 100 nm interlayer. The multilayer with a 300 nm interlayer was more effective in preventing total coating failure and substrate exposure. Conversely, during the scratch test, the multilayer coating with a 500 nm interlayer had the lowest  $H/E$  ratio and functioned better due to improved ductility with an increased critical load,  $L_{c2}$ . The most significant result was obtained from repetitive scratch tests performed at a subcritical load of 1.5 N. It was observed that a 300 nm interlayer required more passes to reach cohesive failure compared to the 100 nm interlayer. However, at the end of the 15th pass both coatings exhibited adhesive failure. In contrast, the coating with a 500 nm interlayer only showed signs of cohesive failure at the given load. Considering the two-contradictory phenomenon in terms of micro mechanical and adhesion properties, it was concluded that the multilayer coating with the 300 nm interlayer exhibited a more gradual wear trend and a 40% and 50%

increase in tool life compared to the coatings with the 100 and 500 nm interlayers, respectively.

The compressive residual stress and the  $H^3/E^2$  ratio decreased as the overall coating thickness was varied from 2  $\mu\text{m}$  to 3  $\mu\text{m}$  with thickness of the interlayer remaining the same. However, the nano-impact test data showed that the 3  $\mu\text{m}$  coating had the best fatigue performance with minimal surface damage. The most striking feature from this result was that the impact behavior was dependant not only on the combination of the load support and micro-structural advantages but also on the overall thickness of the coating. However, the lower  $L_{c2}$  value contributed to lower CPRs in the scratch test due to the combination of high tensile stresses at the surface with significant weakening of the interface. Tool life analysis demonstrated that the 3  $\mu\text{m}$  coating was able to provide protection to the substrate surface by forming a tribo-ceramic film layer. During the running in stage of the milling operation, the thicker coating experienced less surface damage to cause the formation of thermal barrier ceramic tribo-films in a greater amount which critically improved the wear performance of the coating layer.

The second phase of this research considered the effect of WPC on the coated tool's cutting edge geometry, micro-mechanical properties and cutting performance during wet milling of H13 under two different post-treatment conditions: i) variation of WPC process pressures from 0.2 MPa to 0.4 MPa for a duration of 4 seconds; ii) variation of process time from 2 s to 8 s at a WPC pressure of 0.2 MPa. The effect of the aforementioned process parameters on the tool's cutting-edge roundness was insignificant. However, local substrate exposure occurred at a pressure of 0.4 MPa. Thus, the pressure of the process was limited

by the integrity of the cutting edge for the given coating thickness. Additionally, a multi cycle load test showed an increase in hardness as well as  $H^3/E^2$  ratio of the treated coatings along the depth of penetration as the WPC pressure increased. Also, an increase in yield stress caused by the WPC treatment confirmed that the treated coatings with a higher  $H^3/E^2$  ratio tend to be more elastic under the given load compared to the “as deposited” one. Moreover, WPC treatment of the coatings improved their fatigue resistance and reduced the depth-of-penetration under repetitive impact tests. The post-treatment of the coated tools also increased their brittleness, which hindered coating adhesion with increased process pressure. This trend in adhesion of the coating system to the substrate was verified by the ramped load scratch test and the wear test. Post-treatment of a coated tool reduced the critical load of crack initiation at an increasing process pressure. Once the critical load for substrate exposure was reached, the frequency of coating spallation from the wedge gradually increased along with pressure in the treated coating. Micro-chipping occurring in multiple zones along the depth-of-cut during milling can be associated with the increased frequency of spallation of the treated coatings from the wedge during the delamination process, as shown by the ramped load scratch test. This micro-chipping behavior at multiple locations ensured the stable development of a microcrack network at the depth-of-cut under the given strain rate and enabled the material to tolerate large strains without tool fracture at that position. A 35% increase in tool life at a pressure of 0.2 MPa was achieved in the WPC treated coating compared to the “as deposited” coating through a balance between the micromechanical and adhesion properties.

## 5.2 Research Contributions

Given the research gaps in literature for H13 tool steel milling using PVD coated tools under extreme cutting conditions, several experimental approaches are outlined in this research work to improve their tool life and wear behavior. The implementation of these tools in industrial practice could provide an economical alternative to expensive PCBN tools. The major contributions of this dissertation are the following:

This research work demonstrated that the incorporation of an interlayer into a complex multilayer coating improves the adhesion of a coating to the substrate.

Furthermore, it was established that as the interlayer thickness within the multilayer coating structure was varied, tool life enhancement during milling would require a balance between coating micro-mechanical and adhesion properties. A repeated micro scratch test was used to verify that the coating adhesion improved with the increase in interlayer thickness. However, wear performance worsened due to the decrease in load support. Moreover, the successful evaluation of coating adhesion ensures that this technique could be applied to very thin coatings at lower loads to observe coating dominated effects.

This research work introduced WPC for the first time for the post treatment of coatings for this application. A detailed analysis of various process parameters demonstrated that the surface of a coated tool could be superficially strengthened by WPC post treatment. The limitations of this type of coated tool post treatment were also identified.

The most significant contribution of this study was the analysis of the tool wear pattern of a post treated coated tool during the milling process. Changes in coating adhesion

after post-treatment were evaluated and their relationship with the coating failure mode during the scratch test was established.

### 5.3 Directions for Future Work

The findings reported in this thesis open several avenues for future research:

Nano-impact test data was used to quantitatively analyze the low cycle fatigue resistance of multilayer coatings in this thesis. However, an in-situ analysis of the cross-section of the coating through SEM/ FIB could be done at certain intervals between impacts to examine the performance of the multilayer coating with an interlayer in the nano-impact test.

Compressive residual stress was shown to decrease with increasing multilayer thickness. Further analysis on the variation of overall coating thickness could reveal the effect of residual stress on adhesion properties, especially the critical load for crack initiation ( $L_{cl}$ ).

WPC is a recently adopted technique for coating post-treatment. However, according to the literature a pre-treatment process may increase coating adhesion to the substrate. Thus, WPC pre-treatment of the current coating with and without the existing interlayer could be done to understand its effect on coating adhesion.

In this study, WPC treated coated tools were used for the wet milling of H13 involving a semi finishing operation. The application of WPC could be extended to both H13 dry milling and roughing in order to obtain the desired range of cutting conditions that could guarantee minimum tool wear and maximum productivity.

## PUBLICATIONS

1. **Chowdhury S**, Bose B, Yamamoto K, Veldhuis SC (2019) Effect of Interlayer Thickness on Nano-Multilayer Coating Performance during High Speed Dry Milling of H13 Tool Steel. *Coatings* 9 (11):737
2. **Chowdhury S**, Beake B, Yamamoto K, Bose B, Aguirre M, Fox-Rabinovich G, Veldhuis S (2018) Improvement of wear performance of nano-multilayer PVD coatings under dry hard end milling conditions based on their architectural development. *Coatings* 8 (2):59
3. Chowdhury M, **Chowdhury S**, Yamamoto K, Beake B, Bose B, Elfizy A, Cavelli D, Dosbaeva G, Aramesh M, Fox-Rabinovich G (2017) Wear behaviour of coated carbide tools during machining of Ti6Al4V aerospace alloy associated with strong built up edge formation. *Surf. Coat. Technol* 313:319-327
4. **Chowdhury S**, Bose B, Arif A.F.M., Veldhuis S Tool life improvement of coated carbide tools through the application of a novel surface treatment technique-wide peening cleaning (WPC) while wet milling of H13 tool steel. *Manuscript submitted for peer review.*